Spring 2019

Hydrogen Fuel Cell Gasket Handling and Sorting With Machine Vision Integrated Dual Arm Robot

Devin C. Fowler

HYDROGEN FUEL CELL GASKET HANDLING AND SORTING WITH MACHINE VISION INTEGRATED DUAL ARM ROBOT

by

DEVIN FOWLER

(Under the Direction of Daniel Cox)

ABSTRACT

Recently demonstrated robotic assembling technologies for fuel cell stacks used fuel cell components manually pre-arranged in stacks (presenters), all oriented in the same position. Identifying the original orientation of fuel cell components and loading them in stacks for a subsequent automated assembly process is a difficult, repetitive work cycle which if done manually, deceives the advantages offered by automated fabrication technologies of fuel cell components and by robotic assembly processes.

We present an innovative robotic technology which enables the integration of automated fabrication processes of fuel cell components with robotic assembly of fuel cell stacks into a fully automated fuel cell manufacturing line. This task, which has not been addressed in the past uses a Yaskawa Motoman SDA5F dual arm robot with integrated machine vision system. The process is used to identify and grasp randomly placed, slightly asymmetric fuel cell components having a total alpha-plus-beta symmetry angle of 720^{o}, to reorient them all in the same position and stack them in presenters for a subsequent robotic assembly process. The dual arm robot technology is selected for increased productivity and ease of gasket handling during reorientation. The initial position and orientation of the gaskets is identified by image analysis using a Cognex machine vision system with fixed camera. The process was demonstrated as part of a larger endeavor of bringing to readiness advanced manufacturing technologies for

alternative energy systems, and responds the high priority needs identified by the U.S. Department of Energy for fuel cells manufacturing research and development.

INDEX WORDS: Dual arm robotics; Fuel cells; Robotic manufacturing; Robotic assembly; Machine vision system; Flexible materials handling; Robotic fuel cell assembly

HYDROGEN FUEL CELL GASKET HANDLING AND ALIGNMENT WITH MACHINE VISION INTEGRATED DUAL ARM ROBOT

by

DEVIN FOWLER

B.S., University of North Florida, 2016

M.S., Georgia Southern University, 2019

A Thesis Submitted to the Graduate Faculty of Georgia Southern University in Partial Fulfillment of the Requirements for the Degree

MASTER OF SCIENCE

STATESBORO, GEORGIA

HYDROGEN FUEL CELL GASKET HANDLING AND ALIGNMENT WITH MACHINE VISION INTEGRATED DUAL ARM ROBOT

by

DEVIN FOWLER

Major Professor:	Daniel Cox
Committee:	Vladimir Gurau
	Biswanath Samanta

Electronic Version Approved:
May 2018

DEDICATION

To my father, mother, brother, and wife with love.

ACKNOWLEDGMENTS

I would like to especially thank Daniel Cox for bringing me to Georgia Southern University. Without his guidance, I would not have pursued my masters and gained the skills and knowledge that Georgia Southern University has imparted upon me.

I would also like to extend sincere thanks to Vladimir Gurau for his immense contribution of helping the direction of this thesis and for his experience in hydrogen fuel cells.

I would also like to express gratitude to Biswanath Samanta for his knowledge of robotics and mechatronics and for his understanding of graduate school processes.

Lastly, but certainly not least, I would like to thank Allie Fowler for her continuous support. Her patience and encouragement enabled me to write this thesis efficiently.

TABLE OF CONTENTS

Page #

ACKNOWLEDGMENTS 3

LIST OF FIGURES 7

LIST OF TABLES 11

LIST OF EQUATIONS 12

NOMENCLATURE 13

CHAPTER 1. INTRODUCTION 14

1.1 Hydrogen Fuel Cells 14

1.2 Need for Automated Fuel Cell Assembly 14

1.3 Problem Statement 16

1.4 Hypothesis 18

1.5 Experimental Limitations 19

CHAPTER 2. LITERATURE REVIEW 20

2.1 Proton Exchange Membrane Fuel Cells 20

2.1.1 Overview and Advantages 20

2.1.2 History 21

2.1.3 Design 22

2.1.4 Applications and Market Evaluation 23

2.1.5 Technological Challenges 26

2.2 Dual Arm Robotics 27

2.2.1 Dual Arm Robotics Applications 27

2.2.2 Future of 31

2.2.3 Computer Vision Systems in Robotics 32

2.3 Examples of Automated Hydrogen Fuel Cell Construction 33
2.3.1 End Effector Designs 33
2.3.2 Workcell Designs 34
CHAPTER 3. METHODOLOGY 36
3.1 Equipment and Instrumentation Precision 36
3.1.1 Yaskawa Motoman - SDA5F Dual Arm Robot 36
3.1.2 COGNEX ISM1403C Camera 36
3.1.3 Selectively Compliant End-Effector 36
3.2 Robot Mounting Cart and Staging Tables Design and Fabrication 37
3.2.1 Robot Mounting Cart Design 37
3.2.2 Gasket Staging Table and Alignment Table 38
3.3 Fuel Cell Gasket Design and Fabrication 40
3.4 End Effector Design and Fabrication 43
3.5 Programming 46
3.6 Procedure 51
CHAPTER 4. RESULTS 54
4.1 Human Gasket Sortation 54
4.2 Robot Gasket Sortation 56
4.3 Comparison and Analysis 60
4.4 Criteria for Success 61
CHAPTER 5. CONCLUSIONS 62
5.1 Validation of Hypothesis 62

5.2 KNOWLEDGE GAINED FROM PEMFC GASKET SORTING 63

5.3 SUGGESTIONS FOR FUTURE RESEARCH AND APPLICATION 63

REFERENCES 65

APPENDIX A: YASKAWA PROGRAM 69

APPENDIX B: COGNEX PROGRAM 74

APPENDIX C: SDA5F DATA SHEET 75

APPENDIX D: COGNEX ISM1403C DATA SHEET 76

APPENDIX E: ROBOT MOUNTING CART AND STAGING TABLES ITERATIONS 77

APPENDIX F: WORKCELL DESIGN ITERATIONS 83

APPENDIX G: JOB INSTRUCTION 86

LIST OF FIGURES

Page #

Figure 1.1 - Global fuel cell market revenue by product, 2014 - 2025 (USD Million) (top) and global fuel cell market capacity by application, 2015 (MW) (bottom) (Grand View Research 2016). 15

Figure 1.2 - Gasket axis orientation.....17

Figure 1.3 Single PEMFC stack (Sharaf and Orhan 2014, 844).....18

Figure 2.1 - Principals, features, and applications of PEMFCs (Sharaf and Orhan 2014, 812) 20

Figure 2.2 - L-FCEV concept design based on Honda 2005 FCX (Sharaf and Orhan 2014, 830) ... .26

Figure 2.3 - SDA10 automated office chair assembly (Yaskawa Europe GmbH. 2012) 29

Figure 2.4 - Assembly method for the friction-based assembly strategy (left) and dual-arm assembly strategy (right). (Young-Loul, Hee-Chan Song, and Jae-Bok Song 2013).....30

Figure 2.5 - Dual arm robot garment segmentation and folding (Stria et. al. 2019).....31

Figure 2.6 – Examples of image segmentation methods (Nowakowski and Sankowski 2014, Ch. 2.1). 33

Figure 2.7 – “End-effectors used for PEMFC components manipulation: (a) double-acting finger gripper; reproduced with permission from [9]; (b) pneumatic end-effector with suspension mechanism; reproduced from [14]; (c) end-effector with vacuum cups and suspension mechanism used in [7]; (d) pneumatic end-effector; reproduced from [16].” (Gurau, Vladimir, Devin Fowler and Daniel Cox. 2017).....34

Figure 2.8 “General purpose robot workcells for assembly of PEMFC stacks: (a) workcell consisting of 3 KUKA robots with 6 DOF (degrees of freedom); reproduced with permission

from [9]; (b) workcell consisting of a single KUKA robot with 6 DOF; reproduced from [14]" (Gurau, Vladimir, Devin Fowler and Daniel Cox. 2017) 35

Figure 3.1 – Selectively-Compliant End Effector with reference coordinate system.....36

Figure.3.2 – Robot mounting cart design.....37

Figure 3.3 - Robot mounting cart with Yaskawa SDA5F on top and controller housed below 38

Figure 3.4 - Workcell final design with staging table (center left, smaller), alignment table (center right, taller), and SwivelLink® camera mount. 39

Figure 3.5 – Gasket staging and alignment tables (left) and SwivelLink® camera mount (right). The work holding parts in the top left of the left image are 3D printed using ABS. 40

Figure 3.6 - Gasket profile. The top right corner is notched for alignment purposes. 41

Figure 3.7 – Gaskets in the laser cutter (left) and additional cedar residue (right).....42

Figure 3.8 - Stack of cleaned and polished gaskets 42

Figure 3.9 - End effector overview 43

Figure 3.10 - Gasket underneath transparent bottom plate 44

Figure 3.11 - End effector exploded view 44

Figure 3.12 - Symmetry of the end effectors 45

Figure 3.13 - OMAX waterjet fabrication (left) and CNC end stop drilling operation (right).....45

Figure 3.14 - End effector manufactured and assembled 46

Figure 3.15 – "Main Process" programming flowchart for the FS100 47

Figure 3.16 – "Machine Vision Process" flowchart 48

Figure 3.17 - MotoSim EG VRC simulation program during runtime 49

Figure 3.18 - In-Sight® Explorer Easy Builder software HFC notch detection 50

Figure 3.19 - Action list for notch detection cases 51

Figure 3.20 - Experimental Workcell 52

Figure 3.21 - Robot sortation in operation.....53

Figure 3.22 –Manual placement of gasket onto alignment pins 53

Figure 4.1 - Manual gasket sorting time versus run count.....55

Figure 4.2 - False positive from improperly cleaned gasket edge due to laser cutting debris.....57

Figure 4.3 - MotoSim EG VRC Trace Manager (during Online operation).....58

Figure B.1 - Program setup in Cognex EasyBuilder. Trained model (top), Tolerancing (Middle), Trigger and exposure (lower left), and wiring (lower right).....74

Figure C.1 - Yaskawa Motoman SDA5F datasheet.....75

Figure D.1 - Cognex In-Sight® 1403C data sheet.....76

Figure E.1 - Initial alignment table design.....77

Figure E.2 - Fabrication of initial alignment table.....78

Figure E.3 - Initial gasket staging table design.....79

Figure E.4 - Initial gasket staging table design with box placed. 80

Figure E.5 - Fabrication of initial gasket staging table.....81

Figure E.6 - Initial gasket staging table with modified alignment table.....82

Figure F.1 - Initial workcell iteration.....83

Figure F.2 - Second workcell iteration. 84

Figure F.3 - Initial end effector design. 85

Figure G.1 - In-Sight® Explorer 5.4.0 Starting Screen 86

Figure G.2 - Network sensor list.....86

Figure G.3 - Load job file (Top), Accept loading (Middle), and screen after loading (Bottom)...87

Figure G.4 - Run job button location.....87

Figure G.5 - Online button. 88

Figure G.6 - Confirm Go Online popup (press Yes). 88

Figure G.7 - Power switch location for the robot controller 88

Figure G.8 - Controller on screen. 89

Figure G.9 - Grip to enable pendant handshake. 90

Figure G.10 - Release to connect pendant to controller. 91

Figure G.11 - YASKAWA splash screen displayed after connection is successful. 92

Figure G.12 - Main menu after connection completed. 93

Figure G.13 - Screen after touching job on touchscreen controller. 94

Figure G.14 - Job list after touching "Select Job". DFTHEIS job can selected using the "Select" button 95

Figure G.15 - Job screen after selecing DFTHESIS job. 96

Figure G.16 - After switching the pendant key to play 97

Figure G.17 - Press "SERVO ON READY" to enable robot servos. Wait a couple seconds for the servo brakes to disable and the servos to energize before pressing Start. 98

Figure G.18 - Press start on teach pendant to begin the program. 99

LIST OF TABLES

Page #

Table 2.1 - Milestones in fuel cell history (Sharaf and Orhan 2014, 812) 21

Table 4.1 - Results of manual gasket sortation.....54

Table 4.2 - Results of robot gasket sorting experiment 56

Table 4.3 - Gasket sortation categorized trace lengths for each robot.....59

Table 4.4 - Simulated runs using traces in Excel.....59

Table 4.5 - Simulated robot runs with optimized speed 60

LIST OF EQUATIONS

Page #

$H_2 \rightarrow 2H^+ + 2e^-$ ..... Equation 2.1.1 22

$\frac{1}{2}O_2 + 2H^+ + 2e^- \rightarrow H_2O$. ..... Equation 2.1.2 23

$H_2 + \frac{1}{2}O_2 \rightarrow H_2O + W_{ele} + Q_{heat}$. ..... Equation 2.1.3 23

NOMENCLATURE

AFC	Alkaline Fuel Cell
APU	Auxiliary Power Unit
CHP	Combined Heating and Power
CNC	Computer Numerical Control
DFMA	Design for Manufacturing and Assembly
DMFC	Direct Methanol Fuel Cell
DOF	Degree(s) of Freedom
EPS	Emergency Power Supply
GDL	Gas Diffusion Layer
FC	Fuel Cell
H-FCEV	Heavy-Duty Fuel Cell Vehicle
L-FCEV	Light-Duty Fuel Cell Vehicle
LTV	Light Traction Vehicle
MEA	Membrane Electrode Assembly
MSDS	Material Safety Data Sheets
MV	Machine Vision
PEMFC	Polymer Electrolyte Membrane Fuel Cell
PFA	Perfluoroalkoxy Alkane
PLC	Programmable Logic Controller
RAPS	Remote-Area Power Supply
RMFC	Reformed Methanol Fuel Cell
UAV	Unmanned Aerial Vehicle

CHAPTER 1. INTRODUCTION

1.1 Hydrogen Fuel Cells

Fuel cells (FC) use hydrogen and oxygen gas to generate electricity. A fuel cell (FC) is an electrochemical energy converter (EEC) that converts the chemical energy of a fuel directly (without passing through other forms of energy such as thermal or mechanical energy) into DC electricity. Unlike other EECs such as batteries and accumulators which use solid reactants (metals and metal oxides) incorporated into the units, FCs operate as long as they are supplied with a fuel (hydrogen or hydrogen-rich fluid) and an oxidant (oxygen or air). Fuel cells can operate extended times without requiring periodic replacement or recharging. FCs suffer from many challenges currently. The most debilitating challenge of fuel cells is the high cost to purchase and manufacture.

1.2 Need for Automated Fuel Cell Assembly

Due to their fast start-up time, low sensitivity to orientation, and favorable gravimetric power, PEMFCs are particularly suitable for use as prime power for fuel cell vehicles (FCVs), unmanned underwater vehicles (UUVs) and unmanned aerial vehicles (UUVs). As a consequence of the high interest in FCVs and hydrogen, the investment in PEMFC over the past decade easily surpasses all other types of fuel cells combined. PEMFC demand is rising as indicated in Figure 1.1 (Grand View Research 2016). Stationary fuel cell power plants are expected to emerge as the largest application segment and are expected to account for over 70% of the total shipments. Factors such as the flexibility to use different fuels, high efficiency and utilization of direct current are the key factors expected to propel stationary power plant demand (Grand View Research 2016).

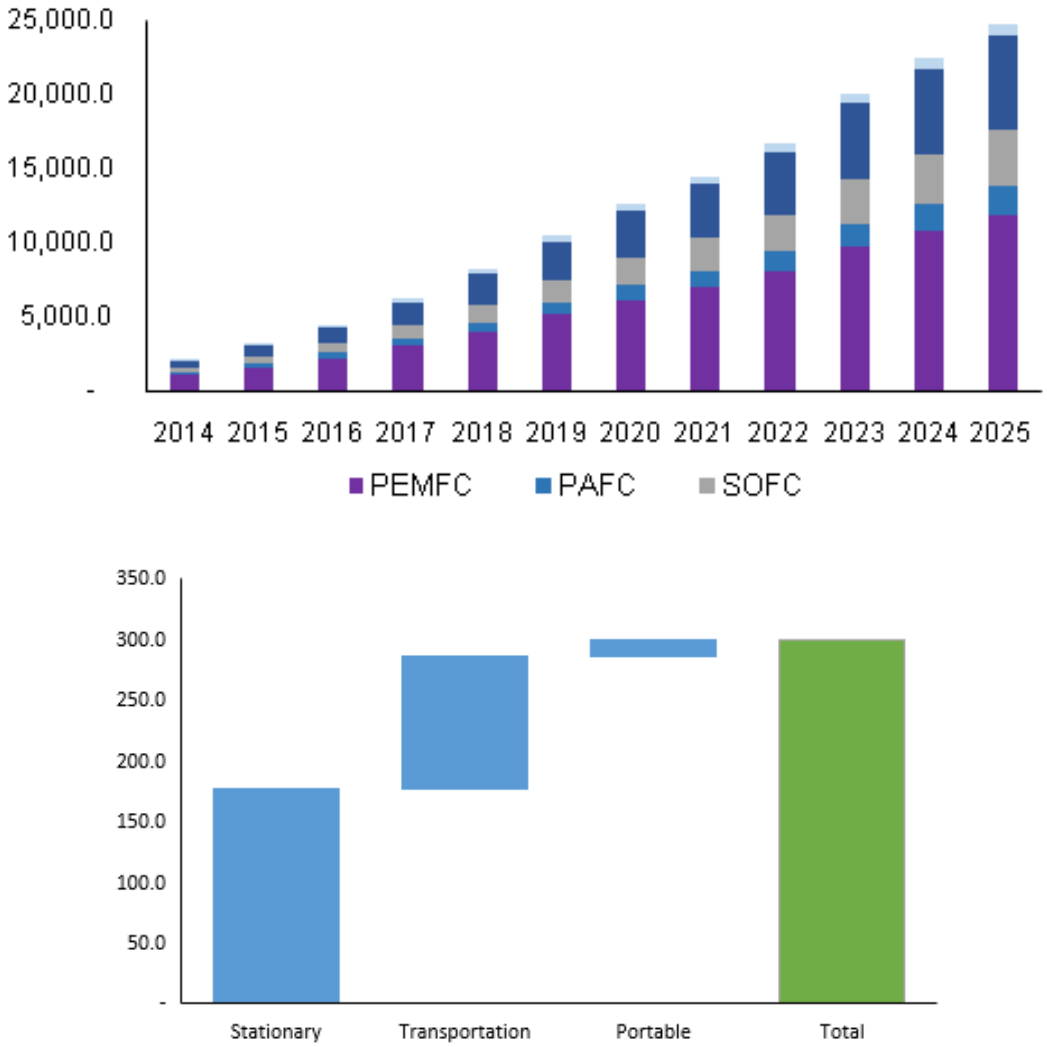

Figure 1.1 - Global fuel cell market revenue by product, 2014 - 2025 (USD Million) (top) and global fuel cell market capacity by application, 2015 (MW) (bottom) (Grand View Research 2016).

The fuel cell stack and its components are currently being manufactured using mostly laboratory fabrication methods that have been scaled up in size, but do not incorporate high-volume manufacturing methods. Manufacturing research and development is needed to prepare advanced manufacturing and assembly technologies that are necessary for low-cost, high volume fuel cell powerplant production. U.S. Department of Energy (DOE) has identified high-priority manufacturing research and development needs for PEMFCs. They include efforts to develop

technologies for high-speed manufacturing of fuel cell components; to develop automated processes for assembling fuel cell stacks; to develop agile, flexible manufacturing and assembly processes; and to establish flexible automated manufacturing technology facilities.

Compared to other types of fuel cells, the PEMFC offers the advantages of delivering higher gravimetric and volumetric power density and for operating at lower temperatures, which result in a quick start up time and less wear on systems components. For these reasons, PEMFCs find today extensive applications in transportation and stationary uses. When compared to other types of fuel cells, PEMFCs dominated the market in recent years in both number of units and in total power shipped, accounting for over 65% of global shipments in 2015. PEMFCs generated a revenue over USD 2 billion in 2015 (Global Markets Insight, 2016) and are expected to generate USD 12 billion in 2025 (Grand View Research, 2016)

1.3 Problem Statement

Gaskets are used in the construction of hydrogen fuel cells (Fig 1.2). The function of the gaskets is to prevent the leaking of fuel cell gasses. Gaskets can be made from a variety of materials but are commonly made of thin poly(tetra)fluoroethylene or rubber sheet (EPDM).

Fuel cell components are inserted in presenters before the robotic assembly process starts, all in the same orientation. In most cases fuel cell components are asymmetric, possessing a total alpha-plus-beta symmetry angle of 720° according to Boothroyd's et al. classification system for manual insertion and fastening processes. This means that the angles through which the components need to be rotated to repeat their orientation is 360° around the axis of insertion, and 360° around an axis perpendicular to the former. Before their insertion in presenters for the subsequent robotic assembly process, components need to be picked from bins where they have a random orientation. Their orientation must be examined relative to two axes of rotation

simultaneously. If necessary, they must be first flipped to bring them with the correct side facing the presenter. This is equivalent to an 180° rotation about axis 1. If necessary, they must then be also rotated in-plane, about axis 2 to bring them in the correct insertion position (Figure 1.2)

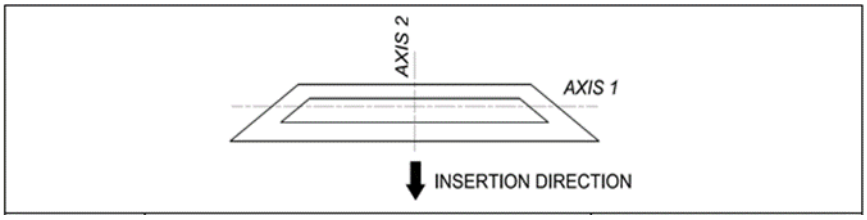

Figure 1.2 - Gasket axis orientation

In particular, fuel cell gaskets are typically only slightly asymmetric, making their orientation examination difficult. PEMFC gaskets are also flexible, flat, thin parts which also makes their manipulation challenging. For example, the gaskets of a PEMFC in the range of a few kW may have the planar area between one hundred to a few hundred cm^2 while their thickness is at submillimeter-scale. This characteristic may lead to a time-consuming sorting and manipulation process. The combined effect of the gasket dimensional characteristic with that of the marginal asymmetry and with the high total alpha-plus-beta symmetry angle makes the gaskets transferring process from their fabrication workcell to the robotic assembly workcell a repetitive work cycle that can cause mental strain and fatigue to human operators. A manual sorting and transferring process of gaskets or other fuel cell components from their manufacturing cell to the assembly line may ultimately defeat the advantages brought by the automated manufacturing processes of fuel cell components and by the robotic assembly process.

The objective of this work is to demonstrate a robotic process of transferring fuel cell components from their fabrication workcell to a robotic fuel cell assembly workcell. This gasket transferring process includes component pickup from a bin where they have a random orientation, handling, orientation examination, reorientation and insertion in the presenter for a

subsequent robotic assembly process. The demonstrated process uses a dual arm robot with integrated machine vision system. This robotic process enables the integration of automated manufacturing processes of fuel cell components with a robotic fuel cell stack assembly process into a fully automated fuel cell manufacturing line. The process was demonstrated with fuel cell gaskets due to increased complexity challenges these components present, but it can be readily used for other fuel cell components such as MEAs and bipolar plates. The process was demonstrated at Georgia Southern University as part of a larger endeavor of bringing advanced manufacturing technologies for alternative energy systems to readiness, and responds the high priority needs identified by the U.S. Department of Energy for fuel cells manufacturing research and development. Grasping these materials by robots can be done by using suction cups to allow for uniform gripping. The use of robotics also allows for better precision.

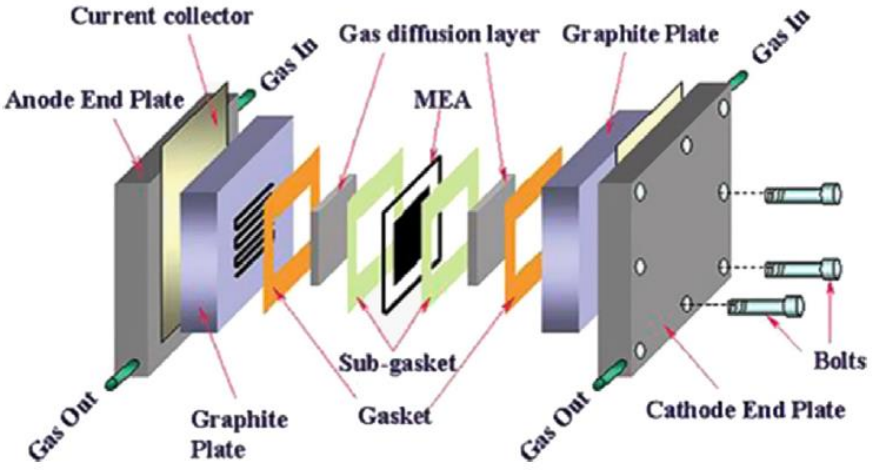

Figure 1.3 Single PEMFC stack (Sharaf and Orhan 2014, 844)

1.4 Hypothesis

If hydrogen fuel cell gaskets are handled with a vision system integrated dual arm robot as compared to using a human, then errors will decrease even if cycle times increase.

1.5 Experimental Limitations

The scope of this work is to demonstrate the feasibility of a manufacturing process aimed to enable the integration of automated manufacturing processes of fuel cell components with the robotic assembly of fuel cell stacks in a single automation line. The gaskets were aligned to a corner before sortation was performed. This allowed the gaskets to be evenly picked up before being scanned (Chapter 3). The robot cycle times were also not completely optimized in terms of robot speed due to potential safety hazards. Ten cleaned gaskets were used during the experiment due to cost limitations.

CHAPTER 2. LITERATURE REVIEW

2.1 Proton Exchange Membrane Fuel Cells

2.1.1 Overview and Advantages

A proton exchange membrane fuel cell (PEMFC) is a modular one-step energy conversion device. A PEMFC converts chemical energy directly to electrical energy. This device is compared to a multi-step energy conversion device such as a combustion engine where energy is converted from chemical to thermal to mechanical to electric. Hydrogen is used as fuel to power fuel cells. Hydrogen fuel cell devices have many advantages over combustion-based energy conversion devices. Some advantages include reduced noise, no pollution during the operation of hydrogen fuel cells, and the capability to obtain hydrogen from renewable sources instead of the depleting fossil fuels used by combustion-based energy conversion devices. (Sharaf and Orhan 2014, 811) These advantages can be viewed in Figure 2.1

Principal of Operation	Features
Electrochemical Energy Conversion	✓ High and Consistent Efficiency ✓ Reduced/Eliminated Harmful Emissions ✓ High Energy Density ✓ Prompt Load-Following ✓ Reduced/Eliminated Noise
Fewer Energy Transformations	✓ High and Consistent Efficiency ✓ Reduced/Eliminated Harmful Emissions ✓ Prompt Load-Following
Runs as Long as Fuel is Supplied	✓ Long Operational Cycles ✓ High Energy Density
Expansion by Adding Cells to a Stack and/or Stacks to a System	✓ Modularity ✓ High Integrability with Renewable Sources
Runs Best on Pure Hydrogen	✓ Reduced/Eliminated Harmful Emissions ✓ High Integrability with Renewable Sources
Static Operation with No Dynamic Parts	✓ Modularity ✓ Reduced/Eliminated Noise
Fuel Reformation Fueling Option	✓ Reduced/Eliminated Harmful Emissions ✓ Long Operational Cycles ✓ Fuel Flexibility
Direct Alcohol Fueling Option	✓ Long Operational Cycles ✓ Prompt Load-Following ✓ Fuel Flexibility

Feature	Application Areas
High and Consistent Efficiency	✓ Propulsion Systems ✓ Light Traction Vehicles ✓ Auxiliary Power Units ✓ Distributed Generation
Reduced/Eliminated Harmful Emissions	✓ Propulsion Systems ✓ Light Traction Vehicles ✓ Auxiliary Power Units ✓ Distributed Generation
Long Operational Cycles	✓ Portable Applications ✓ Propulsion Systems ✓ Light Traction Vehicles ✓ Emergency Back-Up
High Energy Density	✓ Portable Applications ✓ Propulsion Systems ✓ Light Traction Vehicles ✓ Emergency Back-Up
Prompt Load-Following	✓ Propulsion Systems ✓ Light Traction Vehicles ✓ Auxiliary Power Units ✓ Distributed Generation
Modularity	✓ Portable Applications ✓ Auxiliary Power Units ✓ Distributed Generation
Reduced/Eliminated Noise	✓ Propulsion Systems ✓ Light Traction Vehicles ✓ Auxiliary Power Units ✓ Distributed Generation
Fuel Flexibility	✓ Portable Applications ✓ Distributed Generation ✓ Emergency Back-Up
High Integrability with Renewable Sources	✓ Propulsion Systems ✓ Distributed Generation

Figure 2.1 - Principals, features, and applications of PEMFCs (Sharaf and Orhan 2014, 812)

2.1.2 History

The development of the first fuel cell started in the 1800's with Sir William Grove, known as the "father of fuel cell science." "Sir William Grove used his background of electrolysis to conceptualize a reverse process that could be used to generate electricity. Based on this hypothesis, Grove succeeded in building a device that combines hydrogen and oxygen to produce electricity (instead of separating them using electricity). The device, originally labeled a gas battery, came to be known as a fuel cell." (Sharaf and Orhan 2014, 812). The first fully functioning fuel cell was developed in 1959 by Francis Thomas Bacon, which was later licensed and implemented by NASA on the Gemini and Apollo missions (Sharaf and Orhan 2014, 812). Table 2.1.1 is a brief overview of the history and milestones of fuel cells.

Table 2.1 - Milestones in fuel cell history (Sharaf and Orhan 2014, 812)

Year(s)	Milestone
1839	W.R. Grove and C.F. Schönbein separately demonstrate the principals of a hydrogen fuel cell
1889	L. Mond and C. Langer develop porous electrodes, identify carbon monoxide poisoning, and generate hydrogen from coal
1893	F.W. Ostwald describes the functions of different components and explains the fundamental electrochemistry of fuel cells
1896	W.W. Jacques builds the first fuel cell with a practical application
1933-1959	F.T. Bacon develops AFC technology
1937-1939	E. Baur and H. Preis develop SOFC technology
1950	Teflon is used with platinum/acid and carbon/alkaline fuel cells
1955-1958	T. Grubb and L. Niedrach develop PEMFC technology at General Electric

1958-1961	G.H.J. Broers and J.A.A. Ketelaar develop MCFC technology
1960	NASA uses AFC technology based on Bacon's work in its Apollo space program
1961	G.V. Elmore and H.A. Tanner experiment with and develop PAFC technology
1962-1966	The PEMFC developed by General Electric is used in NASA's Gemini space program
1968	DuPont introduces Nafion®
1992	Jet Propulsion Laboratory develops DMFC technology
1990s	Worldwide extensive research on all fuel cell types with a focus on PEMFCs
2000s	Early commercialization of fuel cells

2.1.3 Design

Hydrogen fuel cells are constructed with three main components: a fuel electrode as the anode, an oxidant electrode as the cathode, and an electrolyte inserted between the anode and cathode. The electrode material is porous and covered in a layer of catalyst, which is usually platinum.

Hydrogen gas is pumped into the anode catalyst, which electrochemically separates the gas into hydrogen ions and electrons. This process is represented by Equation 2.1.1

$$H_2 \rightarrow 2H^+ + 2e^- \qquad \text{Equation 2.1.1}$$

After the gas has been separated, the hydrogen ions are drawn through the electrolyte and the electrons are drawn through an external circuit that connects to the cathode. Oxygen gas is pumped into the cathode. The hydrogen ions, oxygen gas, and electrons from the external circuit all combine at the cathode to form water and heat. Equation 2.1.2 represents this process.

$$\frac{1}{2}O_2 + 2H^+ + 2e^- \rightarrow H_2O \qquad \text{Equation 2.1.2}$$

The governing reaction of the entire process is represented by Equation 2.1.3. The combination of hydrogen and oxygen gas produces water, heat, and usable electricity

$$H_2 + \frac{1}{2}O_2 \rightarrow H_2O + W_{ele} + Q_{heat} \qquad \text{Equation 2.1.3}$$

2.1.4 Applications and Market Evaluation

Applications of FC's can be classified as portable, stationary, or transportation based. Fuel cells hold promising potential to become competitive players in a number of markets due to their broad range of applications. And as a result of their high modularity, wide power range, and variation of properties among different types, fuel cells have applications ranging from scooters to large cogeneration power plants as fuel cells can theoretically be used for any energy-demanding application (Sharaf and Orhan 2014, 824).

2.1.4.1 Portable Applications

The two most common portable applications in market focus are portable power generators for personal, emergency, or disaster relief, and portable consumer electronic devices. (Sharaf and Orhan 2014, 824-825) The modularity and high energy density of fuel cells (5–10 times higher energy density than a typical rechargeable battery) make them strong potential candidates for future portable personal electronics. Moreover, portable military equipment is another growing application for portable direct methanol fuel cells (DMFCs), reformed methanol fuel cells (RMFCs), and PEMFCs due to their silent operation, high power and energy density, and low weight compared to current battery- based portable equipment. In addition to lower weight and higher energy density, the fact that fuel cells do not require recharging from an electricity source makes them more favorable in comparison to batteries in the future portables

market. However, their cost and durability are yet to meet set targets (Sharaf and Orhan 2014, 824-825).

2.1.4.2 Stationary Applications

The three most common stationary applications are emergency power supplies (EPS), remote-area power supplies (RAPS), and distributed power or combined heating and power (CHP) generation (Sharaf and Orhan 2014, 825-827).

EPS systems are becoming more commonly used due to the ability to withstand harsh environments, higher energy and power densities, longer operation times, compact size, and modularity (Sharaf and Orhan 2014, 825-827).

The ability to use renewable resources, excellent load-following and high efficiency contributes to the usefulness of PEMFCs for RAPS.

Decentralizing power generation with PEMFCs is also a possibility for near-future implementation. Due to their static nature, lower emissions, excellent load-following, and high efficiency; fuel cells could be used for residential electric power or CHP distributed generation either on a household basis or a larger residential blocks basis. In fact, it is estimated that by 2020, fuel cells could penetrate 50% of the world distributed generation market if cost and durability targets are met (Sharaf and Orhan 2014, 825-827).

2.1.4.3 Transportation Applications

Transportation applications can be categorized into auxiliary power units (APUs), light traction vehicles (LTVs), light-duty fuel cell electric vehicles (L-FCEVs), heavy-duty fuel cell vehicles (H-FCEVs), aerial propulsion, and marine propulsion. (Sharaf and Orhan 2014, 828-838)

APUs can be compared to car batteries in transportation applications. APUs power non-propulsion or secondary systems in a vehicle. (Sharaf and Orhan 2014, 828)

Vehicles such as forklifts, motorcycles, scooters, wheel-chairs, and golf carts fall into the category of LTVs. (Sharaf and Orhan 2014, 828) “Forklifts have been the most successful demonstration of fuel cells in the transportation sector, and one of the most successful demonstrations for fuel cells overall. Forklifts and other material handling vehicles and equipment are exhaustively used in the warehousing and distribution industry, with nearly 2.5 million forklifts in operation in North America.” (Sharaf and Orhan 2014, 828). The success of fuel cell implementation in fork lifts are due to being able to run indoors or in non-ventilated areas, less harmful emissions, high efficiencies, excellent load-following, low maintenance, fast recharge times, longer operation times than conventional batteries, and do not degrade with each recharge as compared to conventional batteries. (Sharaf and Orhan 2014, 828-829).

L-FCEVs and H-FCEVs both utilize fuel cells as the source of electricity to power the primary propulsion system. L-FCEVs primarily include passenger cars, while H-FCEVs include industrial vehicles such as buses, utility-trucks, and other heavy vehicles. (Sharaf and Orhan 2014, 829-832). Figure 2.2 represents a concept design of a modified 2005 Honda FCX L-FCEV (Sharaf and Orhan 2014, 830).

Aerial propulsion is an application of fuel cells that includes space and aviation. Unmanned aerial vehicles (UAVs) are the primary focus of aerial propulsion applications due to the low heat dissipation and static operation for reconnaissance, and higher energy density than conventional batteries allowing for longer flight times (Sharaf and Orhan 2014, 832-833).

Marine applications are largely APU based, with future implications being used in submarines and boats. The issue with fuel cells used for marine application is primarily the durability and corrosion to salt water (Sharaf and Orhan 2014, 833-838).

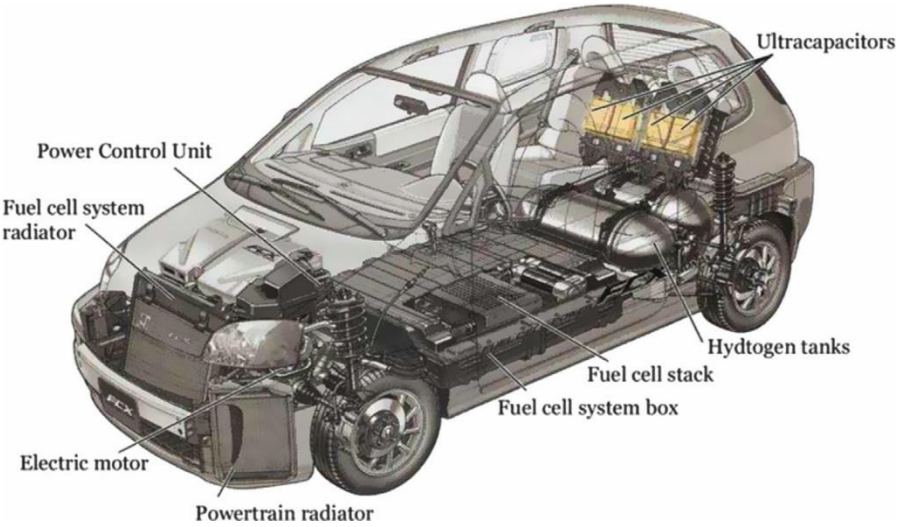

Figure 2.2 - L-FCEV concept design based on Honda 2005 FCX (Sharaf and Orhan 2014, 830)

2.1.5 Technological Challenges

Challenges of fuel cells include high costs, low durability, hydrogen production, flooding and water balance of the cell, parasitic load of auxiliary plant balancing devices, and the lack of standard and internationally accepted codes.

The cost of fuel cells is the primary challenge of their societal implementation. “Experts estimate that the cost-per-kW generated using fuel cells has to drop by a factor of 10 for fuel cells to enter the energy market. Three main reasons behind the current high cost of fuel cell stacks are: the dependence on platinum-based catalysts, delicate membrane fabrication techniques, and the coating and plate material of bipolar plates.” (Sharaf and Orhan 2014, 822-823).

Fuel cell durability is also a fundamental problem, especially for RAPs, marine applications, and other long-term usage applications. Fuel cell durability is also a large factor in

the cost of purchasing fuel cells. The production of hydrogen via steam reformation is also a technological challenge with hydrogen fuel cells. One of the benefits of hydrogen fuel cells is the ability to operate with heavily mitigated pollutant production. With steam reformation, fossil fuels are used to produce hydrogen, which produces pollution and defeats a primary benefit of the HFC (Sharaf and Orhan 2014, 823).

2.2 Dual Arm Robotics

Dual arm manipulation or cooperative manipulation is a broad term for two separate manipulators cooperating to accomplish tasks. There is ambiguity in defining dual arm manipulation. “Two dexterous fingers mounted on the same hand may manipulate a small object using the same principles as two separate manipulators that are moving a large object. In fact, many authors do not distinguish between multi-agent or multi- arm systems.” (Smith 2012, 1340-1353). One proposed classification of dual arm robotics is between coordinated and non-coordinated manipulation. Coordinated manipulation is defined by two arms accomplish the same task and non-coordinated manipulation is defined by two arms performing different tasks. Coordinated manipulation is divided into goal-coordinated and bimanual manipulation. Goal coordinated manipulation is defined by both arms accomplishing the same goal such as typing and bimanual manipulation is defined by both arms physically manipulating the same object. (Smith 2012, 1340-1353)

2.2.1 Dual Arm Robotics Applications

2.2.1.1 Machine Tending

One application of dual arm robots is machine tending. Machine tending is the process of servicing industrial machinery using robots such as tool changes in a CNC or placing steel plates into a waterjet. Dual arm robots are useful to machine tending due to flexibility and the ability to

bimanually grasp materials. A paper written by Geismar et al. details the usefulness of using a dual arm robot to tend three machines simultaneously versus other configurations via computer simulation. The use of a dual arm robot allows for much higher throughput of the machine shop as compared to using either three operators or three robots. “Via a computational study, we have quantified the gains realized by using a dual-arm robot under a variety of circumstances in these smaller cells. We have also delineated the parameters under which a dual-arm robot generates higher throughput than a single-arm/dual-gripper robot. For two-machine cells that produce multiple part types, we showed how a special, easily understood and implemented class of dual-arm cycles dominates all single-arm/single-gripper cycles.” (Geismar, et. al 2012)

2.2.1.2 Assembly

Dual arm robots are also commonly used in assembly applications due to their flexibility and wide range of motion. Integrating dual arm robots into manufacturing facilities for the purposes of assembly is very practical due to the ability to replace human workers. Figure 2.4 represents a Yaskawa Motoman SDA10 assembling an office chair. This demonstration shows the flexible tooling of the dual arm robot as it grips a screwdriver and various parts of the assembly. Certain larger parts of the assembly are bimanually grasped to allow for stability of placement. By using both arms, the complexity of the workcell is much more compact than using one robot with special holding tooling. This can reduce the cost of the workcell and allow for better modularity for a changing design. (Yaskawa Europe GmbH. 2012)

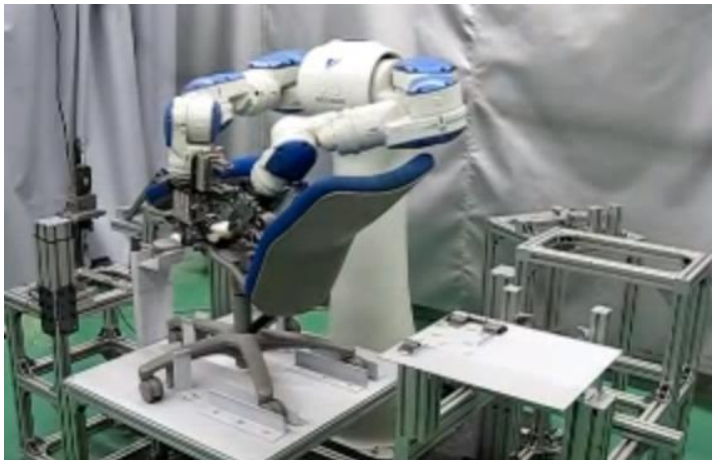

Figure 2.3 - SDA10 automated office chair assembly (Yaskawa Europe GmbH. 2012)

Another example of the efficacy of using dual arm robots for assembly was used by Kim Young -Loul, Hee-Chan Song, and Jae-Bok Song. In this study, a dual arm robot was employed to close the lid of a box without the use of a jig. Two methods were compared; one method relied on the use of friction on the bottom of the box in order for a manipulator to assemble the lid on to the box, and the other relied on the use of a second manipulator to grip the box during the lid assembly. Both methods employed force sensing to accommodate for the slippage and misalignment of the lid with respect to the box. During the friction assembly strategy, the lid on the box is rotated and slid against the top edge of the box to align one edge of the box. This process is repeated for the second edge of the box to ensure alignment. After the lid is positioned, the manipulator pushed the lid down onto the box completing the assembly. During the dual arm assembly strategy, the same method is employed, but the base is kept in place by the second manipulator. The advantage of using the second manipulator is to reduce the use of a jig and not rely on the friction between the box and the surface it is rests on as this can vary depending on applications. (Young-Loul, Hee-Chan Song, and Jae-Bok Song 2013)

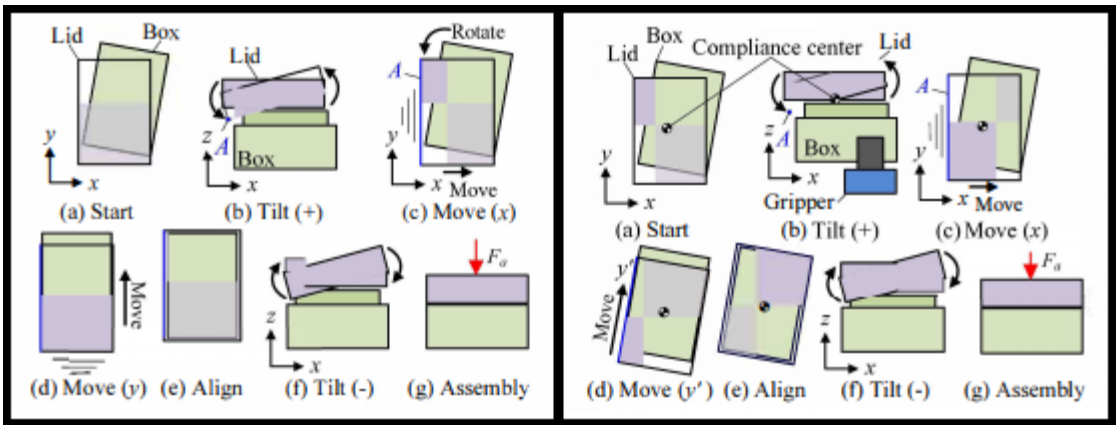

Figure 2.4 - Assembly method for the friction-based assembly strategy (left) and dual-arm assembly strategy (right). (Young-Loul, Hee-Chan Song, and Jae-Bok Song 2013)

2.2.1.3 Sorting

Another application of dual arm robotics is sorting. Sorting is the process of arranging items systematically. The use of dual arm robots allows for a variety of items to be sorted with precision and accuracy. Employing dual arm robots also allows multiple objects to be sorted at once. This allows a complex workcell to be reduced, and allows for repurposing if the product changes at much less cost than by using a fixed system.

In a paper written by Stria et al., a vision sensing dual arm robot was used to sort various garments. The garments were segmented into contours from the camera, and then the dual arm robot executed folding. By segmenting the garment into contours, landmark points were determined, and the folded model was generated. Figure 2.5 represents the garment segmentation and folding operations (Stria et. al. 2019). “It is shown how folded variants of the unfolded model can be derived automatically. Universality and usefulness of the model is demonstrated by its favorable performance within the completely folding procedure, which is applicable to a variety of garments categories (towel, pants, shirt, etc.) and evaluated experimentally using the two-armed robot. The principal novelty with respect to the state of the art is in the new garment

polygonal model and its manipulation planning algorithm which leads to the speed up by two orders of magnitude.” (Stria et. al. 2019)

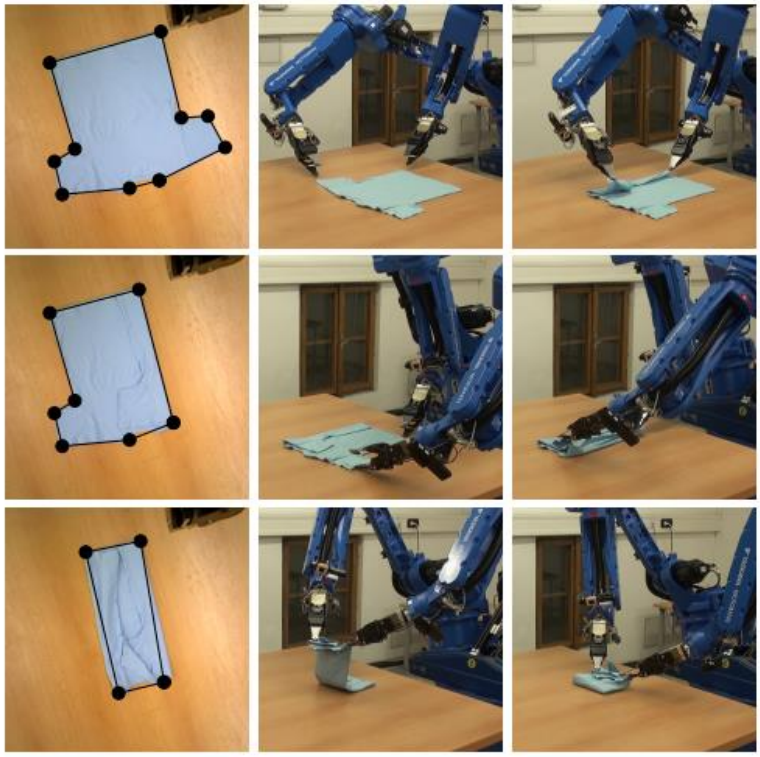

Figure 2.5 - Dual arm robot garment segmentation and folding (Stria et. al. 2019).

2.2.2 Future of

Many aspects will influence the future of dual arm robotics. One proposed future avenue for better incorporation of dual arm robotics is the integration of system theory with tools from cognitive methodologies, specifically the consideration of vision and learning capabilities in feedback design (Smith 2012, 1340-1353). The applications of allowing the robot to adjust according to global knowledge of the environment allows for advanced control. This control can allow for higher levels of collaboration between the manipulators of the robot and humans. (Smith 2012, 1340-1353)

Utilization of machine learning would allow for complex interaction between multiple robots and humans. Tasks that are more complex can be completed by utilizing higher level of coordination. This tier of coordination would involve both robots and humans taking on roles of leadership of followership and would require careful planning and safety measures. “Current state of the art typically employs different types of compliance, such as admittance or impedance control approaches, putting the human in complete control. However, for robots to truly replace parts of the human work-force, we will need systems that can participate actively, as leaders as well as followers in collaborative tasks.” (Smith 2012, 1340-1353).

2.2.3 Computer Vision Systems in Robotics

Machine Vision (MV) is the process of using imaging devices such as cameras or radars to transmit visual data such as pictures of videos to a computer to gain a better understanding of the images, videos, or live streams. The applications of MV include manufacturing, biometry, security, and more. To gain a better understanding of the image, it must first be segmented in a process known as image segmentation. “Image segmentation divides an input image into regions matching separate objects, visible in the image by finding in the image analyzed cohesive regions which are characterized by similar values of some attribute (e.g. lightness) or a set of features (e.g. texture). In this way, objects of interests are extracted for further processing such as description or recognition. The result of image segmentation should allow one to define the geometric features of objects placed in a scene as accurately as possible with the minimum computational complexity.” (Nowakowski and Sankowski 2014, Ch. 2.1). Methods of image segmentation include pixel, edge, region, model, and graph-based methods (Figure 2.6).

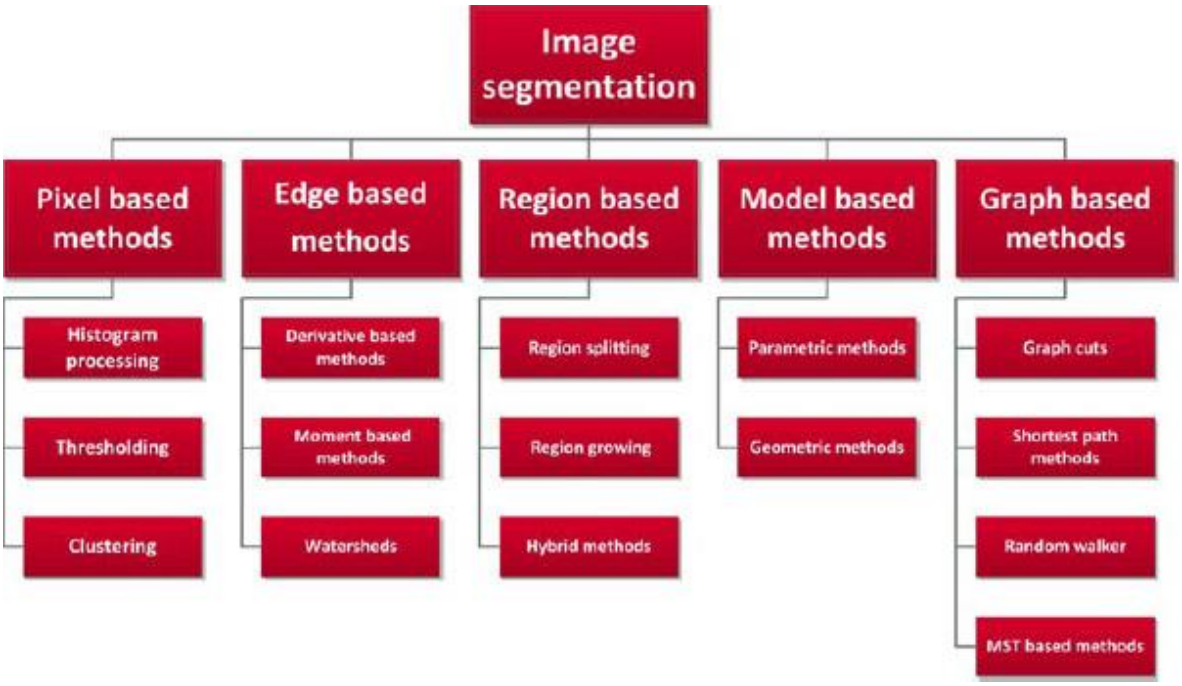

Figure 2.6 – Examples of image segmentation methods (Nowakowski and Sankowski 2014, Ch. 2.1).

2.3 Examples of Automated Hydrogen Fuel Cell Construction

2.3.1 End Effector Designs

The design of end effectors for assembly of PEMFC construction initially used finger grippers for grasping of the bipolar plates and pneumatic grippers for grasping of MEAs and gaskets. The use of finger grippers required submillimeter accuracy and incorporated feeders and vision systems. Later designs of end effectors allowed for more flexibility and cost reduction. These designs incorporated vacuum cups and suspension mechanisms, which reduce the need for vision systems. Later designs of end effectors also utilize passively compliant mechanisms, which allow for flexibility that is not present in most robots and assist in placement (Gurau, Vladimir, Devin Fowler and Daniel Cox. 2017).

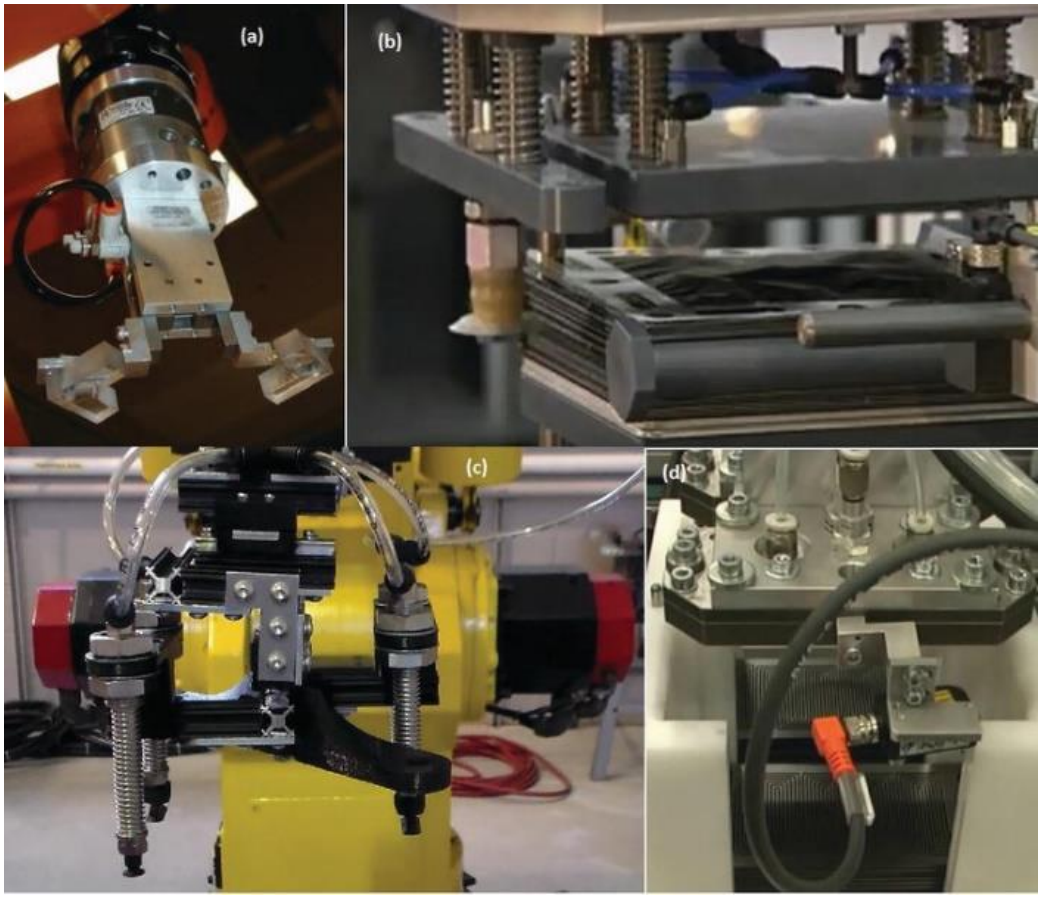

Figure 2.7 – “End-effectors used for PEMFC components manipulation: (a) double-acting finger gripper; reproduced with permission from [9]; (b) pneumatic end-effector with suspension mechanism; reproduced from [14]; (c) end-effector with vacuum cups and suspension mechanism used in [7]; (d) pneumatic end-effector; reproduced from [16].” (Gurau, Vladimir, Devin Fowler and Daniel Cox. 2017)

2.3.2 Workcell Designs

Workcells for PEMFC stack assembly have been successfully demonstrated using fixed automation lines, multiple robots, and single robots. Two assembly strategies are used for automated assembly. The first strategy assembles and tests individual cells before adding them to the stack. The second strategy assembles the entire stack at once. The first strategy benefits from additional testing and servicing, but at the cost of more manufacturing operations.

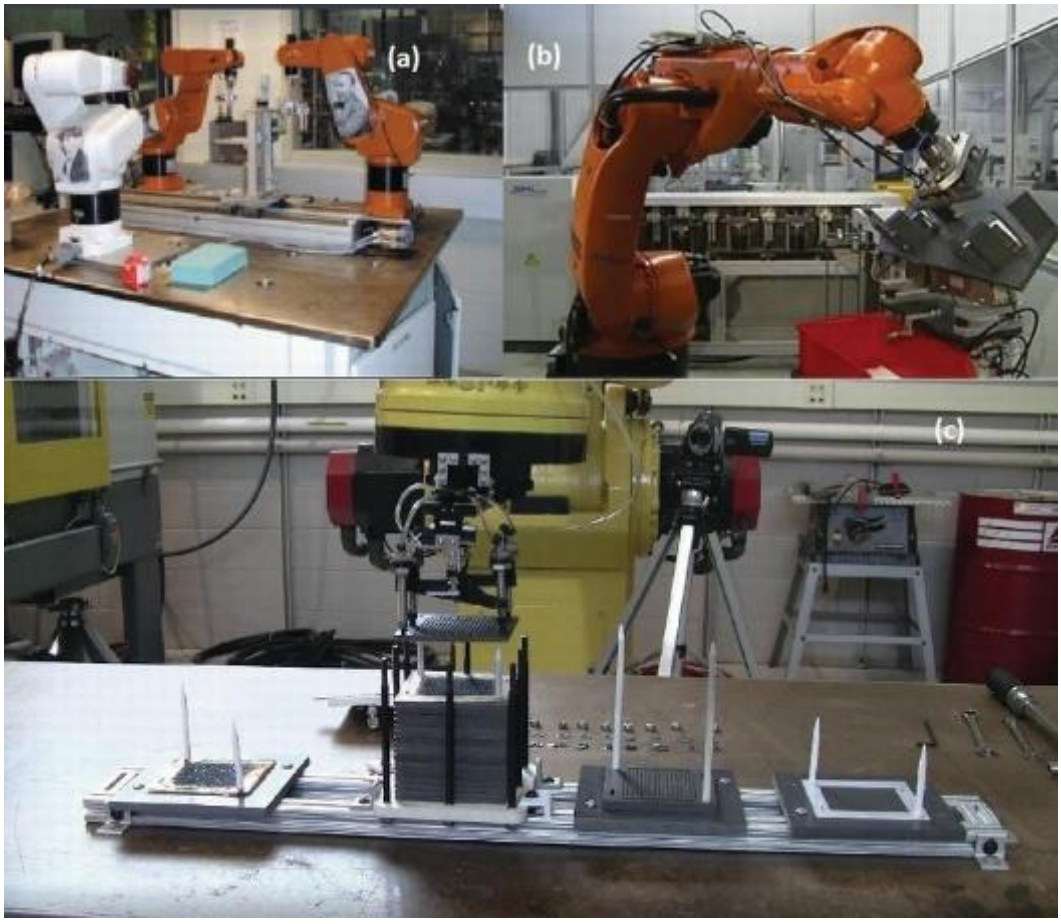

Figure 2.8 “General purpose robot workcells for assembly of PEMFC stacks: (a) workcell consisting of 3 KUKA robots with 6 DOF (degrees of freedom); reproduced with permission from [9]; (b) workcell consisting of a single KUKA robot with 6 DOF; reproduced from [14]” (Gurau, Vladimir, Devin Fowler and Daniel Cox. 2017)

CHAPTER 3. METHODOLOGY

3.1 Equipment and Instrumentation Precision

3.1.1 Yaskawa Motoman - SDA5F Dual Arm Robot

The SDA5F robot used for the experiment has a 5 kg payload per arm with a 1,118 mm vertical reach, 845 mm horizontal reach per arm, and ±0.06 mm repeatability. Each arm has seven axes with a single axis for base rotation. (Appendix C)

3.1.2 COGNEX ISM1403C Camera

The ISM1403C camera used in this experiment had 128MB of image processing memory, measured 8.8mm diagonal with 4.4 x 4.4µm sq. pixels (1600 x 1200 resolution), had an electronic shutter speed of 27µs to 1000ms 7 full frames per second, and had a CCD alignment variability of ±0.127mm from lens C-mount axis to center of imager. (Appendix D)

3.1.3 Selectively Compliant End-Effector

The fabricated end effector utilized linear rails and springs to move in three degrees of freedom. Horizontally in both X and Y (with respect to the end effector pointing towards the base) the system allowed for ±3mm and Vertically (Z-axis) the end effector had a compliance of 50mm. Figure 3.1 represents the end effector and associated reference coordinate system.

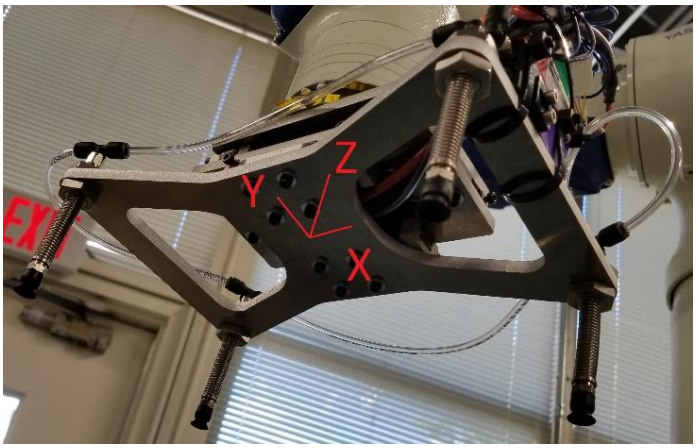

Figure 3.1 – Selectively-Compliant End Effector with reference coordinate system

3.2 Robot Mounting Cart and Staging Tables Design and Fabrication

3.2.1 Robot Mounting Cart Design

The robot mounting cart was the first apparatus designed. This was done at the beginning of the experiment to allow for the robot and controller to be secured before any robot motion was performed as to prevent potential hazard. The cart design began by designing a 4ft by 4ft by 0.25-inch plate with both mounting locations for the SDA5F and a bolt hole pattern for flexible mounting options. The bolt hole pattern was chosen to be 0.5-inch holes spaced 2 inches apart. The mounting holes were moved 2.5 inches from the edge of the top plate to allow the SDA5F to interface with a conveyor and to be near the steel tube frame for rigidity. The height of the cart was determined by finding the height of the FS100 controller and allowing for 0.25-inch clearance. This small clearance was chosen to avoid too much height added to the cart while still being able to fit the controller into the frame and underneath the robot to prevent unplanned collision between the robot and controller and to prevent instability. The 2-inch by 0.25-inch tube that was used for the frame was chosen for maximum strength and rigidity (Figure 3.2)

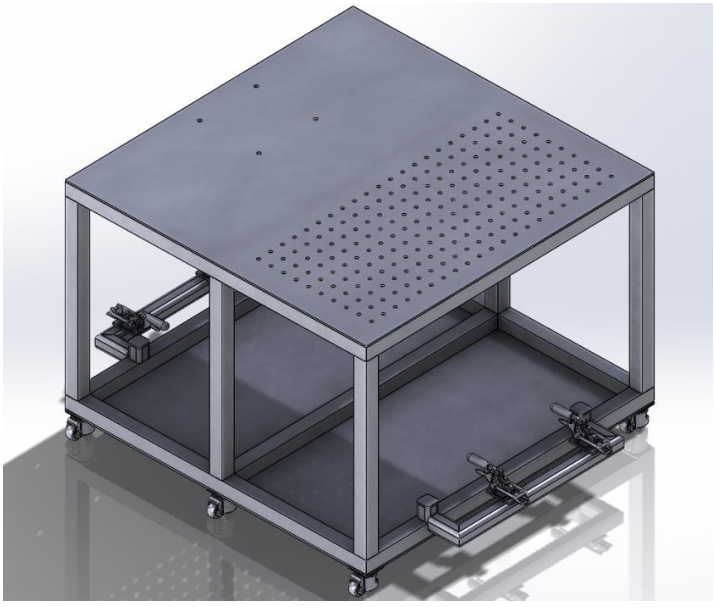

Figure.3.2 – Robot mounting cart design

3.2.1.1 Manufacturing of Robot Mounting Cart

Once the cart was designed, the fabrication process began. The steel tubing was cut to length and welded. The top plate was waterjet to allow for accurate mounting hole locations. Figure 3.3 represents the finished cart with the SDA5F and controller. The controller was placed opposite of the robot to allow for the center of gravity of the system to be closer to the center of the cart to prevent instability.

Figure 3.3 - Robot mounting cart with Yaskawa SDA5F on top and controller housed below

3.2.2 Gasket Staging Table and Alignment Table

The staging and alignment table were designed such that both of the manipulator arms were able to pick up and place gaskets while avoiding singularities and without crashing into each other. This design was performed experimentally by manually moving the manipulators to positions of interest (pick, place, scan, etc.) and recording the positions that worked with minimal articulation or translational difficulty when jogging.

The design of the tables and camera mounts were iterated several times. Initially the camera was positioned such that the gasket was viewed when it was in the staging table. This prevented the ability to see the gaskets when a manipulator was picking. This also caused detection errors due to the transparency of the gasket so a different approach was taken. The new design allowed the manipulators to scan the gasket after picking. Since scanning occured with only the gripper behind the gasket, the semitransparency of the gasket was mitigated, and scanning was found to be more accurate. Figure 3.4 represents the final design of the workcell.

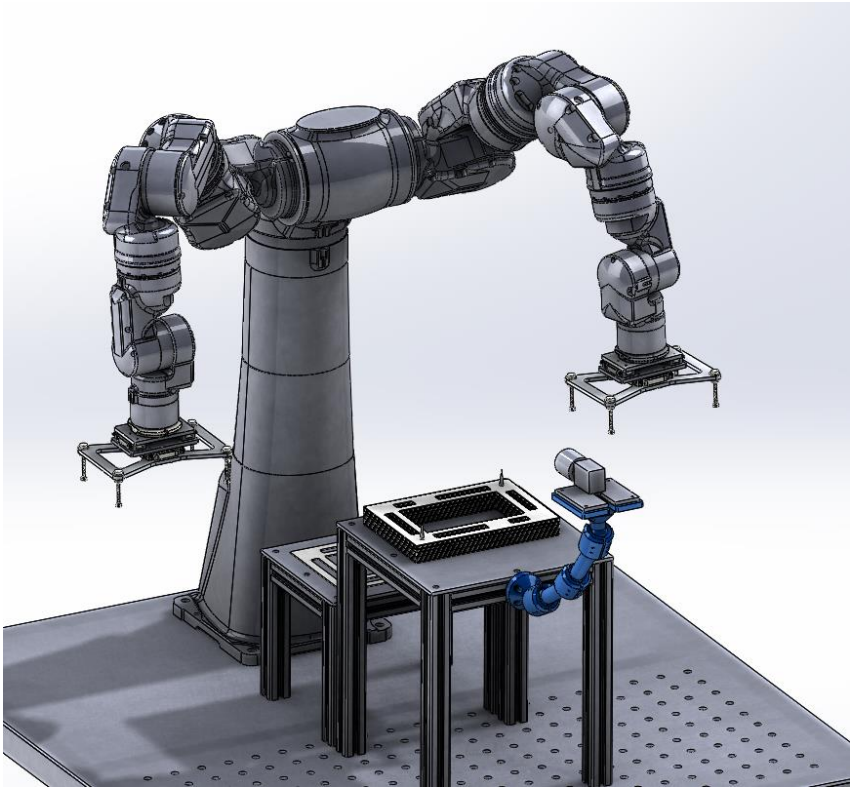

Figure 3.4 - Workcell final design with staging table (center left, smaller), alignment table (center right, taller), and SwivelLink® camera mount.

The staging table and alignment tables were fabricated using 1.5-inch 8020 aluminum extrusion (Figure 3.5). The top of each table was fabricated from waterjet 0.25-inch aluminum plate to accurately place holes for the alignment pins and work holding fixtures. The 8020 aluminum also allowed for the attachment of the camera mount, which was made from

SwivelLink® connectors. The SwivelLink® connectors allowed for ease of camera manipulation in six degrees of freedom.

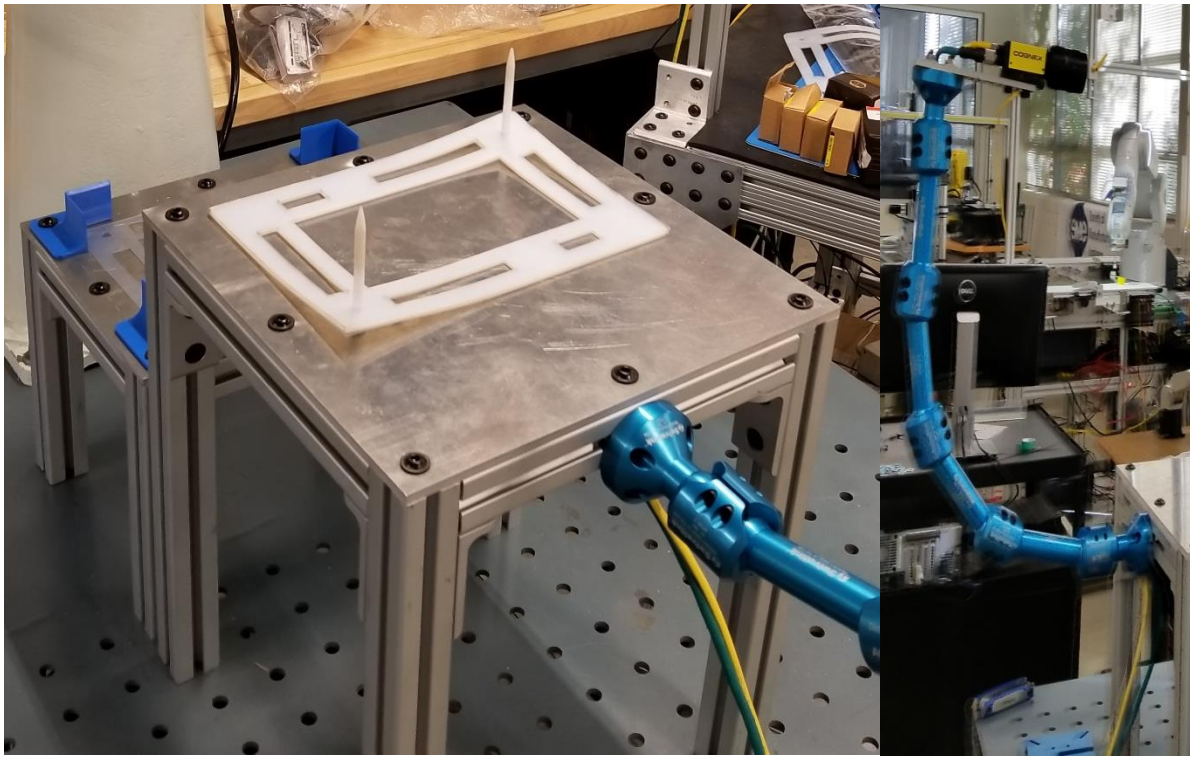

Figure 3.5 – Gasket staging and alignment tables (left) and SwivelLink® camera mount (right). The work holding parts in the top left of the left image are 3D printed using ABS.

3.3 Fuel Cell Gasket Design and Fabrication

The fuel cell gasket was designed by Dr. Gurau. The purpose of a fuel cell gasket is to prevent the hydrogen gas and oxygen from escaping their flow channels. This prevents flow between the cathode and anode. Flat gaskets instead of O-rings or other shapes have been demonstrated to insulate better. The current design has the outside dimensions equal to the dimensions of the bipolar plates, the inside dimensions are those of the gas diffusion layers (GDLs). GDLs are components of the membrane electrode assemblies (MEAs) and their principal role is to distribute the reactant gasses over the active area of the MEAs. The GDLs must be surrounded by the gaskets in the fuel cell assembly without overlap. This is why there

are alignment pins. The other gasket cuts are for the inlet and outlet manifolds of hydrogen, air, coolant fluid, and for alignment pins. The gasket geometry is similar to the MEA and bipolar plate designs.

The gasket thickness must be roughly 80% of the GDL thickness. Its material must withstand the operational temperature of the fuel cell, which in this case is between 120 and 200 degrees Celsius. Teflon does not turn out to be a good material for this since it deforms permanently under compression. Another material candidate is perfluoroalkoxy alkane (PFA) which is recommended by the MEA manufacturer. From previous experiments performed by Vladimir Gurau, the fuel cells leaked when made from PFA. Silicone does not perform well in acidic environments in accordance to the MSDS, but silicone performs well at high temperatures and most importantly, is flexible, which makes it a good sealant. Vladimir Gurau is currently researching the best material to fabricate the gaskets time of writing. 0.35 mm PFA is the material that the gaskets used in this experiment are made from.

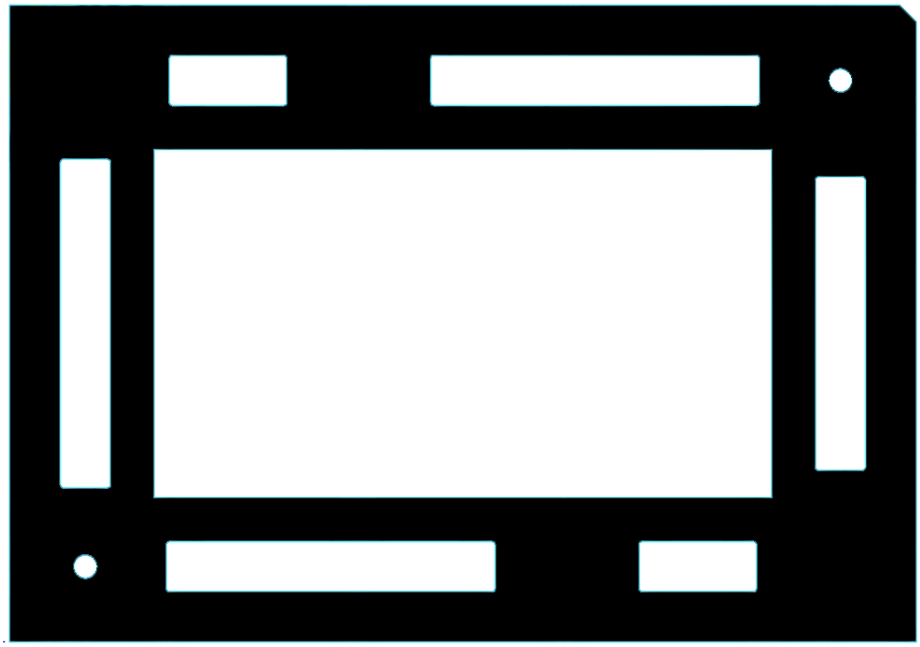

Figure 3.6 - Gasket profile. The top right corner is notched for alignment purposes.

The gaskets were fabricated using a laser cutter to ensure precision (Figure 3.7, left). The mechanism used for catching the gaskets was cedar wood, as using the onboard slats would result in the gasket falling through and inaccurate cutting due to the flexible material.

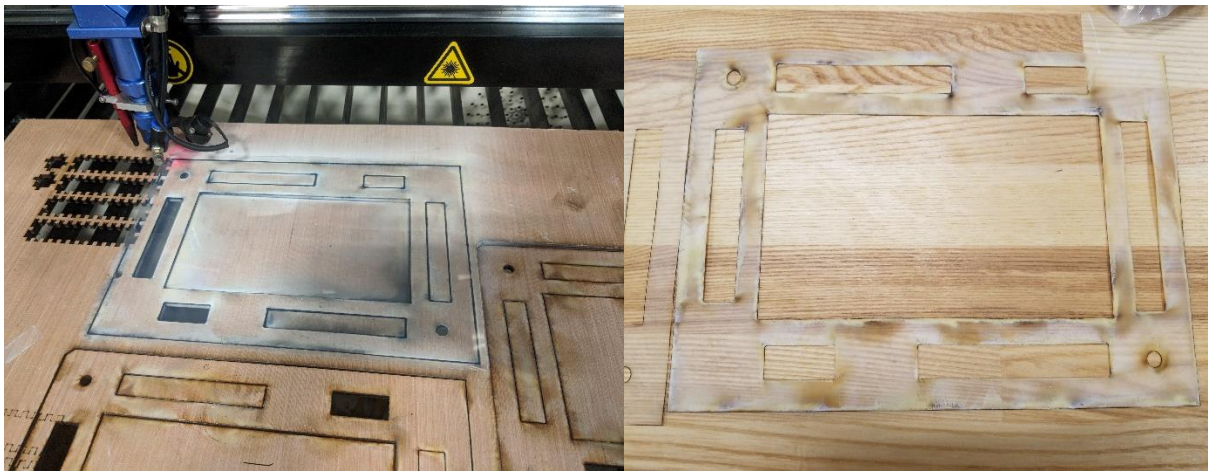

Figure 3.7 – Gaskets in the laser cutter (left) and additional cedar residue (right).

The work holding cedar sheet created an additional problem, as the laser burned through the PFA leaving residue on the gasket edges and faces (Figure 3.7, right). The gaskets were washed with isopropyl alcohol to clean the burned material from the edges and faces. After scrubbing the gaskets most of the residue material was removed (Figure 3.8).

Figure 3.8 - Stack of cleaned and polished gaskets

3.4 End Effector Design and Fabrication

The purpose of the end effector was to grasp the flexible gasket material while also remaining compliant. The compliance of the end effector was to prevent misalignment between the alignment holes in the gasket and the alignment pins during placement.

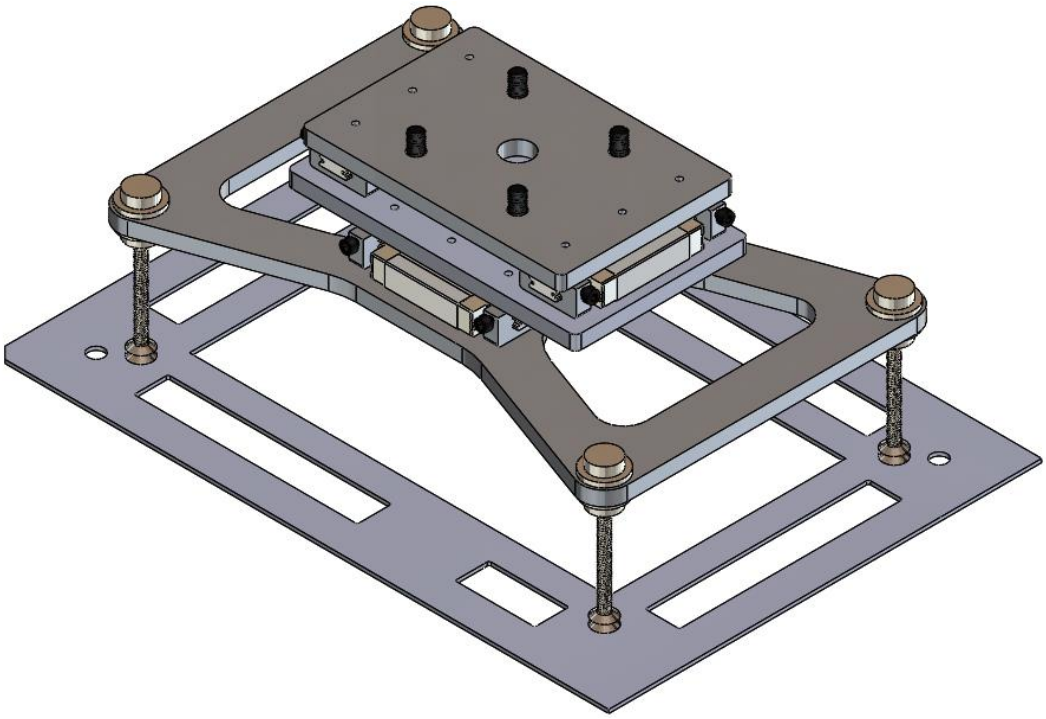

Figure 3.9 - End effector overview

The purpose of the bottom plate (with reference to Figure 3.9) was to hold the level compensators that are attached to the suction cups. The design of the bottom plate was dependent on the geometry of the gasket. Figure 3.10 represents the final bottom plate design with a superimposed picture of the gasket and the placement of the suction cups. The placement of the suction cups was designed such that there would be sufficient suction regardless of the four orientations of the gaskets and sufficient suction regardless of the motion of the end effector. The suction cups also accomplish the task of providing rigidity to the gasket's alignment holes when locating.

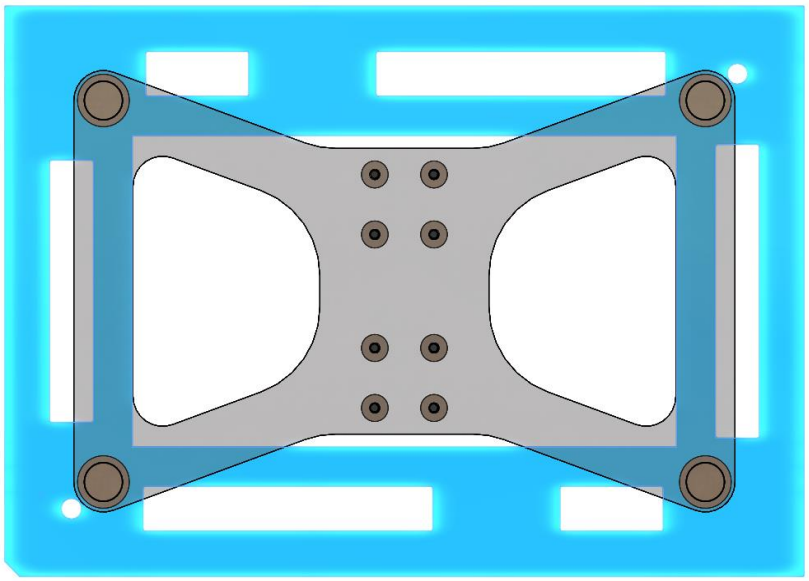

Figure 3.10 - Gasket underneath transparent bottom plate

The purpose of the middle and top plates was to allow for compliance in two degrees of freedom (DOF) when locating the gaskets to the alignment pins. This two DOF compliance was accomplished by using two sets of linear carriages and rails, where the sets were oriented 90 degrees from each other. The design of the top plate was dependent on the “wrist” of the SDA5F. Both the top and middle plates have holes to allow the SDA5F’s air and electrical lines to pass though. Figure 3.11 represents the exploded view of the end effector.

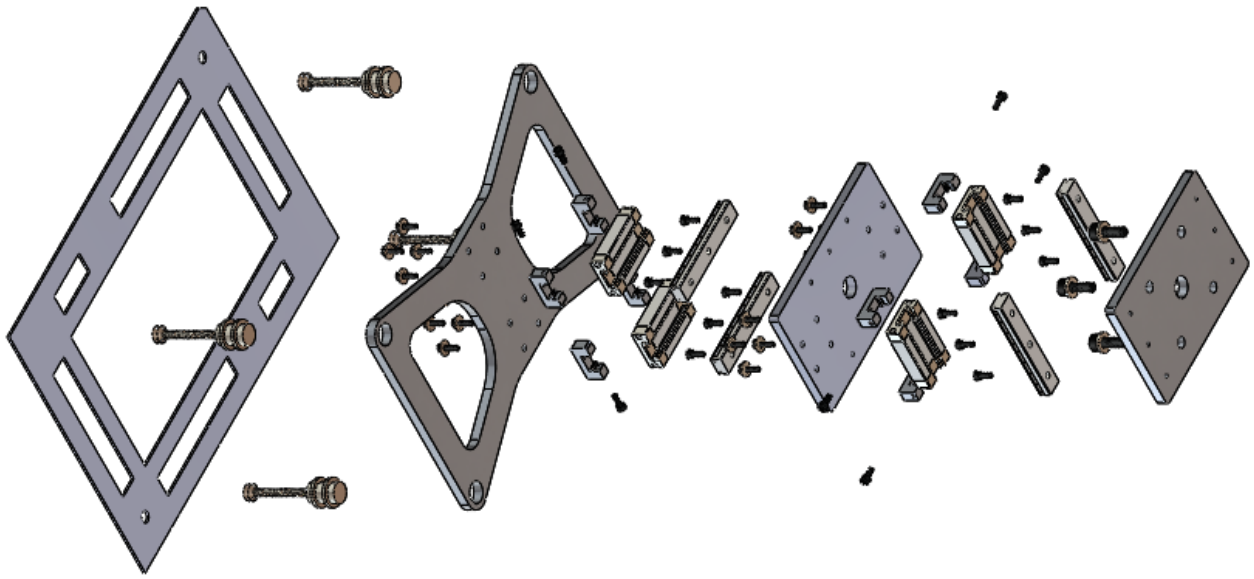

Figure 3.11 - End effector exploded view

The end effector was also symmetric to allow for ease of transfer of a gasket from one manipulator to another. This symmetry also made it much easier to program the transfer process, as both end effectors were aligned such that the suction cups touched each other (Figure 3.12)

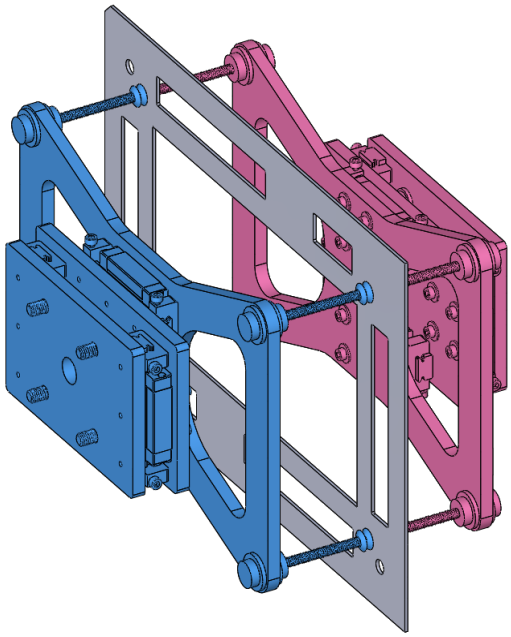

Figure 3.12 - Symmetry of the end effectors

Fabrication of the end effector primarily relied upon OMAX waterjet (Figure 3.13). The plates and rail end stops were first waterjet. The rail end stops were then put into a CNC machine to fabricate the hole for the adjustable screw. Both the plates and end stops were then tapped.

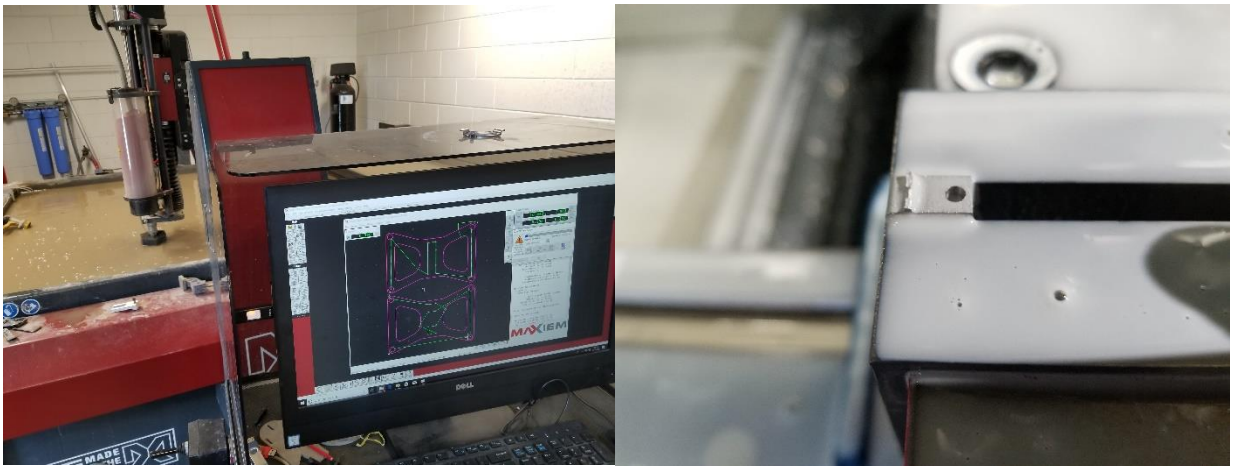

Figure 3.13 - OMAX waterjet fabrication (left) and CNC end stop drilling operation (right)

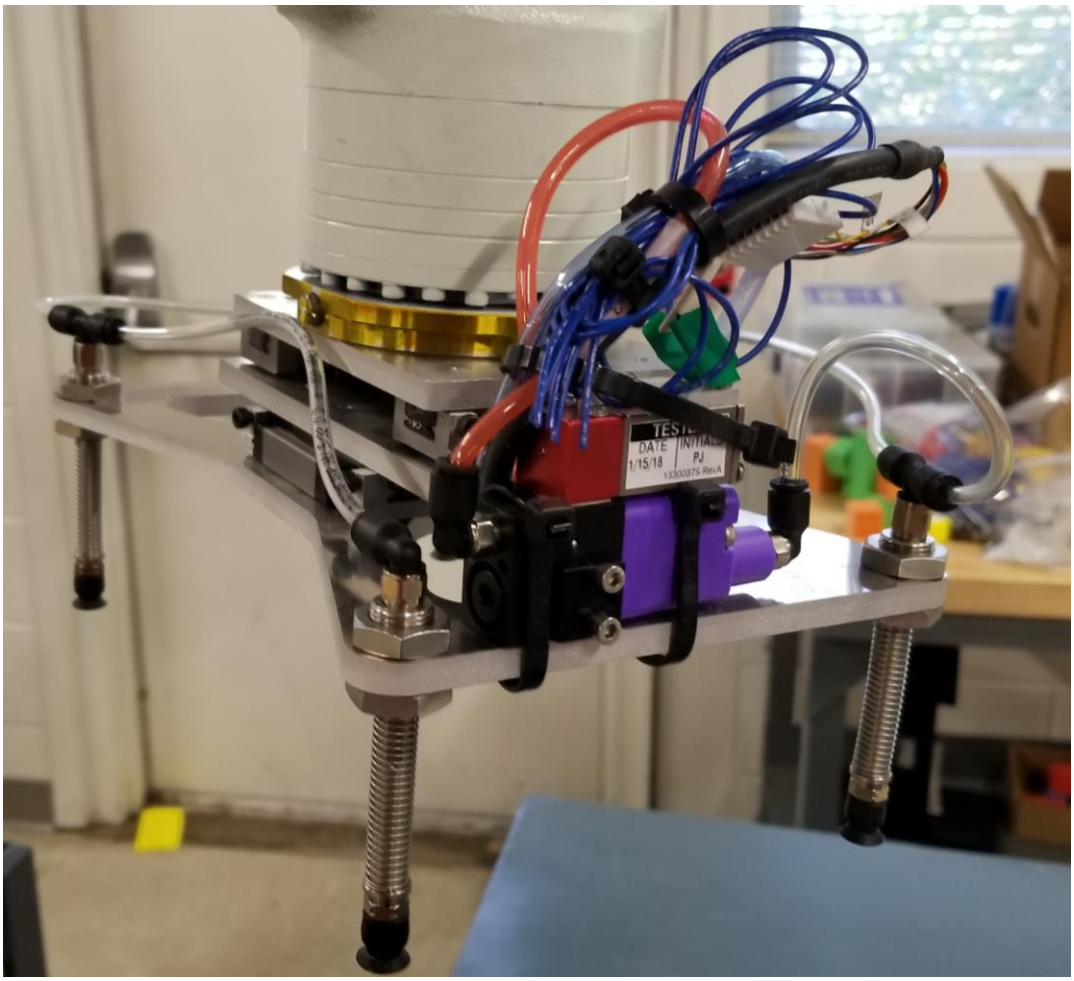

Figure 3.14 - End effector manufactured and assembled

After the plates, rails, and rail end stops were assembled, the end effector was affixed to the robot. Air and electrical lines were routed to the ANVER solenoid vacuum unit and suction cups. Caution was used to prevent the lines from being cut too short so other experiments could be performed later. The unit was tested to ensure proper suction was available and that it responded to the controller. This was determined to be satisfactory and the end effectors were considered completed (Figure 3.14).

3.5 Programming

The program running on the FS100 controller to control the SDA5F robot used the INFORM III programming language. The program running on the In-Sight® CIO-MICRO-CC

I/O controller that received inputs from the ISM1403C camera used the In-Sight® Explorer software. Pseudocode program flowcharts (Figure 3.15 & 3.16) were developed before the programs were written. The flowcharts were used to develop ideas and generate the paths required to accomplish the goals of the experiment.

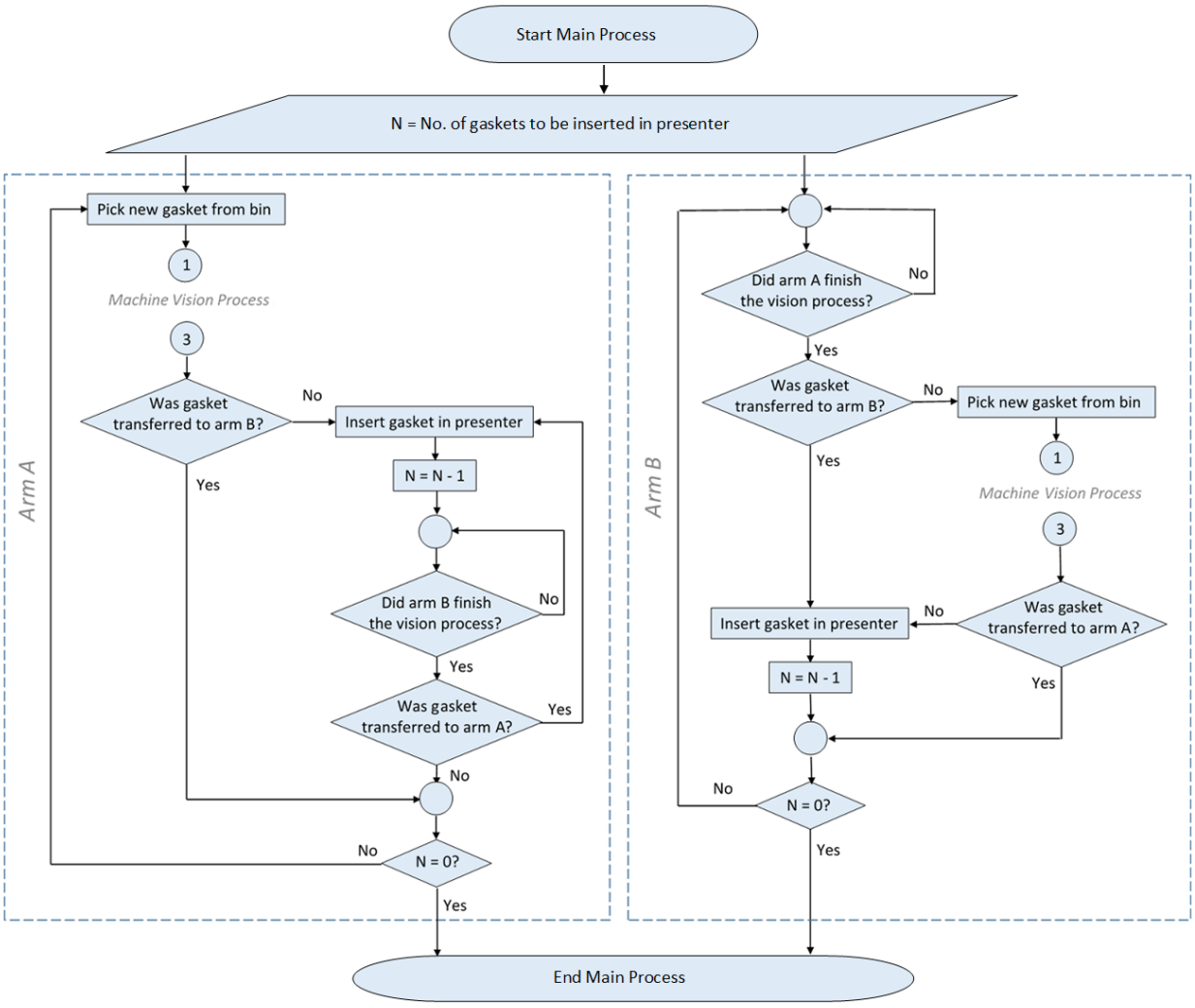

Figure 3.15 – "Main Process" programming flowchart for the FS100

The "Machine Vision Process" flowchart was completed in tandem with the "Main Process" flowchart. This flowchart (Figure 3.16) indicated what manipulator process to employ (Place, Rotate, Flip, or Flip-Rotate) depending on the result of the inputs from the COGNEX

program. Both flowcharts were designed to work synchronously during the gasket sortation process. Once the flowcharts were completed, the programs were written.

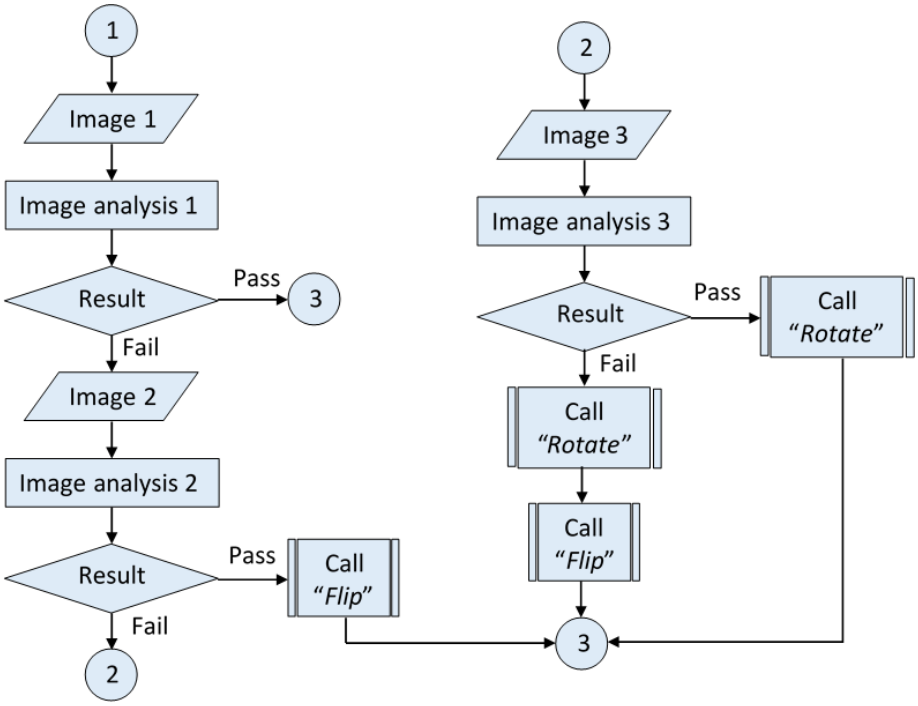

Figure 3.16 – "Machine Vision Process" flowchart

The programs were simulated using MotoSim EG VRC before they were run. This prevented the possibility of unwanted collision and allowed for better control and path iteration. The MotoSim EG VRC program allowed for simulated inputs that were manually controlled during program runtime. The ability to simulate inputs allowed for testing of all gasket orientations for both manipulators. The MotoSim EG VRC program also allowed for the importing of CAD models (Figure 3.17). This allowed for better control and understanding of the manipulator locations at all times during the experiment. The "Online Function" of the MotoSim EG VRC software allowed for visual indicating of where the robot was during operation (Figure 3.17) This allowed for validating the accuracy of the imported CAD models versus the physical construction. Once the simulated program was written, it was easily transferred from the

computer to the FS100 controller via FTP. This allowed for rapid development and deployment of programs and programming updates.

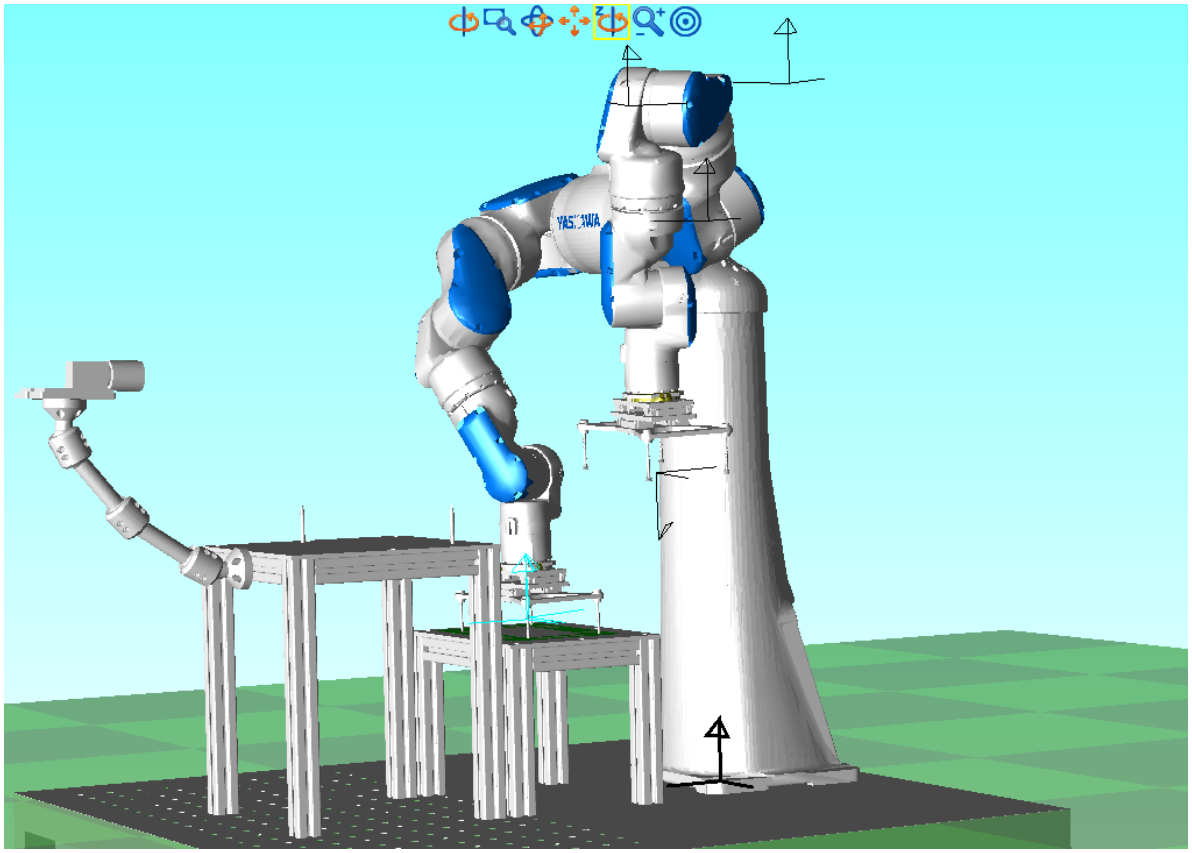

Figure 3.17 - MotoSim EG VRC simulation program during runtime

The machine vision program was written using the In-Sight® Explorer software. The "Easy Builder" function allowed for ease of computer vision development. An edge model was trained that looked for the HFC gasket notched corner (4 red squares in Figure 3.18). The SDA5F would bring the gasket into the top left position and scan for the gasket notch. If that notch was not detected, then the SDA5F would bring the gasket to the second position and scan for the notch. This process repeated until the notch was found. If the notch was never found, the

robot program would end. Once the notch was found, a corresponding action would occur and the camera program would restart (Figure 3.19).

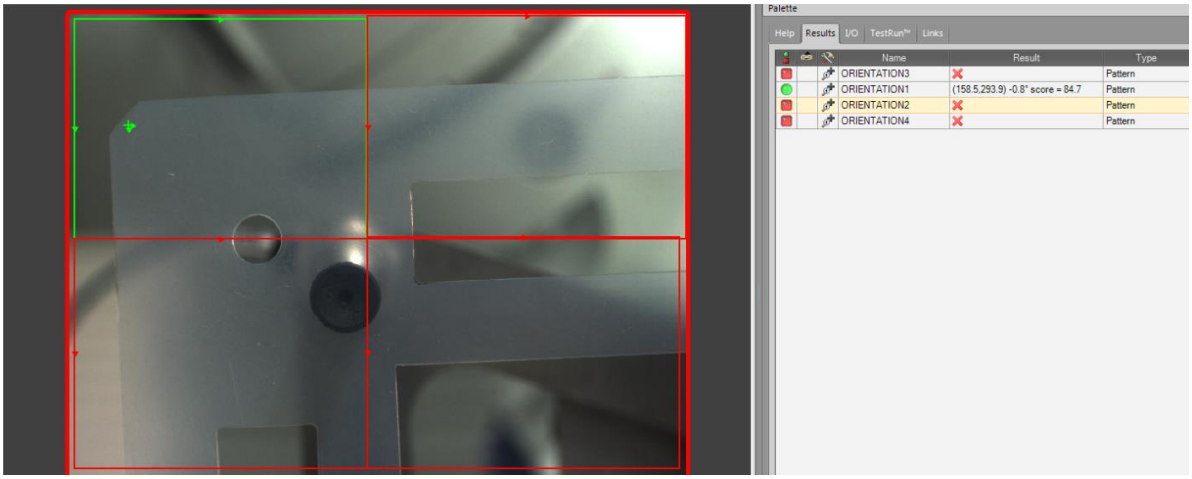

Figure 3.18 - In-Sight® Explorer Easy Builder software HFC notch detection

Case one from Figure 3.19 would signal for the current manipulator to place the gasket onto the alignment pins without rotating around Axis 1 or Axis 2. While the manipulator is placing the gasket onto the alignment pins for case one, the opposite manipulator is grabbing a part to allow for continuous motion and to decrease the cycle time of the system. Case two would only occur if case one failed, and would rotate the gasket around Axis 1 by transferring the gasket to the opposite manipulator before insertion. Once the gasket is transferred to the opposite manipulator for case two, the initial manipulator would move to grab another gasket to decrease cycle time. Case three would only occur if the previous cases failed, and would rotate the gasket around Axis 2 by rotating the "Wrist" joint of the manipulator. While the current manipulator is rotating the gasket and inserting in case three, the opposite manipulator is moving to pick a gasket in the same method as case one. Case four would only occur if the other three cases failed, and would rotate both around Axis 1 and Axis 2 by transferring the gasket to the other manipulator then rotating it using the "Wrist" joint. Once the gasket is transferred to the opposite

manipulator for case four, the initial manipulator would move to grab another gasket to decrease cycle time using the same method as case two.

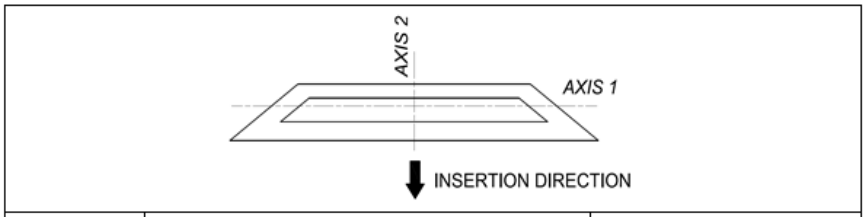

		Image No.				Action	
		1	2	3	4	Flip about *Axis 1*	Rotation about *Axis 2*
Results Image Analysis	Case 1	Pass	No further inspections needed			No	No
	Case 2	Fail	Pass	No further inspections needed		Yes	No
	Case 3	Fail	Fail	Pass	No further inspections needed	No	180°
	Case 4	Fail	Fail	Fail	Pass	Yes	180°

Figure 3.19 - Action list for notch detection cases

3.6 Procedure

This experiment compared hydrogen fuel cell gasket sortation time and accuracy of both a human and dual arm robot. This comparison was done to test the efficacy of using a dual arm robot with machine vision versus a human worker for gasket sortation. The dual arm robot was utilized to allow for ease of manipulation and reorientation of the flexible HFC gasket. Figure 3.20 represents the robot workcell of the hydrogen fuel cell gasket sortation experiment which utilized a Yaskawa SDA5F dual arm manipulator and Cognex ISM1403C camera system.

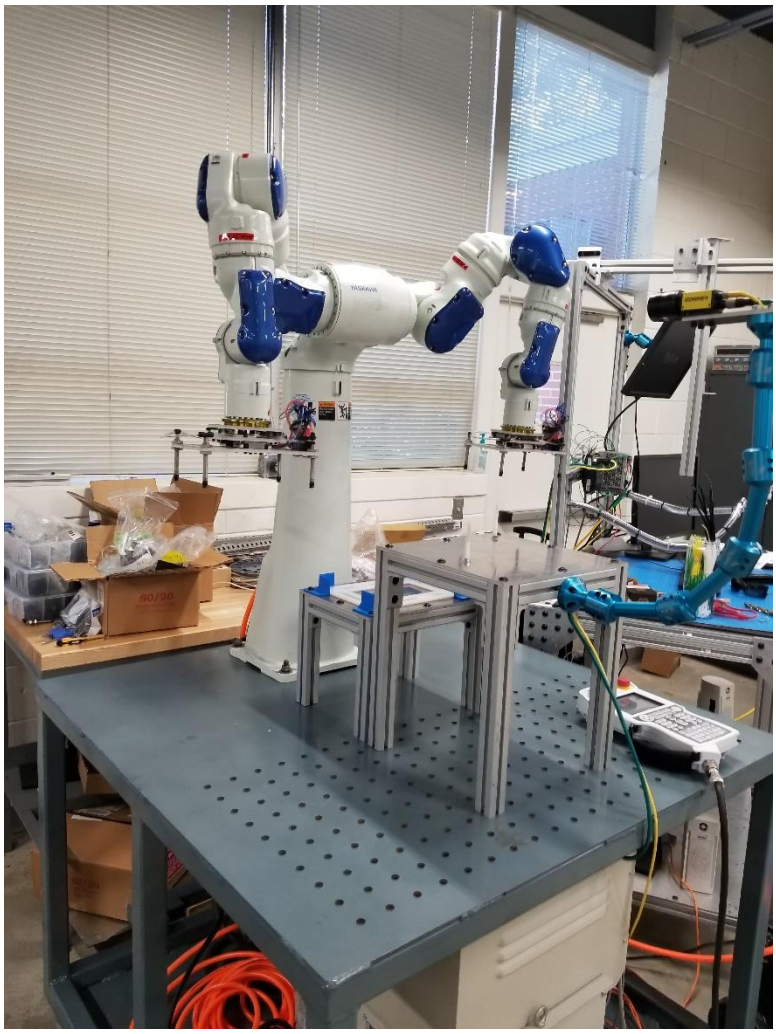

Figure 3.20 - Experimental Workcell

The robot began by first picking one gasket and moving it to be scanned by the camera. Depending on the signal from the COGNEX camera program the robot had four cases:

1. Place the gasket on the alignment pins without rotating the gasket.
2. Rotate the gasket then place the gasket on the alignment pins.
3. Transfer the gasket to the other robot arm then place the gasket on the alignment pins.
4. Transfer the gasket to the other robot arm, rotate the gasket, then place the gasket on the alignment pins.

While one arm was placing the current gasket, the other arm was moving to grab the next one (Figure 3.21). This allowed for continuous motion and optimized productivity. After the gaskets were all sorted, the stack was carefully analyzed manually to check the accuracy of the robot system. Manual timing with a stopwatch was used to determine cycle times.

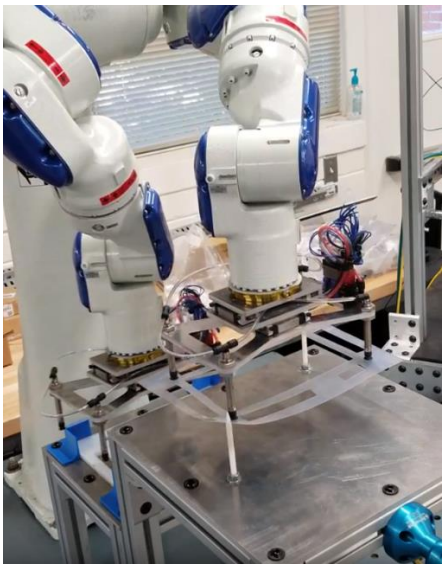

Figure 3.21 - Robot sortation in operation

The next step was to gather information about the human worker. A group of five randomly selected individuals was chosen to sort the gaskets manually. A box of randomly oriented gaskets was placed in front of the students and the goal was set to align and place the gaskets as soon as possible while retaining accuracy (Fig 3.22). Manual timing with a stopwatch was used to determine cycle times.

Figure 3.22 –Manual placement of gasket onto alignment pins

CHAPTER 4. RESULTS

4.1 Human Gasket Sortation

The results from the human sorting experiment are represented in Table 4.1, with the time being represented as Minutes:Seconds.Milliseconds. This is the result of ten randomly oriented HFC gaskets being sorted three times by five human subjects with one untimed practice run per human that occurred before data was collected. The average time for all five subjects to sort the HFC gaskets was 1:23.25 with 9.94s standard deviation.

Human	Run 1	Errors Run 1	Run 2	Errors Run 2	Run 3	Errors Run 3	Average Time	Standard Deviation
1	01:46.88	2	01:43.99	0	01:43.76	0	01:44.88	00:01.42
2	01:24.23	0	01:19.12	0	01:18.62	0	01:20.66	00:02.53
3	01:39.30	0	01:32.12	0	01:25.63	0	01:32.35	00:05.58
4	01:34.84	0	01:34.04	0	01:26.84	0	01:31.91	00:03.60
5	01:10.27	0	01:08.95	0	01:04.96	0	01:08.06	00:02.26

Table 4.1 - Results of manual gasket sortation

During the first run for Human 1 there were two errors observed. Errors are defined as gaskets that were not stacked in the proper orientation. The proper orientation was defined with the notched corner located to the top right (Figure 3.6). Even though there were only three runs for Human 1, there were two errors. This might indicate that repetitive work is subject to error. Error is also likely due to the small notched corner of the HFC gasket and the material being translucent. An improperly sorted HFC gasket could cause early failure of the HFC, decrease efficiency, or prevent its operation entirely due to flow restrictions. “A recent study showed that a manual assembly process of a 20-cell PEMFC stack lasted on average 50% longer than the robotic assembly process. The delays in the manual operations, as compared to the operations performed by the robot, were in part due to periodic breaks necessary for the human operator performing a repetitive work cycle. These delays are expected to increase significantly as the size of the fuel cell stack increases.” (Gurau, Vladimir, Devin Fowler and Daniel Cox. 2017)

For each human run three was the lowest time, run two was the second lowest time, and run one was the longest time. This indicates that there was a learning curve for each human (Figure 4.1). More runs would need to be conducted to see the effects of the learning curve and to determine the minimum time that the human needed to complete the cycle. The trendline was modeled as linear due to performing three runs, but true models of the learning curve may tend to be exponential as there is likely a minimum cycle time.

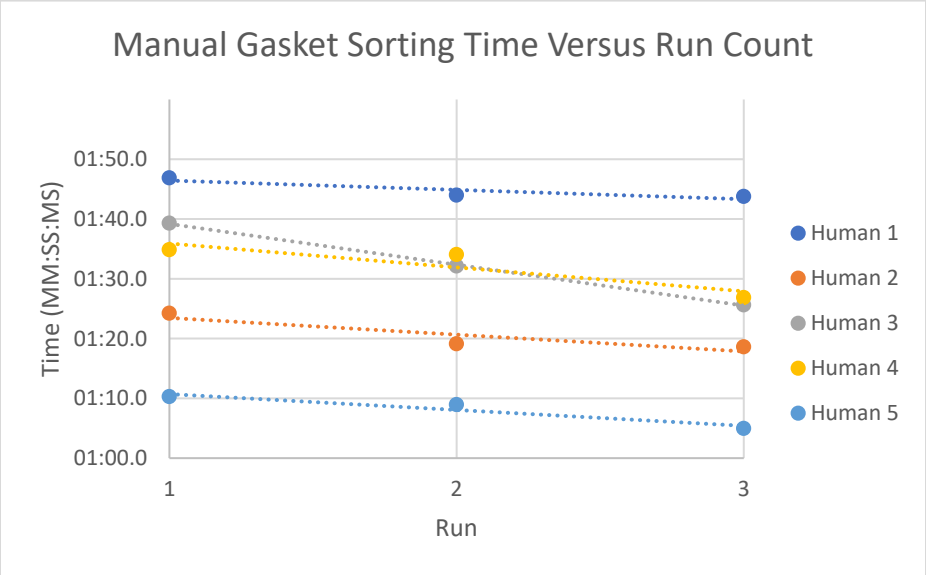

Figure 4.1 - Manual gasket sorting time versus run count

A stopwatch was used to determine the cycle times for each human worker. This approach can be subject to error, as human reaction time can affect the measurements. Humans take 180-200 milliseconds to register visual stimulus and respond (Jain et. al. 2015). Another possible way to capture cycle times would be to use a high-speed camera and playback the cycle times.

Each human subject was asked to share their opinions about the experiment:

- “The experiment was annoying; it was easy to phase out and just work. I feel like muscle memory caused error”

- “Interesting and harsh. Caused me to push myself and was mindless like gaming”
- “Mindless, but alright. It could get old”
- “Dark surfaces would make it easier for sorting”
- “Boring and easy”

4.2 Robot Gasket Sortation

The results of the robot sorting experiment are listed in Table 4.2, with the time being represented as Minute:Second:Millisecond. This data represents the time required to sort ten randomly sorted HFC gaskets onto alignment pins. The time was taken with a stopwatch. Timing began when the robot started the program and was stopped after the last gasket was placed.

Run	Time	Errors
1	04:10.15	0
2	04:13.85	0
3	04:16.37	0
4	04:20.40	0
5	04:16.25	0
6	04:40.13	0
Average	04:19.53	0
Std. Dev.	00:09.71	0

Table 4.2 - Results of robot gasket sorting experiment

No errors were present during the robotic sorting data collection, which should be expected due to the implementation of a camera system. This was due to fine tuning the camera system by changing the rotational, translational, and scale tolerances for the edge detection methods and by iterating programming changes. Some errors were present prior to tuning that

had to be addressed. The ambient lighting in the room with the camera would change throughout the course of the day due to sunlight. This was corrected by closing all blinds and gathering data only at night. Edges that were also improperly cleaned resulted in false positives (Figure 4.2). This was corrected by properly cleaning the edges of the gaskets with isopropyl-alcohol and testing. Another error would occur when the gripper was seen on camera and would send false positives to other detection regions. This was corrected by altering the robot code to only accept one signal at a time (Appendix A).

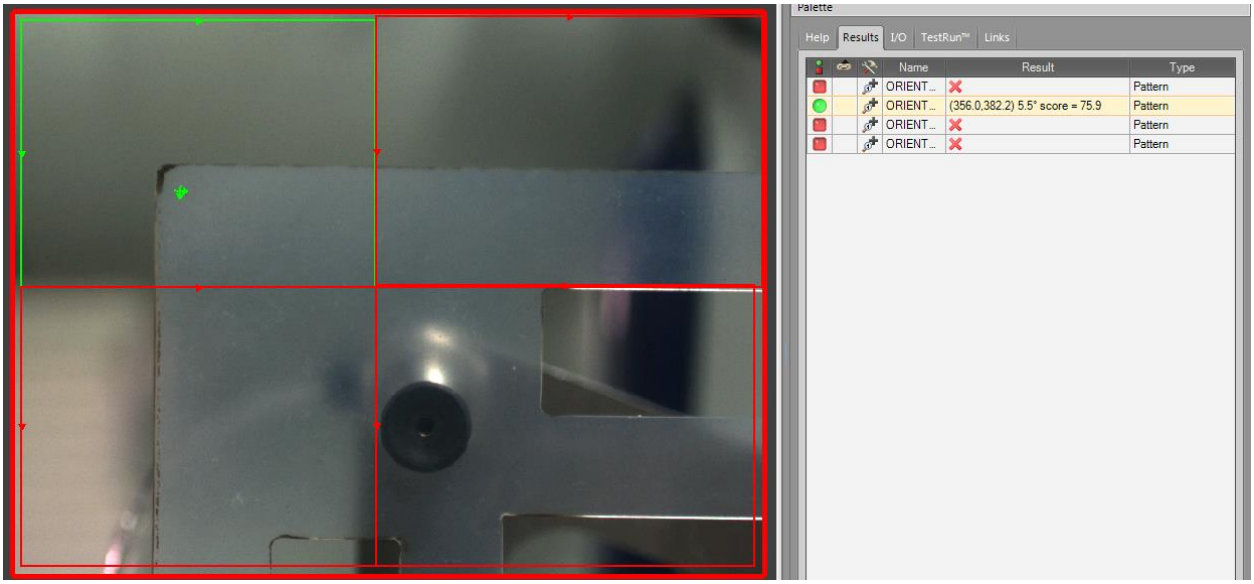

Figure 4.2 - False positive from improperly cleaned gasket edge due to laser cutting debris.

Due to the limitation of the vacuum equipment used, the speed of the robot was limited during the experiment as high speeds would release the gasket. Optimization of the robot speed was not prioritized during the experiment due to the dangers involved. The robot moves were run at relatively low speeds, but the traces of the robot were recorded using MotoSim EG VRC's "Online Function". These traces were used for the calculation of the theoretical max speeds and minimum cycle times. Traces are the path of the tooling of the robot manipulator measured as length (Figure 4.3). These lengths can help to compare robot moves to see which move is shorter for optimization purposes. Traces can also be used to determine the theoretical time that a robot

would require to accomplish a move by applying the robot's maximum linear speed. Since robot moves can be either joint interpolated or linear interpolated, the theoretical movement time is an approximation.

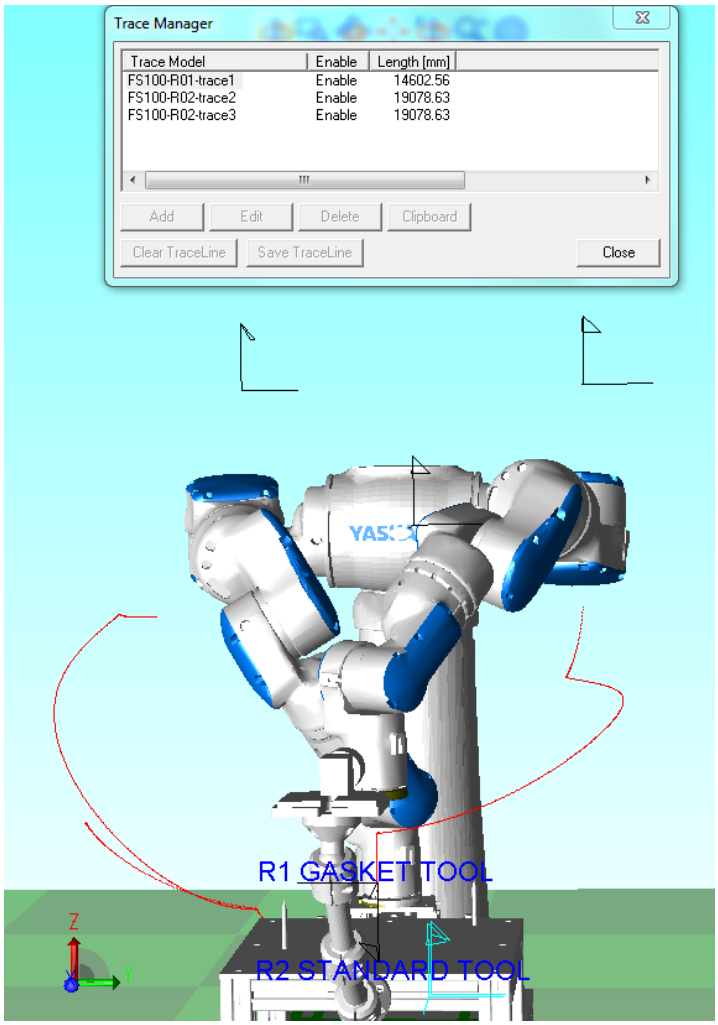

Figure 4.3 - MotoSim EG VRC Trace Manager (during Online operation)

Each of the robot moves were categorized and traces were recorded during the experiment (Table 4.3). Since each gasket was randomly oriented, the moves had to be recorded separately and for each case to ensure all moves were regarded. During case two and four a handoff would occur and the robot would move back to pick a gasket. During case one and three the robot would either place or rotate the gasket and return to the home position (Figure 3.15).

ID	Robot 2	Trace (mm)
1	Home to Pick Entry	481.96
2	Pick Entry to Camera Scan Case 1	738.79
3	Move from Scan 1 to Scan 2	205.92
4	Move from Scan 2 to Scan 3	148.10
5	Move from Scan 3 to Scan 4	233.75
6	Case 1 to Home	2440.87
7	Case 2 to Pick Entry	3938.44
8	Case 3 to Home	1309.57
9	Case 4 to Pick Entry	4232.70
10	Home to Assist Robot 1 then Home	3084.88

ID	Robot 1	Trace (mm)
11	Home to Pick Entry	518.80
12	Pick Entry to Camera Scan Case 1	716.03
13	Move from Scan 1 to Scan 2	221.74
14	Move from Scan 2 to Scan 3	156.04
15	Move from Scan 3 to Scan 4	243.36
16	Case 1 to Home	1394.31
17	Case 2 to Pick Entry	3845.67
18	Case 3 to Home	1264.51
19	Case 4 to Pick Entry	4135.25
20	Home to Assist Robot 2 then Home	3192.37

Table 4.3 - Gasket sortation categorized trace lengths for each robot.

Once the trace lengths were determined, the theoretical time of each move ID could be determined from the linear maximum speed of 1500 mm/s. Fifteen runs were simulated using Excel to determine the average optimized time (Table 4.4). The trace lengths were summated and divided by 1500 to determine the cycle time. The trace length in the sixth row per gasket (Lines 6, 12, 18, etc.) was not counted due to the shortest move during a synchronous move (both robots moving at once) slows down to accommodate for the longer move.

Line	Gasket No.	Case No.	Change picking manipulator	R1 ID	R2 ID	R1 Length	R2 Length
1	1	3	Yes		1		481.96
2					2		738.79
3					3		205.92
4					4		148.1
5					8		1309.57
6				11		518.8	
7	2	2	No	12		716.03	
8				13		221.74	
9				17		3845.67	
10							
11							
12					10		3084.88
13	3	3	Yes	12		716.03	
14				13		221.74	
15				14		156.04	
16				18		1264.51	
17							
18					1		481.96
19					2		738.79
20					6		2440.87

Table 4.4 - Simulated runs using traces in Excel

The results of the fifteen runs are displayed in Table 4.5. The average time of the simulated runs decreased the time by 90.1%. This indicates that there is a lot of improvements that can be made for optimizing cycle times. The actual numerical value of the optimized sorting robot should be only considered as a theoretical minimum, as it does not account for acceleration and deceleration of the robot, joint interpolation, or equipment limitations such as vacuum gripper systems. It is also worth remarking that the robot only needs to move as fast or slightly faster than the rest of the manufacturing cell. These results also make the assumption that the points that were taught for the moves are in optimum positions, which is not accurate.

Run	Time (ss.ms)
1	20.17
2	25.77
3	27.91
4	24.71
5	28.69
6	27.45
7	27.40
8	23.99
9	21.91
10	26.94
11	26.38
12	22.34
13	30.22
14	25.31
15	25.93
Average	
Std. Dev.	2.71

Table 4.5 - Simulated robot runs with optimized speed

4.3 Comparison and Analysis

The average cycle time for manual gasket sorting was 1:23.25 and the average cycle time for robot gasket sorting was 4:19.52. The robotic sorting method took an average of 2:56.27 more time to sort the gaskets than the manual method, or about 17.63 extra seconds per gasket.

This extra time is caused from a variety of factors such as the design choice of scanning each corner of the gasket separately with a one second delay and robot moves between each scan for reliability. The robot was also not optimized for speed due to the risks involved and due to equipment limitation. If the robot was optimized for speed there could be a significant decrease in cycle times.

Errors in sorting only occurring during human trials. Robotic sorting was error free for the six runs that occurred. This was due to the controlled environment of the sorting cell that only sorted gaskets during nighttime, and only used ten of the same cleaned gaskets. As more data is collected in future experimentation and iterations, errors may occur such as with uncleaned gaskets or ambient light interference. Conversely, as more manual sorting is performed there is likely probability that errors will occur especially due to the labor being repetitive.

Human workers found the experiment to be dull and repetitive even after a few minutes of work. Employment of human workers over long shifts can result in other potential problems such as arthritis or the development of a twitch. The learning curve that was present in the human trials indicated that faster cycle times could be attained after more runs were completed, unlike the fixed cycle times of the robot. Learning curves tend to be exponential, so an approximate minimum cycle time for human workers can be determined with more data.

4.4 Criteria for Success

Success of the experiment was accepted if the errors during robot sorting were less than those during human sorting, which implies that the implementation of a vision integrated dual arm robot is feasible.

CHAPTER 5. CONCLUSIONS

5.1 Validation of Hypothesis

We demonstrate a novel robotic process of transferring fuel cell components from their fabrication workcell to a robotic fuel cell assembly workcell. The process was demonstrated with fuel cell gaskets due to increased complexity challenges these components present, but it can be readily used for other fuel cell components such as MEAs and bipolar plates. These components transferring process includes component pickup from a bin where they have a random orientation, handling, orientation inspection, reorientation and insertion in a presenter for a subsequent process. The demonstrated process uses a dual arm robot with integrated machine vision system. This robotic process enables the integration of automated manufacturing processes of fuel cell gaskets with a robotic fuel cell stack assembly process previously demonstrated into a fully automated fuel cell manufacturing line. The robot productivity was compared to the productivity of five human subjects. For a short task the robot was outperformed by the human subjects. It is however expected that the robot productivity will be significantly higher than that of the humans over an eight hour shift due to its constant work pace and no downtime needed for food and rest. The experiment demonstrates that for such dull, repetitive work cycles human error is possible even for short tasks.

The results of the experiment satisfy the hypothesis, as errors during robotic sorting decreased even though cycle times increased. This implies that the implementation of the vision integrated dual arm robot is feasible for long term manufacturing, due to the potential failures that could occur if a gasket was not properly stacked. It was also proven during the MotoSim simulation that the cycle times for the robot can decrease after motion optimization has been performed.

5.2 Knowledge Gained from PEMFC Gasket Sorting

Using a vision integrated dual arm robot for PEMFC gasket sorting can be beneficial, as stacking errors can be eliminated. By picking then scanning the semitransparent gasket material, the chance of falsely detecting manufacturing features is greatly reduced versus scanning before picking. The utilization of vacuum suction cups helped to grasp the thin flexible gasket material, as other forms of grippers would not be viable. The selectively compliant end effectors helped to reduce misalignment during stacking, as contact between the holes in the gasket and the alignment pins during placement would translate the end effector resulting in better positioning.

5.3 Suggestions for Future Research and Application

Future research of PEMFC gasket sorting is inevitable as demand for PEMFC production continues to increase. Researching better methods of gasket sorting before the demand will prove vital for manufacturing, and will result in better preparedness for this demand.

Understanding the effects of robot optimization on cycle time will be beneficial for mass production. The cycle time of the current experiment is unoptimized to prevent the risk of high impact collision. Cycle times will need to decrease as demand increases, and experimentation may be necessary to determine how to increase the speed of the robot. Advances in speed can result from eliminating unnecessary robot moves, increasing the speed of current moves, or mechanical changes such as the relocation of gaskets, cameras, and tables.

Utilizing a stamp for cutting the gasket profile will eliminate the burn marks left from laser cutting. The additional step of cleaning burn marks on the gaskets after the laser cutting process will also be removed. By eliminating a process step, less automation will be required resulting in cost reduction. Using a stamp will also remove the utilization of a laser cutter, which are expensive. Stamps will require maintenance as they wear over time.

The implementation of MotoSight 2D would increase the accuracy of gasket alignment onto the stack, as individual gasket positions could be communicated to the robot. MotoSight 2D allows for the COGNEX camera to communicate via Ethernet/IP to the Yaskawa programmable logic controller (PLC). Data from the COGNEX camera can include the position of the gaskets, their rotation, flaws, whether they are present, and their orientation.

Implementation of better lighting control would allow for more consistent operation of the COGNEX camera. This experiment utilized the camera at night to mitigate uncontrolled light sources from permeating into the scan area. Using brighter lights and covers could mitigate these uncontrolled light sources and allow for runtime of the scanning operation during a wider range.

REFERENCES

Global Markets Insight, 2016, “Fuel Cell Market Size by Application (Stationary, Portable, Transport), by Product (PEMFC, DMFC, SOFC), Industry Analysis Report, Regional Outlook (U.S, Canada, Germany, UK, Japan, South Korea, South Africa, Brazil), Application Potential, Price Trends, Competitive Market Share & Forecast, 2016 – 2024”, https://www.gminsights.com/industry-analysis/fuel-cell-market

Grand View Research. 2016. “Fuel Cell Market Analysis By Product (PEMFC, PAFC, SOFC, MCFC), By Application (Stationary, Transportation, Portable) And Segment Forecast, 2018 - 2025.” *Fuel Cell Market Size, Growth Forecast | Industry Analysis Report, 2025*. Accessed January 1, 2018. https://www.grandviewresearch.com/industry-analysis/fuel-cell-market.

Umberto, Lucia. 2014. “Overview on fuel cells.” *Renewable and Sustainable Energy Reviews*, 30: 64-169. Accessed January 1, 2018. https://doi.org/10.1016/j.rser.2013.09.025.

Ho, Jonathan C., Ewe-Chai Saw, Louis Y.Y. Lu, John S. Liu. 2014. “Technological barriers and research trends in fuel cell technologies: A citation network analysis.” *Technological Forecasting and Social Change*, 82: 66-79. Accessed January 1, 2018. https://doi.org/10.1016/j.techfore.2013.06.004.

Mekhilef S., R. Saidur, A. Safari. 2012. “Comparative study of different fuel cell technologies.” *Renewable and Sustainable Energy Reviews*, 16 (1): 981-989. Accessed February 1 2018. https://doi.org/10.1016/j.rser.2011.09.020.

Salvendy, Gavriel. 2012. *Handbook of Human Factors and Ergonomics*. Hoboken: Wiley, 2012. *eBook Academic Collection (EBSCOhost)*

Makris, Sotiris, Panagiota Tsarouchi, Aleksandros-Stereos Matthaiakis, Athanasios Athanasatos, Xenofon Chatzigeorgiou, Michael Stefos, Konstantinos Giavridis, Sotiris Aivaliotis,. 2017.

"Dual arm robot in cooperation with humans for flexible assembly." *CIRP Annals*, 66 (1): 13-16. Accessed April 1 2018. https://doi.org/10.1016/j.cirp.2017.04.097.

Geismar, Neil, U. V. Manoj, Avanthi Sethi, and Chelliah Sriskandarajah. 2012. "Scheduling Robotic Cells Served by a Dual-Arm Robot." *IIE Transactions* 44 (3): 230–48. doi:10.1080/0740817X.2011.618174.

Stria, Jan, Daniel Prusa, Vaclav Hlavac, Libor Wagner, Vladimir Petrik, Pavel Krsek, and Vladimir Smutny. 2014. "Garment perception and its folding using a dual-arm robot." *2014 IEEE/RSJ International Conference On Intelligent Robots & Systems* 61. *Complementary Index*, EBSCO*host* (accessed February 10, 2018).

Panagiota Tsarouchi, Sotiris Makris, George Michalos, Michael Stefos, Konstantinos Fourtakas, Konstantinos Kaltsoukalas, Dimitris Kontrovrakis, George Chryssolouris. 2014 "Robotized Assembly Process Using Dual Arm Robot." *Procedia CIRP* 23: 47-52. https://doi.org/10.1016/j.procir.2014.10.078.

Zhao, Yuanshen, Liang Gong, Chengliang Liu, Yixiang Huang. 2016. "Dual-arm Robot Design and Testing for Harvesting Tomato in Greenhouse." *IFAC-PapersOnLine* 49 (16):161-165. https://doi.org/10.1016/j.ifacol.2016.10.030.

Boothroyd G., Dewhurst P., and Knight W.A., 2011, Product Design for Manufacture and Assembly, 3rd ed., CRC Press, Boca Raton

Krüger, J, G. Schreck, D. Surdilovic. 2011. "Dual arm robot for flexible and cooperative assembly." *CIRP Annals* 60 (1): 5-8. https://doi.org/10.1016/j.cirp.2011.03.017.

Jiménez Moreno, Robinson, and Oscar Fernando Aviles. 2017. "Humanoid Robot Cooperative System by Machine Vision." *International Journal Of Online Engineering* 13, no. 12: 162-173. *Engineering Source*, EBSCO*host*(accessed February 11, 2018).

Nowakowski, Jacek, and Dominik Sankowski. 2014. *Computer Vision In Robotics And Industrial Applications*. [Hackensack] New Jersey]: World Scientific, 2014. *eBook Academic Collection (EBSCOhost)*, EBSCO*host* (accessed February 11, 2018).

Smith, Christian, Yiannis Karayiannidis, Lazaros Nalpantidis, Xavi Gratal, Peng Qi, Dimos V. Dimarogonas, Danica Kragic. 2012. "Dual arm manipulation - A survey" *Robotics and Autonomous Systems* 60 (10): 1340-1353. https://doi.org/10.1016/j.robot.2012.07.005.

Sharaf, Omar, and Orhan, Mehet. 2014. "An Overview of Fuel Cell Technology: Fundamentals and Applications." *Renewable and Sustainable Energy Reviews* 32: 811-53. Accessed December 19, 2017. https://doi.org/10.1016/j.rser.2014.01.012

Grover, Mikell. 2008. *Automation, Production Systems, and Computer-Integrated Manufacturing*. Lehigh University: Pearson Education Inc.

Kim, Young-Loul, Hee-Chan Song, Jae-Bok Song. 2013. "Force control based jigless assembly strategy of a unit box using dual-arm and friction." *IEEE ISR 2013*: 1-3. Accessed January 1 2019. doi: 10.1109/ISR.2013.6695701

Jain A, Bansal R, Kumar A, Singh K D. 2015. "A comparative study of visual and auditory reaction times on the basis of gender and physical activity levels of medical first year students." *Int J App Basic Med Res* 5:124-127. Accessed January 1 2019. http://www.ijabmr.org/text.asp?2015/5/2/124/157168

Yaskawa Europe GmbH. 2012. "Motoman dual arm robot assembling a chair" YouTube video, 2:53. Posted March 21, 2012. Accessed January 1 2019. https://www.youtube.com/watch?v=r3fUsoLCSrY

Gurau, Vladimir, Devin Fowler and Daniel Cox. 2017. "Robotic Technologies for Proton Exchange Membrane Fuel Cell Assembly." *Proton Exchange Membrane Fuel Cell, Tolga Taner,*

IntechOpen, DOI: 10.5772/intechopen.71470. Available from: https://www.intechopen.com/books/proton-exchange-membrane-fuel-cell/robotic-technologies-for-proton-exchange-membrane-fuel-cell-assembly

U.S. Department of Energy. “Roadmap on Manufacturing R&D for the Hydrogen Economy”, https://www.hydrogen.energy.gov/pdfs/roadmap_manufacturing_hydrogen_economy.pdf [Accessed: 9/4/2017]

APPENDIX A: YASKAWA PROGRAM

```
/JOB
//NAME DFTHESIS
//POS
///NPOS 2,2,0,37,0,0
///TOOL 1
///POSTYPE PULSE
///PULSE
C00000=36748,73480,-59006,-135983,-5400,55307,135520
///TOOL 0
C00001=35303,70861,-71500,31711,9975,73656,139229
BC00000=0
BC00001=0
///POSTYPE ROBOT
///RECTAN
///RCONF 0,0,0,0,0,0,0,0,0,0,0,0,0,0,0,0,0,0,0,0,0,0,0,0,0
P00010=174.871,378.359,-381.747,-176.9929,-2.7270,177.4608,64.2257
P00011=201.993,268.510,-549.719,178.9106,0.2916,-179.7702,79.5182
P00012=180.120,-2.113,-575.698,-179.5420,-0.2050,-179.7857,79.6096
P00013=180.441,-1.824,-650.648,-179.4972,-0.9848,-178.5543,79.5087
///RCONF 1,0,0,0,0,0,0,0,0,0,0,0,0,0,0,0,0,0,0,0,0,0,0,0,0
P00014=267.358,2.728,-363.028,-178.8864,31.0926,-177.6595,81.4110
///RCONF 0,0,0,0,0,0,0,0,0,0,0,0,0,0,0,0,0,0,0,0,0,0,0,0,0
P00015=465.953,113.329,-148.103,-71.7424,87.4549,-72.3554,95.2066
P00016=468.126,-106.006,-132.741,-71.7543,87.4493,-72.3651,67.9985
P00017=468.116,-106.383,18.940,-71.7636,87.4366,-72.3708,68.0036
P00018=467.324,122.669,3.805,-71.8437,87.4375,-72.4491,68.0028
P00019=454.036,0.887,-398.293,-179.6439,-0.6160,179.8856,68.0004
P00020=454.048,1.044,-437.137,-179.6434,-0.6123,179.8832,68.0013
///RCONF 1,0,0,0,0,0,0,0,0,0,0,0,0,0,0,0,0,0,0,0,0,0,0,0,0
P00021=411.071,386.540,-354.940,-179.3569,-1.0258,-178.8551,68.0006
///RCONF 0,0,0,0,0,0,0,0,0,0,0,0,0,0,0,0,0,0,0,0,0,0,0,0,0
P00022=459.672,-3.033,-354.878,-179.9352,0.1783,1.3267,78.1309
P00023=457.038,-3.409,-434.412,-179.9408,0.1786,-0.3230,78.1279
P00024=293.691,234.891,11.453,83.5042,-88.8072,9.4504,66.8987
P00025=297.039,21.560,17.216,147.2015,-87.8805,-53.1763,66.8975
P00026=379.653,489.348,-372.773,165.3738,25.0526,135.0668,78.0885
P00027=456.150,235.212,-162.706,-164.7138,45.5306,-164.9474,66.7034
P00028=456.128,235.201,-162.729,175.5213,-47.3212,0.1733,66.7036
///TOOL 1
P00049=426.687,-308.820,-273.273,179.4829,-0.1120,2.8885,-80.5597
P00050=242.104,-414.985,-375.366,179.3255,-0.8318,-1.2651,-69.9702
```

```
P00051=192.893,-194.317,-499.923,-179.4348,-0.0016,4.2809,-80.5464
///RCONF 1,0,0,0,0,0,0,0,0,0,0,0,0,0,0,0,0,0,0,0,0,0,0,0,0
P00052=184.950,-7.807,-585.451,-179.6187,1.2456,3.0606,-80.6470
P00053=185.536,-9.063,-651.082,-179.6183,1.2482,3.0613,-80.6497
///RCONF 0,0,0,0,0,0,0,0,0,0,0,0,0,0,0,0,0,0,0,0,0,0,0,0,0
P00054=190.780,-18.761,-457.521,178.9727,-0.6651,4.2029,-80.5586
///RCONF 1,0,0,0,0,0,0,0,0,0,0,0,0,0,0,0,0,0,0,0,0,0,0,0,0
P00055=451.352,98.429,-128.825,117.0647,-89.3530,64.0167,-77.5319
P00056=463.725,-105.129,-134.000,116.7684,-89.3528,64.3158,-92.6516
P00057=463.061,-113.336,10.648,94.1126,-89.2645,87.3021,-80.5671
P00058=441.969,105.781,17.186,94.1205,-89.4344,87.1237,-80.5533
P00059=463.078,-16.036,-387.849,178.6721,0.5364,1.0834,-80.5575
P00060=463.222,-11.174,-441.713,178.6723,0.5378,1.0824,-80.5574
P00061=460.197,-13.441,-352.318,-179.6625,-0.1300,-178.9521,-80.5684
P00062=457.185,-14.717,-435.591,-179.6658,-0.1316,-178.9609,-80.5676
P00063=306.794,-232.297,-7.243,21.8454,-88.5514,-108.3287,-80.5546
///RCONF 0,0,0,0,0,0,0,0,0,0,0,0,0,0,0,0,0,0,0,0,0,0,0,0,0
P00064=291.317,20.210,15.515,21.9513,-88.5534,-108.4352,-80.5549
///RCONF 1,0,0,0,0,0,0,0,0,0,0,0,0,0,0,0,0,0,0,0,0,0,0,0,0
P00065=260.084,-359.810,-94.257,-146.1283,-30.7801,167.0442,-73.3087
P00066=276.388,-662.367,-147.056,-133.5678,-4.1946,154.6813,-92.3909
//INST
///DATE 2018/09/01 16:43
///ATTR SC,RW
///GROUP1 RB2,BS2
///GROUP2 RB1,BS1
NOP
*START
DOUT OT#(7) ON
MOVJ P050 VJ=D001 PL=0  +MOVJ P010 VJ=D001
MOVJ P051 VJ=D001 PL=0  +MOVJ P010 VJ=D001
MOVJ P052 VJ=D001 PL=0  +MOVJ P010 VJ=D001
MOVL P053 V=D002 PL=0  +MOVL P010 V=D002
DOUT OT#(5) ON
TIMER T=0.250
MOVL P052 V=D002 PL=0  +MOVL P010 V=D002
MOVJ P054 VJ=D001 PL=0  +MOVJ P010 VJ=D001
*R2SCAN
MOVJ P055 VJ=D001 PL=0  +MOVJ P010 VJ=D001
TIMER T=1.000
IFTHEN IN#(10)=ON
        JUMP *R2ROT
ENDIF
```

```
MOVJ P056 VJ=D001 PL=0  +MOVJ P010 VJ=D001
TIMER T=1.000
IFTHEN IN#(12)=ON
        MOVJ P066 VJ=D001 PL=0  +MOVJ P024 VJ=D001
        JUMP *R2FLROT
ENDIF
MOVJ P057 VJ=D001 PL=0  +MOVJ P010 VJ=D001
TIMER T=1.000
IFTHEN IN#(14)=ON
        JUMP *R2PLACE
ENDIF
MOVJ P058 VJ=D001 PL=0  +MOVJ P010 VJ=D001
TIMER T=1.000
IFTHEN IN#(16)=ON
        JUMP *R2FLIP
ENDIF
JUMP *BREAK
*R1SCAN
MOVJ P050 VJ=D001 PL=0  +MOVJ P015 VJ=D001
TIMER T=1.000
IFTHEN IN#(10)=ON
        JUMP *R1ROT
ENDIF
MOVJ P050 VJ=D001 PL=0  +MOVJ P016 VJ=D001
TIMER T=1.000
IFTHEN IN#(12)=ON
        JUMP *R1FLROT
ENDIF
MOVJ P050 VJ=D001 PL=0  +MOVJ P017 VJ=D001
TIMER T=1.000
IFTHEN IN#(14)=ON
        JUMP *R1PLACE
ENDIF
MOVJ P050 VJ=D001 PL=0  +MOVJ P018 VJ=D001
TIMER T=1.000
IFTHEN IN#(16)=ON
        JUMP *R1FLIP
ENDIF
JUMP *BREAK
*R2PLACE
MOVJ P059 VJ=D001 PL=0  +MOVJ P011 VJ=D001
MOVL P060 V=D002 PL=0  +MOVJ P012 VJ=D001
DOUT OT#(5) OFF
```

```
MOVL P059 V=D002 PL=0  +MOVL P013 V=D003
DOUT OT#(1) ON
TIMER T=0.500
MOVJ P049 VJ=D001 PL=0  +MOVL P012 V=D002
MOVJ P050 VJ=D001 PL=0  +MOVJ P014 VJ=D001
JUMP *R1SCAN
*R1PLACE
MOVJ P051 VJ=D001 PL=0  +MOVJ P019 VJ=D001
MOVJ P052 VJ=D001 PL=0  +MOVL P020 V=D002
DOUT OT#(1) OFF
MOVL P053 V=D003 PL=0  +MOVL P019 V=D002
DOUT OT#(5) ON
TIMER T=0.500
MOVL P052 V=D002 PL=0  +MOVJ P021 VJ=D001
MOVJ P054 VJ=D001 PL=0  +MOVJ P010 VJ=D001
JUMP *R2SCAN
*R2ROT
MOVJ P061 VJ=D001 PL=0  +MOVJ P011 VJ=D001
MOVL P062 V=D002 PL=0  +MOVJ P012 VJ=D001
DOUT OT#(5) OFF
MOVL P061 V=D002 PL=0  +MOVL P013 V=D003
DOUT OT#(1) ON
TIMER T=0.500
MOVJ P049 VJ=D001 PL=0  +MOVL P012 V=D002
MOVJ P050 VJ=D001 PL=0  +MOVJ P014 VJ=D001
JUMP *R1SCAN
*R1ROT
MOVJ P051 VJ=D001 PL=0  +MOVJ P022 VJ=D001
MOVJ P052 VJ=D001 PL=0  +MOVL P023 V=D002
DOUT OT#(1) OFF
MOVL P053 V=D003 PL=0  +MOVL P022 V=D002
DOUT OT#(5) ON
TIMER T=0.500
MOVL P052 V=D002 PL=0  +MOVJ P021 VJ=D001
MOVJ P054 VJ=D001 PL=0  +MOVJ P010 VJ=D001
JUMP *R2SCAN
*R2FLIP
MOVJ P063 VJ=D001 PL=0  +MOVJ P024 VJ=D001
MOVL P064 V=D003 PL=0  +MOVL P025 V=D003
DOUT OT#(1) ON
DOUT OT#(5) OFF
MOVL P063 V=D003 PL=0  +MOVL P024 V=D003
MOVJ P065 VJ=D001 PL=0  +MOVJ P028 VJ=D001
```

```
JUMP *R1ROT
*R1FLIP
MOVJ P063 VJ=D001 PL=0  +MOVJ P024 VJ=D001
MOVL P064 V=D003 PL=0  +MOVL P025 V=D003
DOUT OT#(1) OFF
DOUT OT#(5) ON
MOVL P063 V=D003 PL=0  +MOVL P024 V=D003
MOVJ P061 VJ=D001 PL=0  +MOVJ P026 VJ=D001
JUMP *R2ROT
*R2FLROT
MOVJ P063 VJ=D001 PL=0  +MOVJ P024 VJ=D001
MOVL P064 V=D003 PL=0  +MOVL P025 V=D003
DOUT OT#(1) ON
DOUT OT#(5) OFF
MOVL P063 V=D003 PL=0  +MOVL P024 V=D003
MOVJ P065 VJ=D001 PL=0  +MOVJ P027 VJ=D001
JUMP *R1PLACE
*R1FLROT
MOVJ P063 VJ=D001 PL=0  +MOVJ P024 VJ=D001
MOVL P064 V=D003 PL=0  +MOVL P025 V=D003
DOUT OT#(1) OFF
DOUT OT#(5) ON
MOVL P063 V=D003 PL=0  +MOVL P024 V=D003
MOVJ P059 VJ=D001 PL=0  +MOVJ P026 VJ=D001
JUMP *R2PLACE
*BREAK
MOVJ C00000 BC00000 VJ=D001 PL=0  +MOVJ C00001 BC00001 VJ=D001
DOUT OT#(1) OFF
DOUT OT#(5) OFF
END
```

APPENDIX B: COGNEX PROGRAM

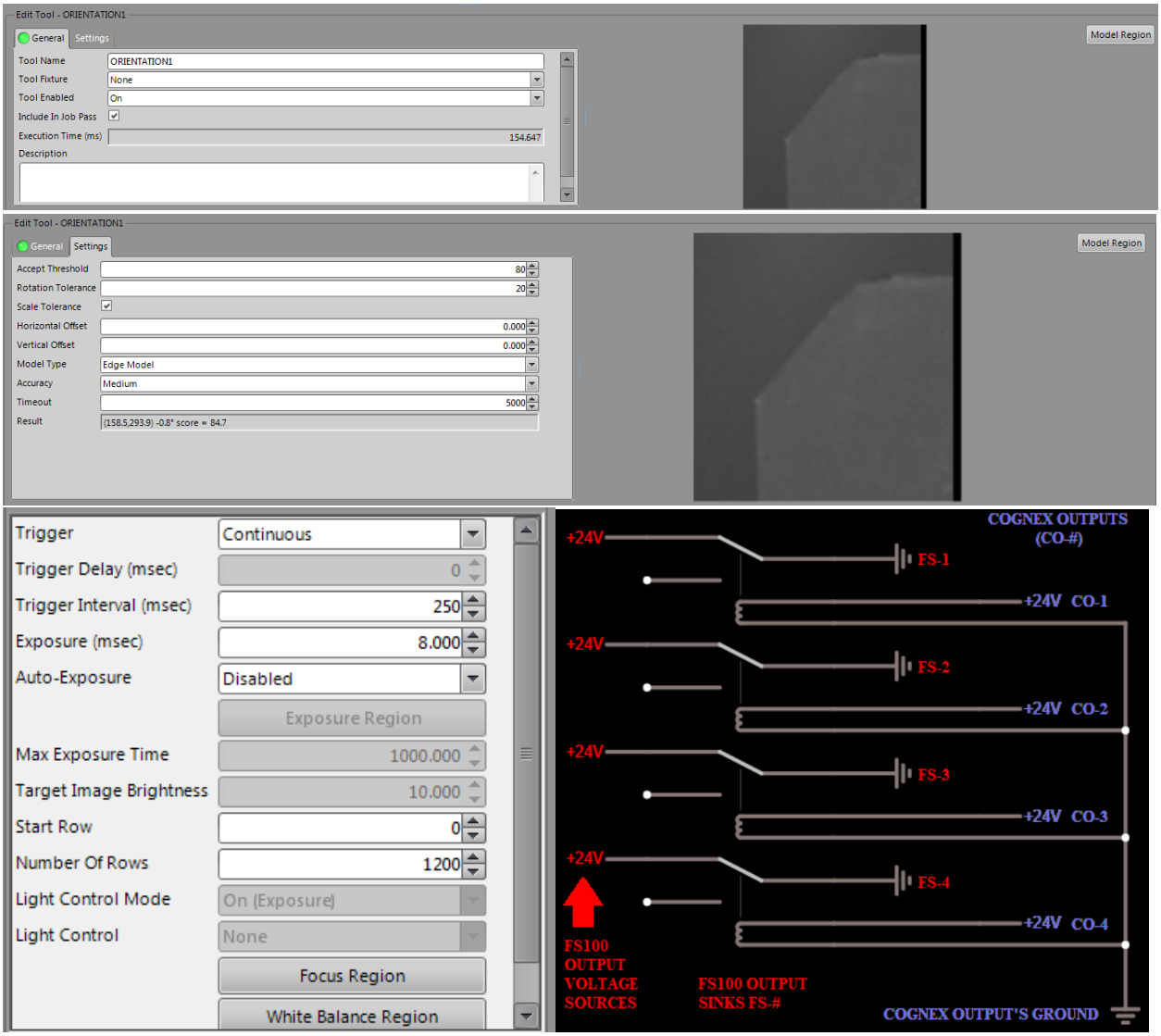

Figure B.1 - Program setup in Cognex EasyBuilder. Trained model (top), Tolerancing (Middle), Trigger and exposure (lower left), and wiring (lower right).

APPENDIX C: SDA5F DATA SHEET

SDA5F ROBOT

All dimensions are metric (mm) and for reference only. Please request detail drawings for all design/engineering requirements.

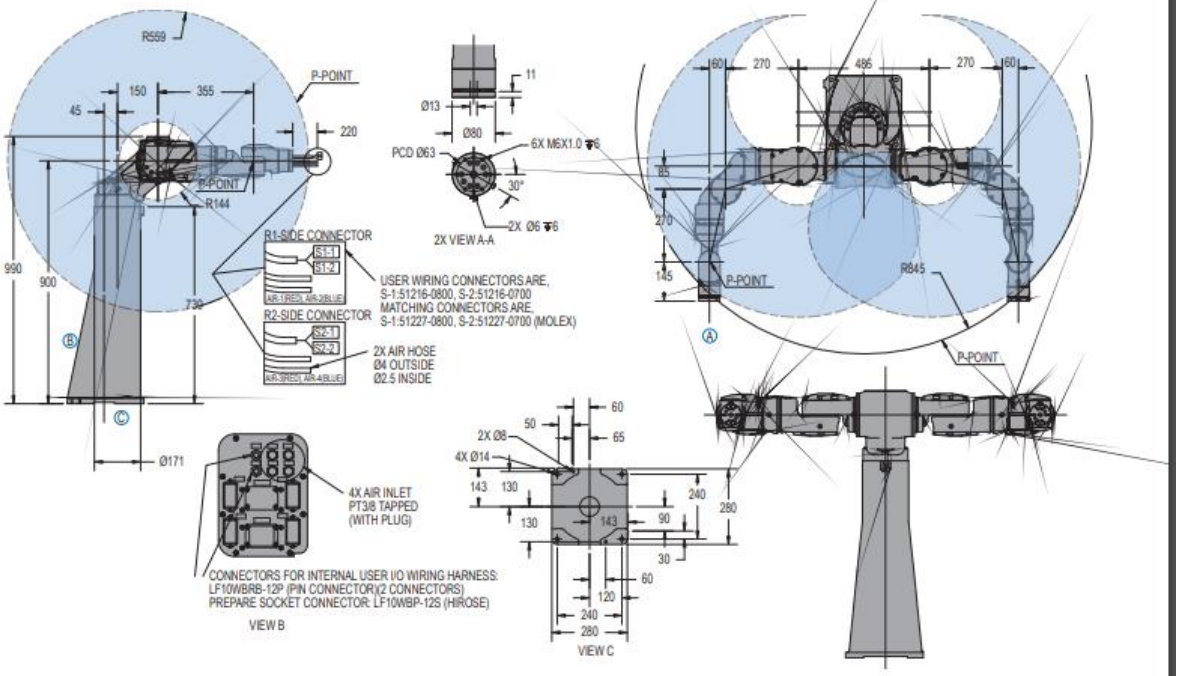

SDA5F SPECIFICATIONS

Structure		Articulated
Mounting		Floor
Controlled Axes		15 (7 axes per arm plus base rotation)
Payload		5 kg (11 lbs)/arm
Horizontal Reach per Arm		845 mm (33.3")
Horizontal Reach (P-point to P-point)		1,690 mm (66.5")
Vertical Reach		1,118 mm (44")
Repeatability		±0.06 mm (±0.003")
Maximum Motion Range	Rotation-Axis (Waist) L-Axis (Lower Arm) E-Axis (Elbow) U-Axis (Upper Arm) R-Axis (Upper Arm Twist) B-Axis (Wrist Pitch/Yaw) T-Axis (Wrist Twist)	±170° ±110° ±170° +115° / -90° ±180° ±110° ±180°
Maximum Speed	Rotation-Axis S-Axis L-Axis E-Axis U-Axis R-Axis B-Axis T-Axis	200°/s 200°/s 200°/s 200°/s 200°/s 200°/s 230°/s 350°/s
Approximate Mass		110 kg (242.6 lbs)
Power Consumption		1.4 kVA
Allowable Moment	R-Axis B-Axis T-Axis	14.7 N • m 14.7 N • m 7.35 N • m
Allowable Moment of Inertia	R-Axis B-Axis T-Axis	0.45 kg • m² 0.45 kg • m² 0.11 kg • m²

FS100 CONTROLLER SPECIFICATIONS*

Dimensions (mm)	470 (w) x 200 (h) x 420 (d) (18.5" x 7.9" x 16.5")
Approximate Mass	20 kg (44.1 lbs)
Cooling System	Direct cooling
Ambient Temperature	During operation: 0° to 40° C (32° to 104° F) During transit and storage: -10° to 60° C (14° to 140° F)
Relative Humidity	90% max. non-condensing
Primary Power Requirements	Single-phase or 3-phase power, 200/230 VAC at 50/60 Hz (MPP3, MPK2, MH6F, HP20F require 3-phase)
External Transformer (optional)	For 480/575 VAC installations
Digital I/O NPN-Standard PNP-Optional	Standard I/O: 16 inputs/16 outputs Max. I/O (optional): 168 inputs and 168 outputs
Position Feedback	Absolute encoder
Program Memory	JOB: 10,000 steps, 1,000 instructions CIO Ladder: 1,500 steps
Pendant Dim. (mm)	169 (w) x 314.5 (h) x 50 (d) (6.7" x 12.4" x 2")
Pendant Weight	.998 kg (2.2 lbs)
Interface	One Compact Flash slot; One USB port (1.1)
Pendant Playback Buttons	Teach/Play/Remote Keyswitch selector Servo On, Start, Hold, and Emergency Stop Buttons
Programming Language	INFORM III, menu-driven programming, MotoPlus SDK (C language) – optional
Maintenance Functions	Displays troubleshooting for alarms
Number of Robots/Axes	Up to 2 robots, 16 axes (requires 2 controllers)
Multi Tasking	Up to 6 concurrent jobs, 1 system job
Fieldbus	All common networks supported
Ethernet	10 Base T/100 Base TX
Safety	Dual-channel Emergency Stop Pushbuttons, 3-position Enable Switch, Manual Brake Release

Note: Use DX100 controller for arc welding applications.
* See FS100 Controller data sheet (DS-509) for complete specifications

www.motoman.com

YASKAWA
MOTOMAN ROBOTICS

MOTOMAN ROBOTICS
100 AUTOMATION WAY, MIAMISBURG, OHIO 45342
TEL: 937.847.6200 ■ FAX: 937.847.6277

Figure C.1 - Yaskawa Motoman SDA5F datasheet

APPENDIX D: COGNEX ISM1403C DATA SHEET

Table 3-1: In-Sight Micro Vision System Specifications

Specification		In-Sight 1020/1050	In-Sight 1100/1110	In-Sight 1100C	In-Sight 1400/1410	In-Sight 1400C	In-Sight 1403/1413	In-Sight 1403C
Minimum Firmware Requirement		In-Sight version 4.1.0		In-Sight version 4.3.0	In-Sight version 4.1.0	In-Sight version 4.3.0	In-Sight version 4.1.0	In-Sight version 4.3.0
Memory	**Job/Program**	64MB non-volatile flash memory; unlimited storage via remote network device.						
	Image Processing	128MB						
Image	**Sensor**	1/3-inch CCD					1/1.8-inch CCD	
	Sensor Properties	5.92mm diagonal, 7.4 x 7.4µm sq. pixels					8.8mm diagonal, 4.4 x 4.4µm sq. pixels	
	Resolution (pixels)	640 x 480					1600 x 1200	
	Electronic Shutter Speed	16µs to 1000ms					27µs to 1000ms	
	Acquisition[1]	Rapid reset, progressive scan, full-frame integration.						
		256 grey levels (8 bits/pixel)		24 bit color	256 grey levels (8 bits/pixel)	24 bit color	256 grey levels (8 bits/pixel)	24 bit color
		Gain/Offset controlled by software.						
		60 full frames per second		57 full frames per second	60 full frames per second	58 full frames per second	14 full frames per second	7 full frames per second
	Lens Type	CS-mount and C-mount (with 5mm extension, included).						
	CCD Alignment Variability[2]	±0.127mm (0.005in), (both x and y) from lens C-mount axis to center of imager.						

Figure D.1 - Cognex In-Sight® 1403C data sheet.

APPENDIX E: ROBOT MOUNTING CART AND STAGING TABLES ITERATIONS

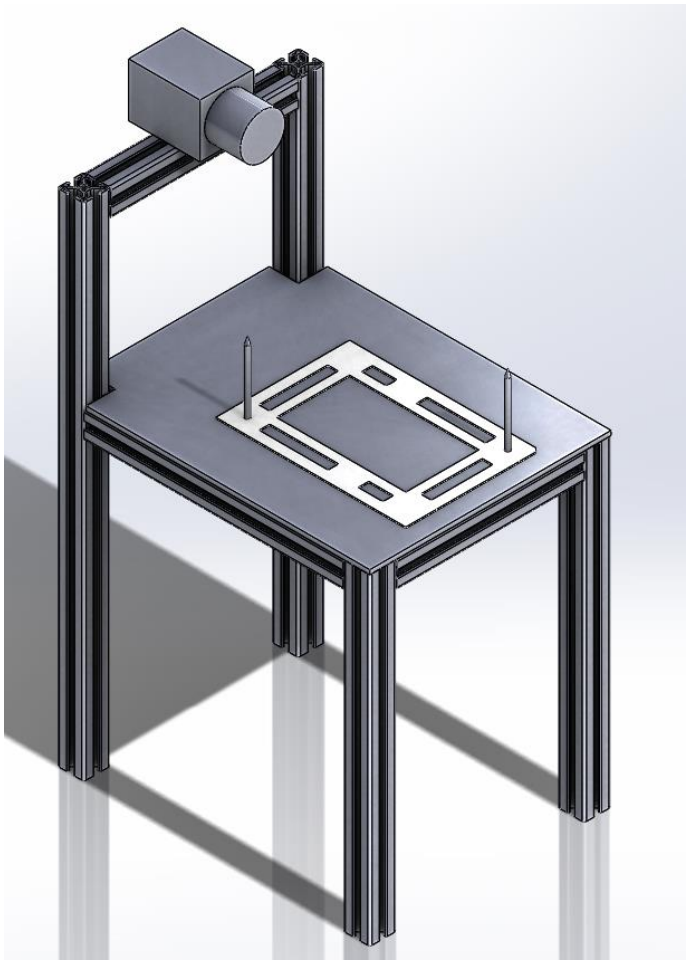

Figure E.1 - Initial alignment table design

Figure E.2 - Fabrication of initial alignment table.

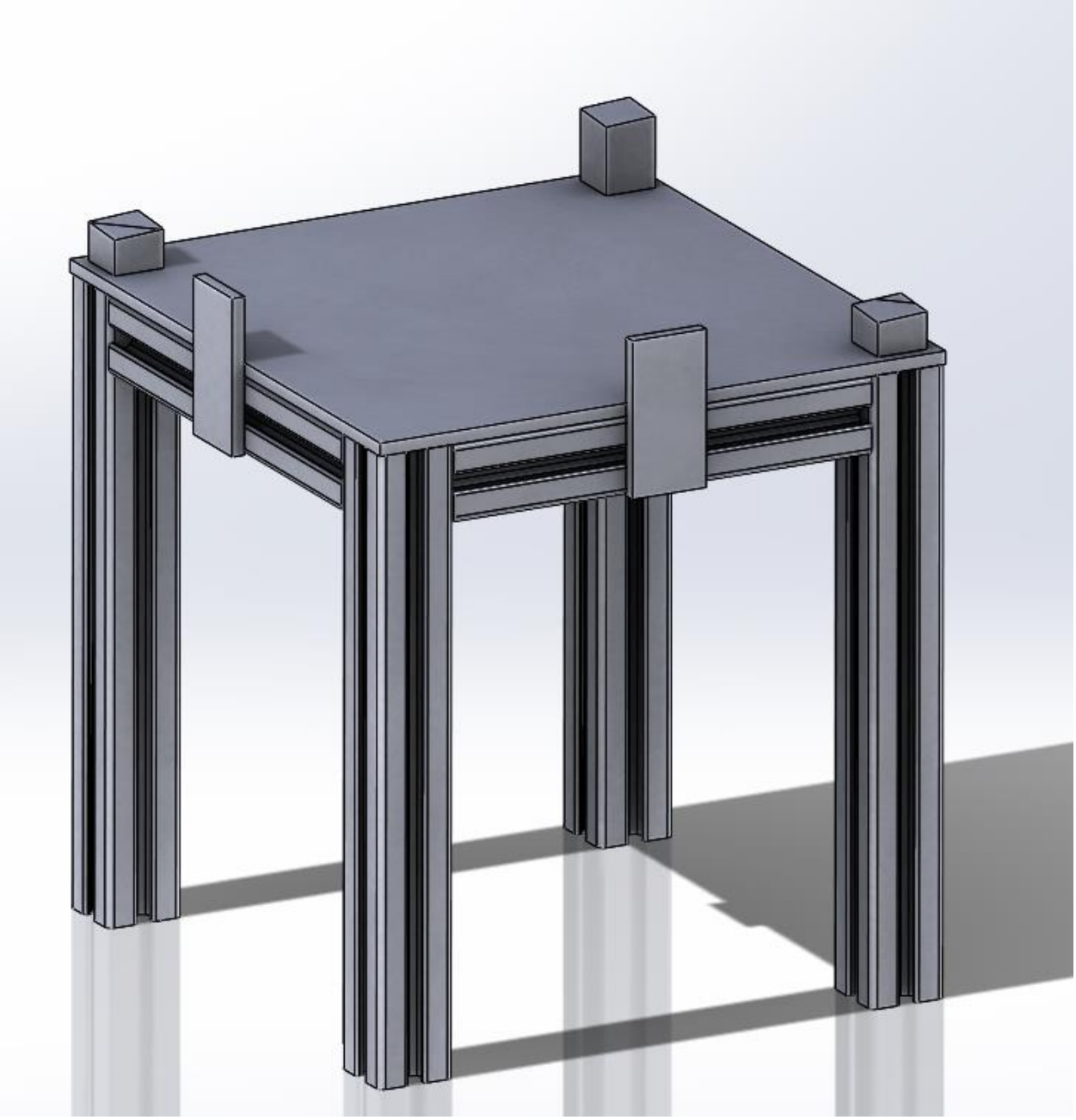

Figure E.3 - Initial gasket staging table design.

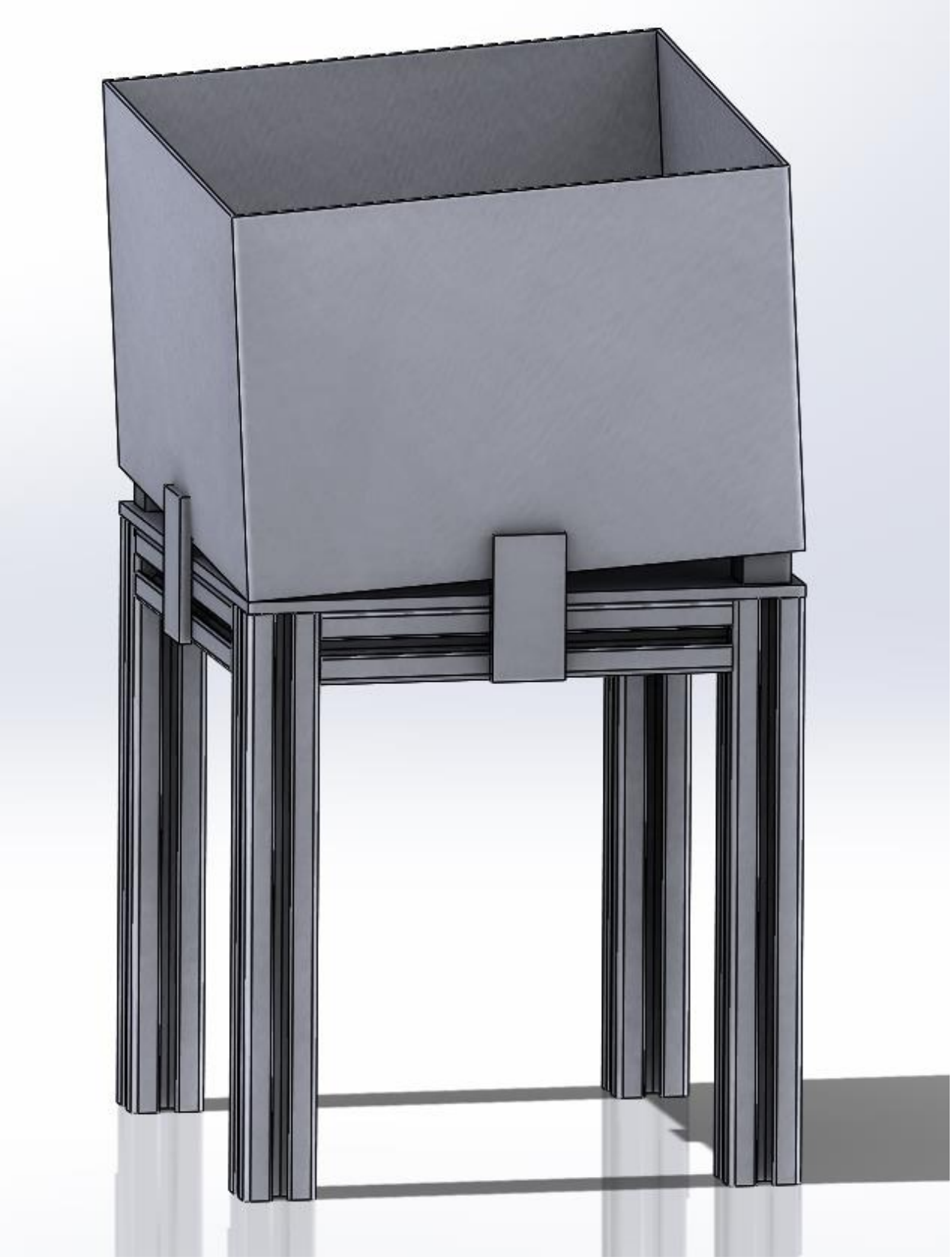

Figure E.4 - Initial gasket staging table design with box placed.

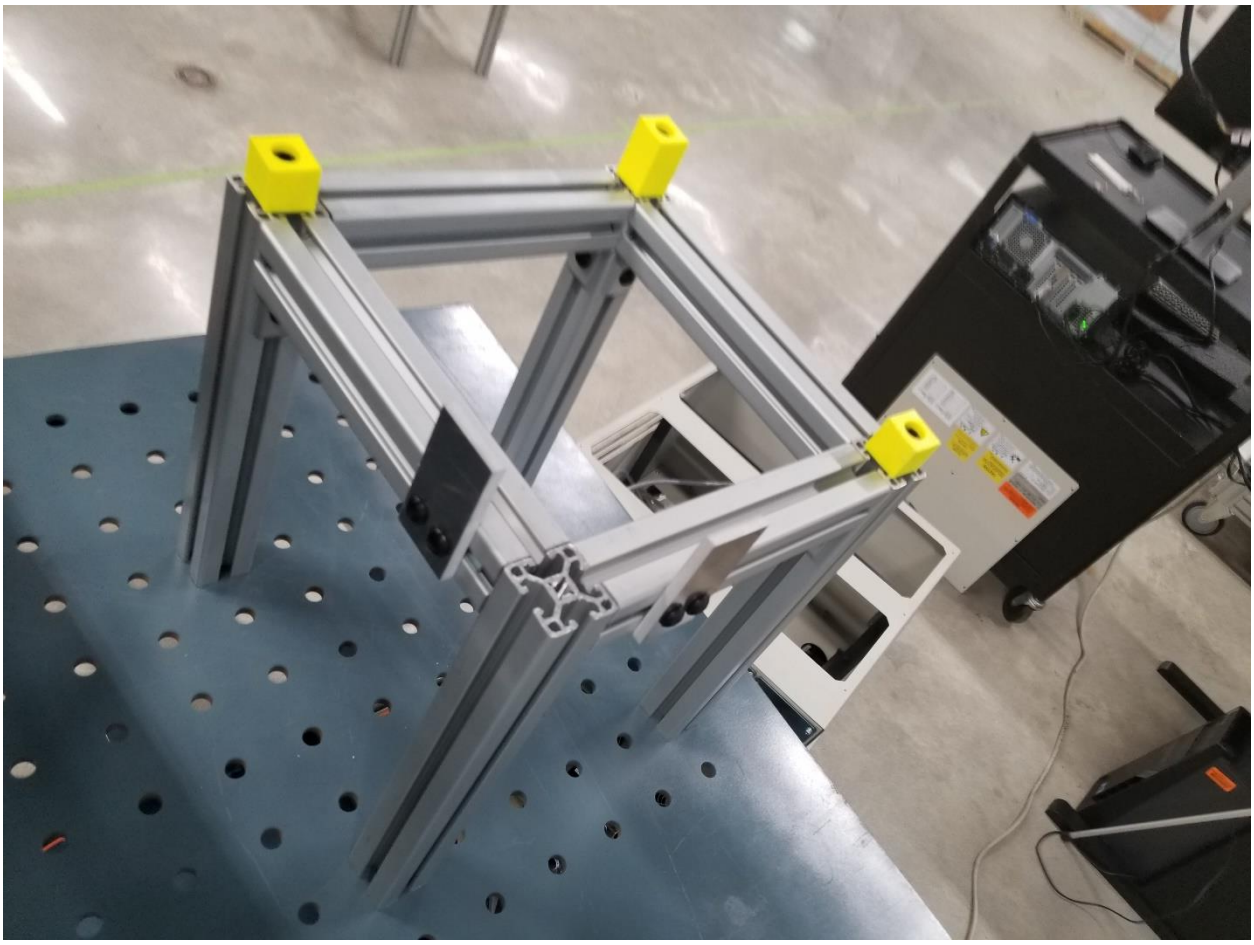

Figure E.5 - Fabrication of initial gasket staging table.

Figure E.6 - Initial gasket staging table with modified alignment table.

APPENDIX F: WORKCELL DESIGN ITERATIONS

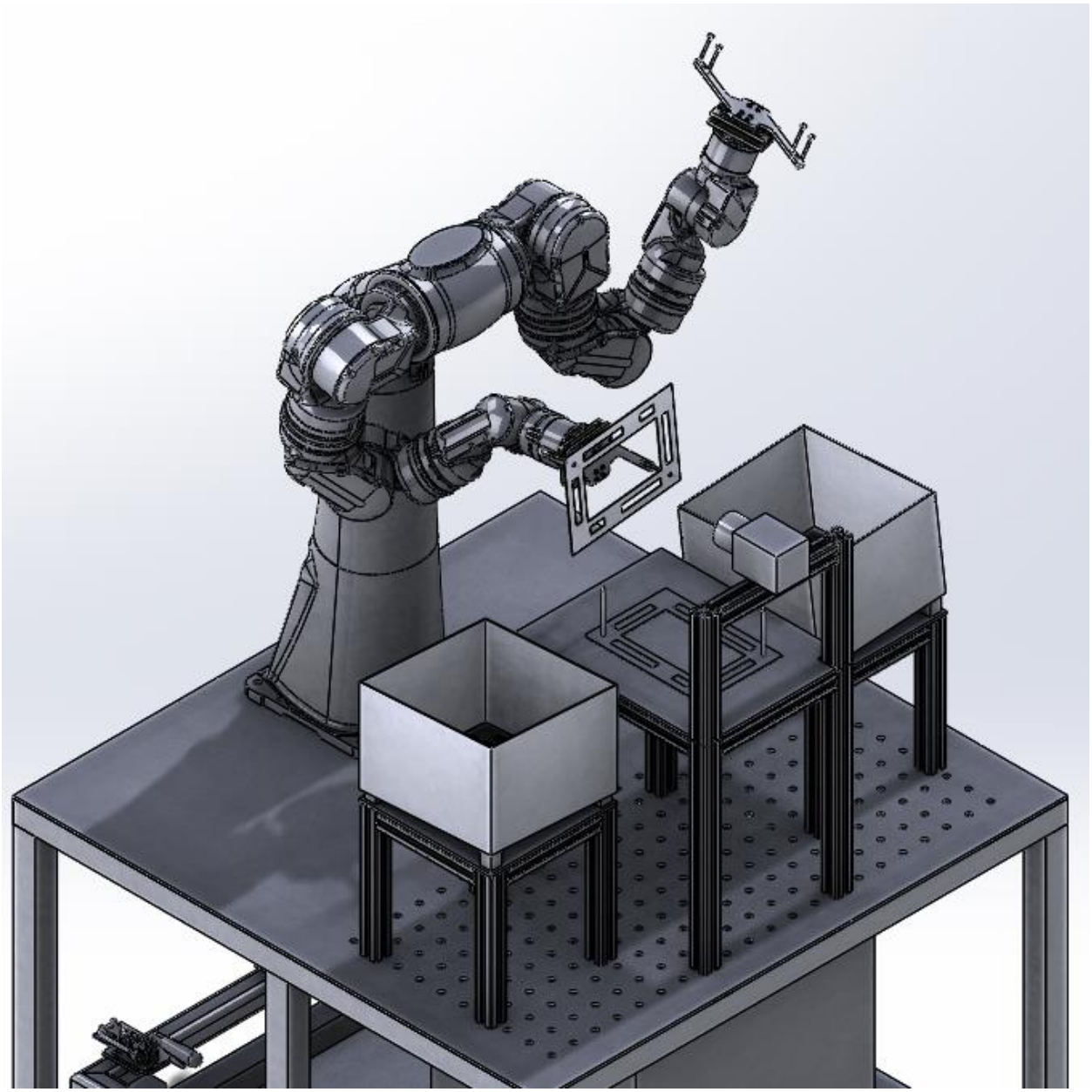

Figure F.1 - Initial workcell iteration.

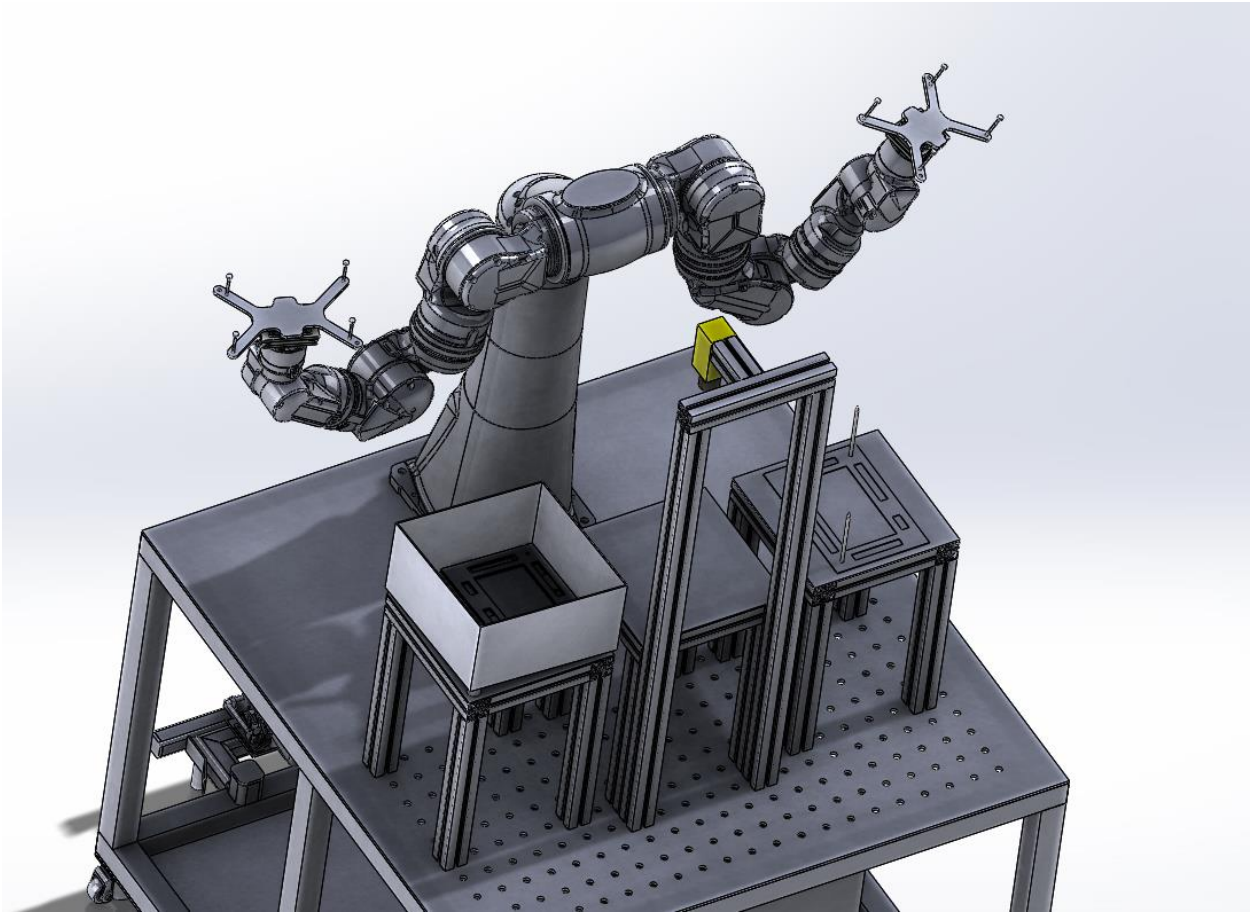

Figure F.2 - Second workcell iteration.

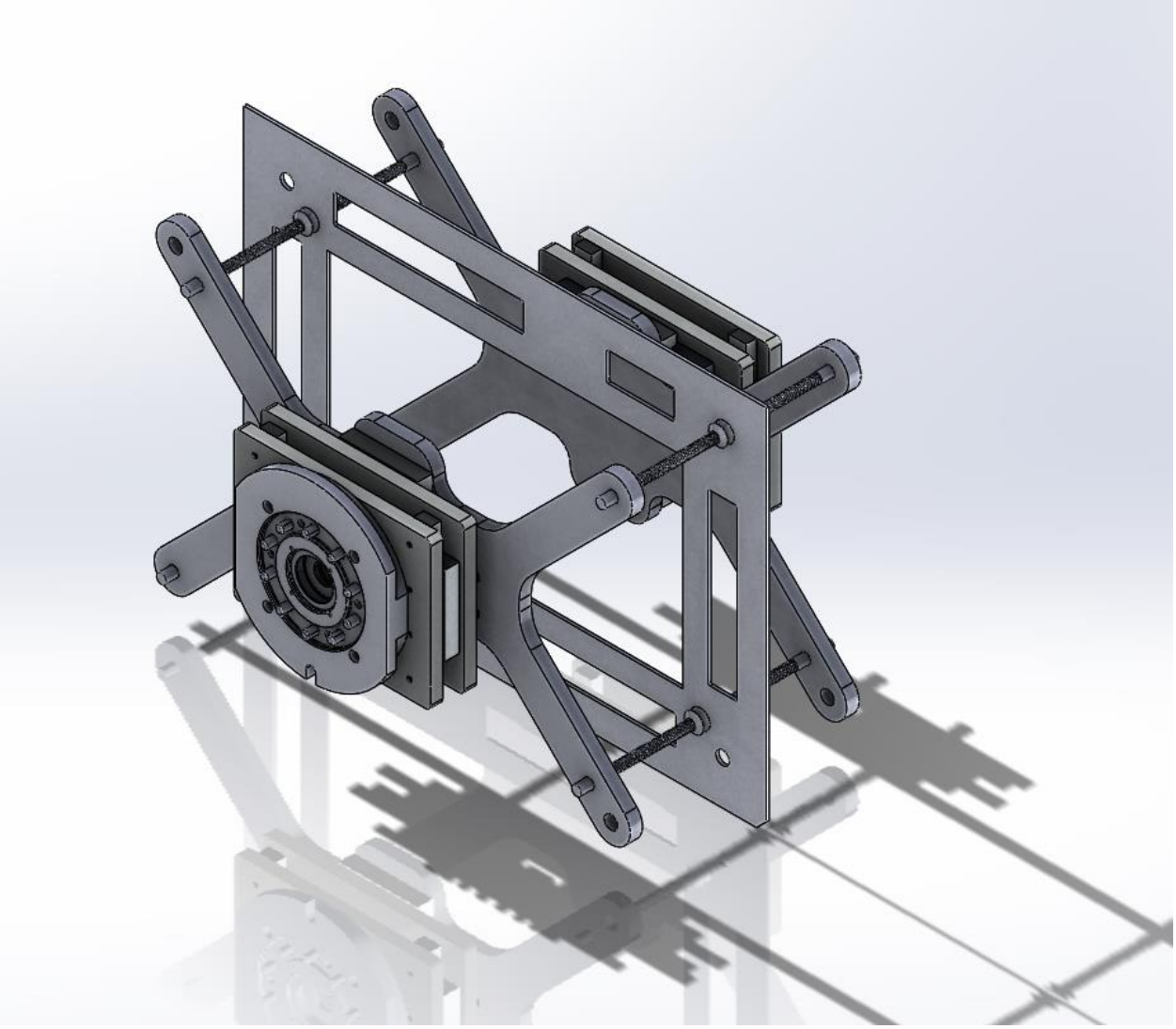

Figure F.3 - Initial end effector design.

APPENDIX G: JOB INSTRUCTION

Step 1: Open Cognex In-Sight® Explorer 5.4.0.

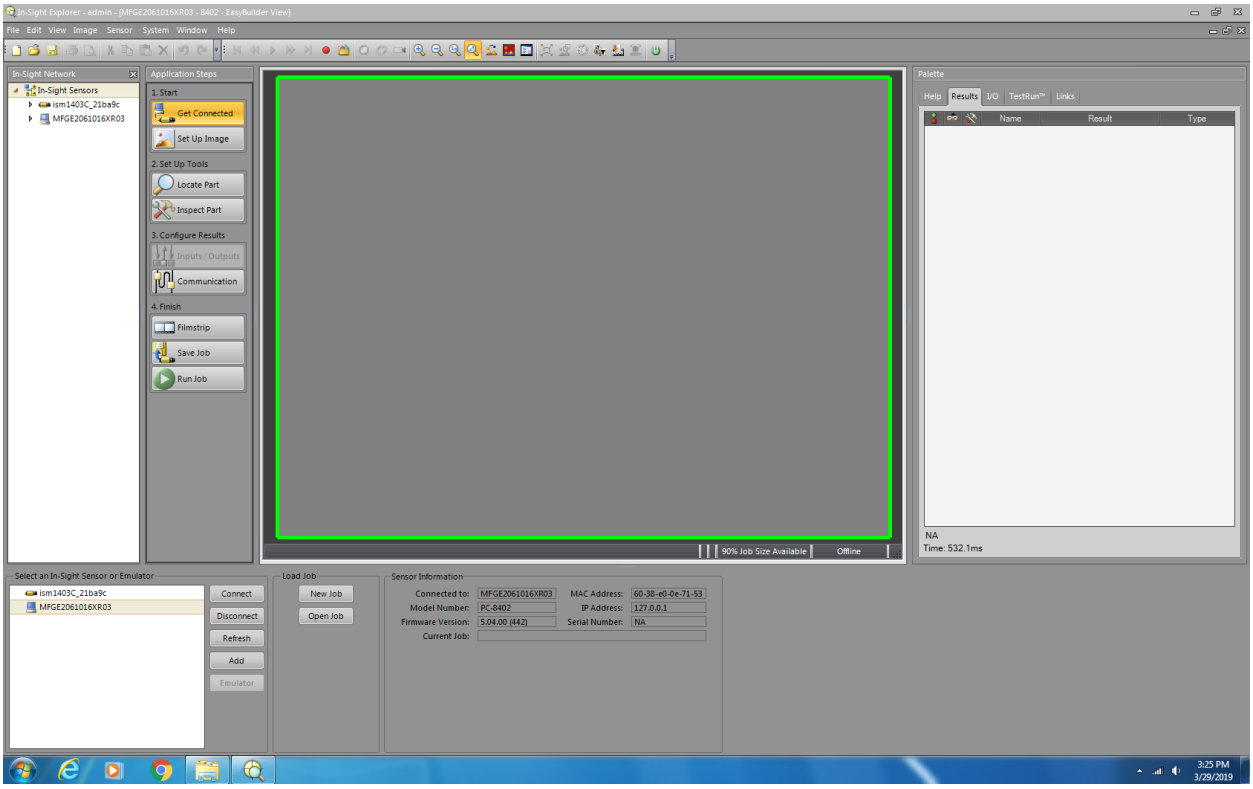

Figure G.1 - In-Sight® Explorer 5.4.0 Starting Screen

Step 2: Connect to the ISM1403C camera by double clicking the “ism1403C_21ba9c” name.

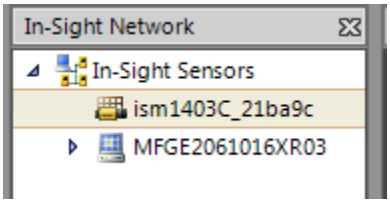

Figure G.2 - Network sensor list.

Step 3: Open the job file available online at:

https://drive.google.com/open?id=1qBZCrd5So2qzWCFQED_FhqbOvtL01u_k

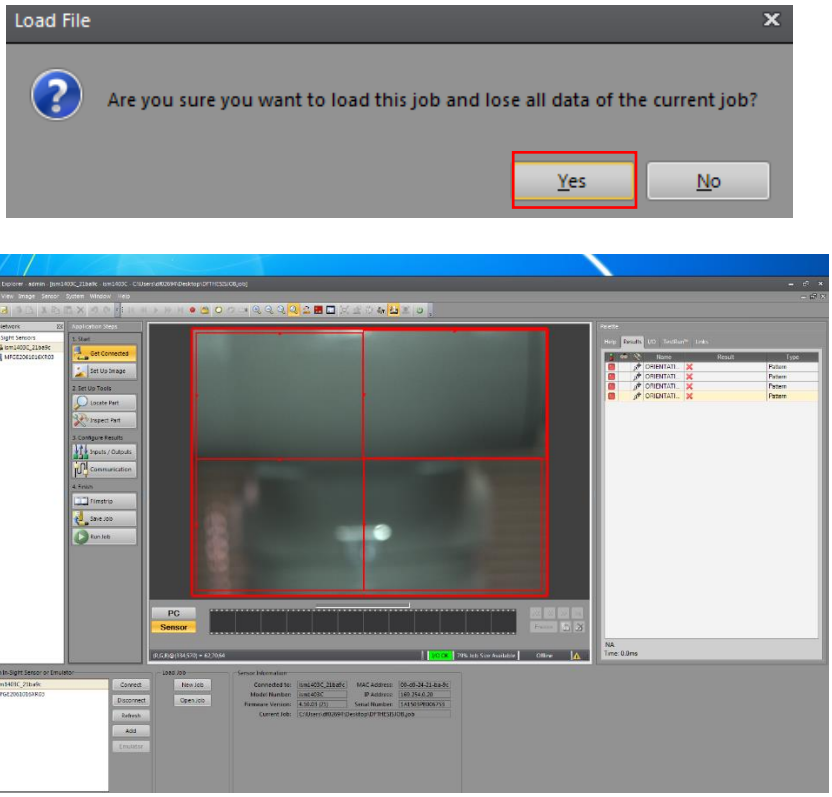

Figure G.3 - Load job file (Top), Accept loading (Middle), and screen after loading (Bottom)

Step 4: Go Online with the camera by selecting “Run Job” on the left side of the screen, then pressing “Online”. The camera will then activate.

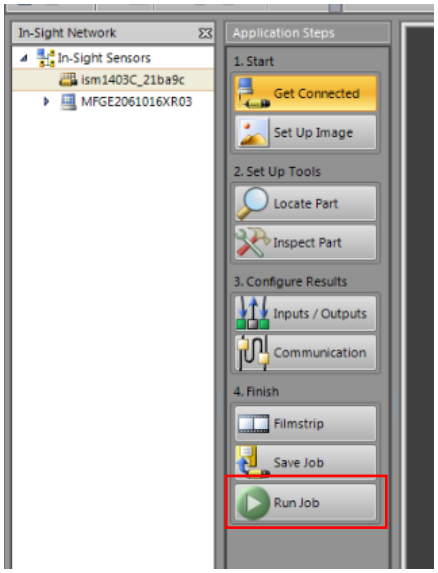

Figure G.4 - Run job button location.

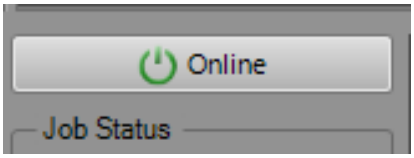

Figure G.5 - Online button.

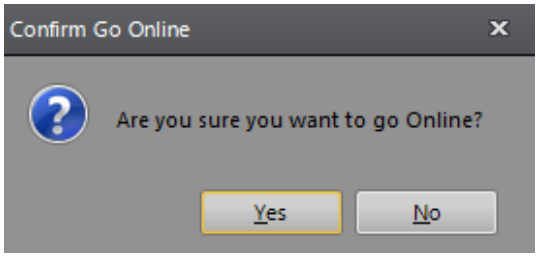

Figure G.6 - Confirm Go Online popup (press Yes).

Step 5: Turn on the robot controller.

Figure G.7 - Power switch location for the robot controller

Step 6: Enable the teach pendant after robot controller is powered.

Figure G.8 - Controller on screen.

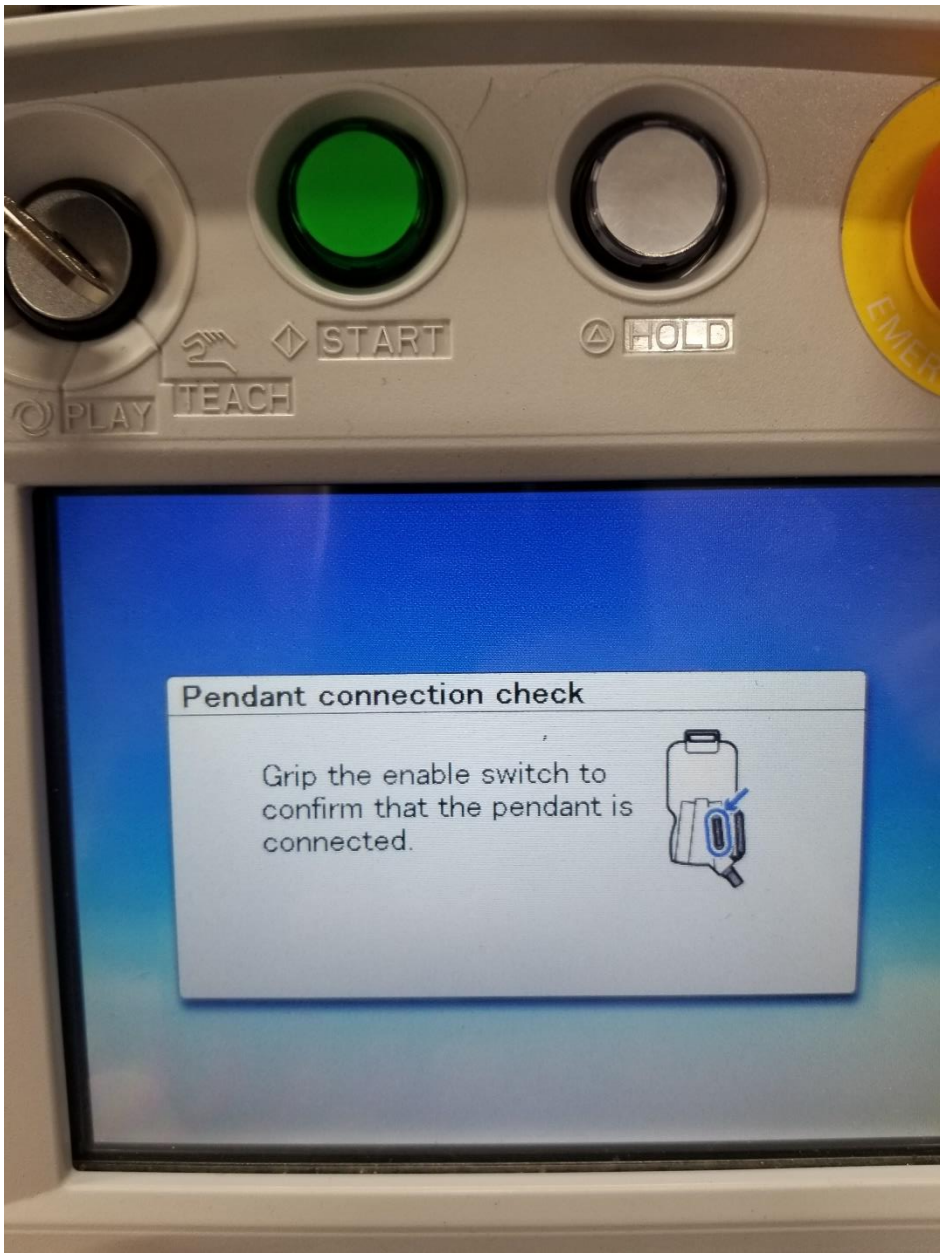

Figure G.9 - Grip to enable pendant handshake.

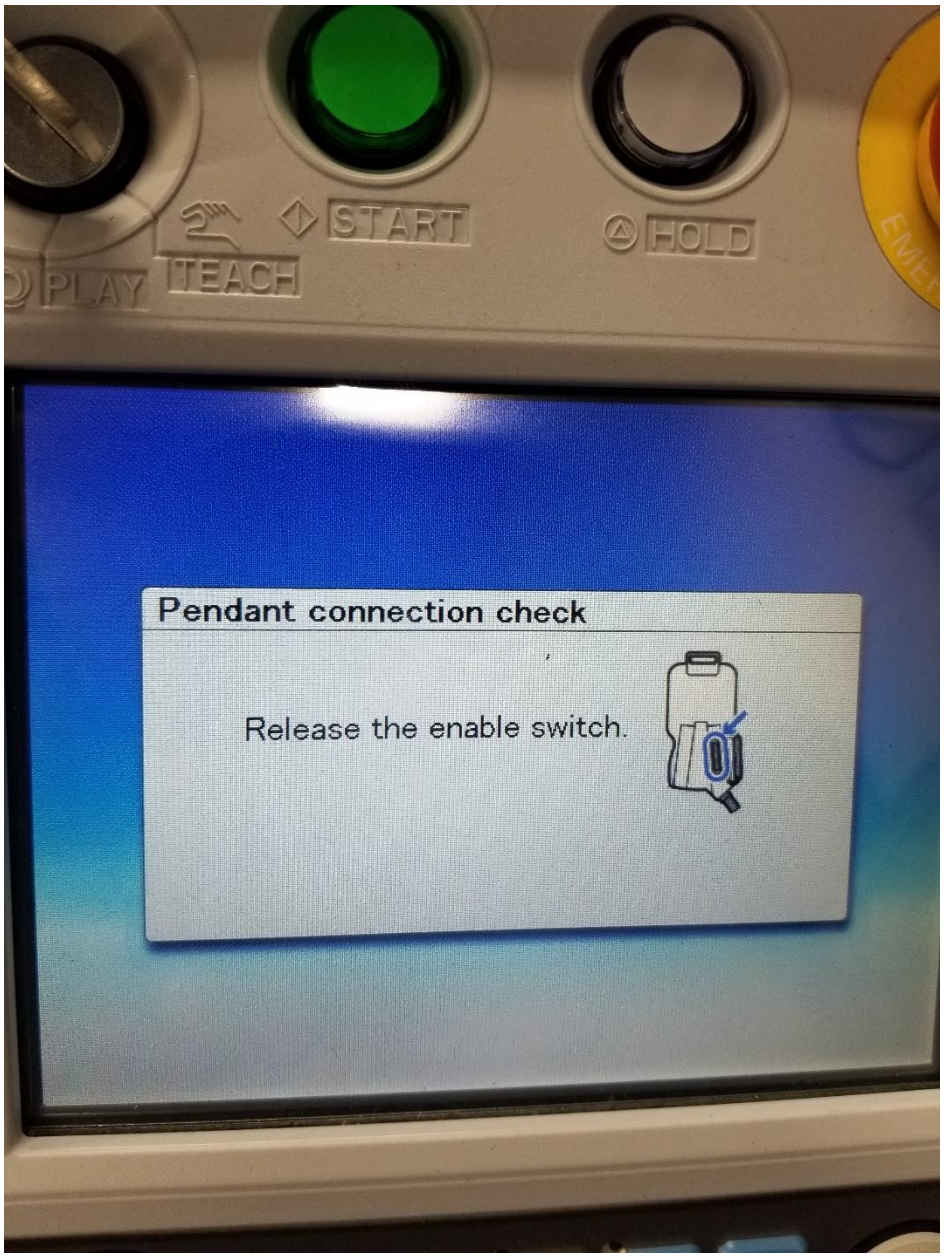

Figure G.10 - Release to connect pendant to controller.

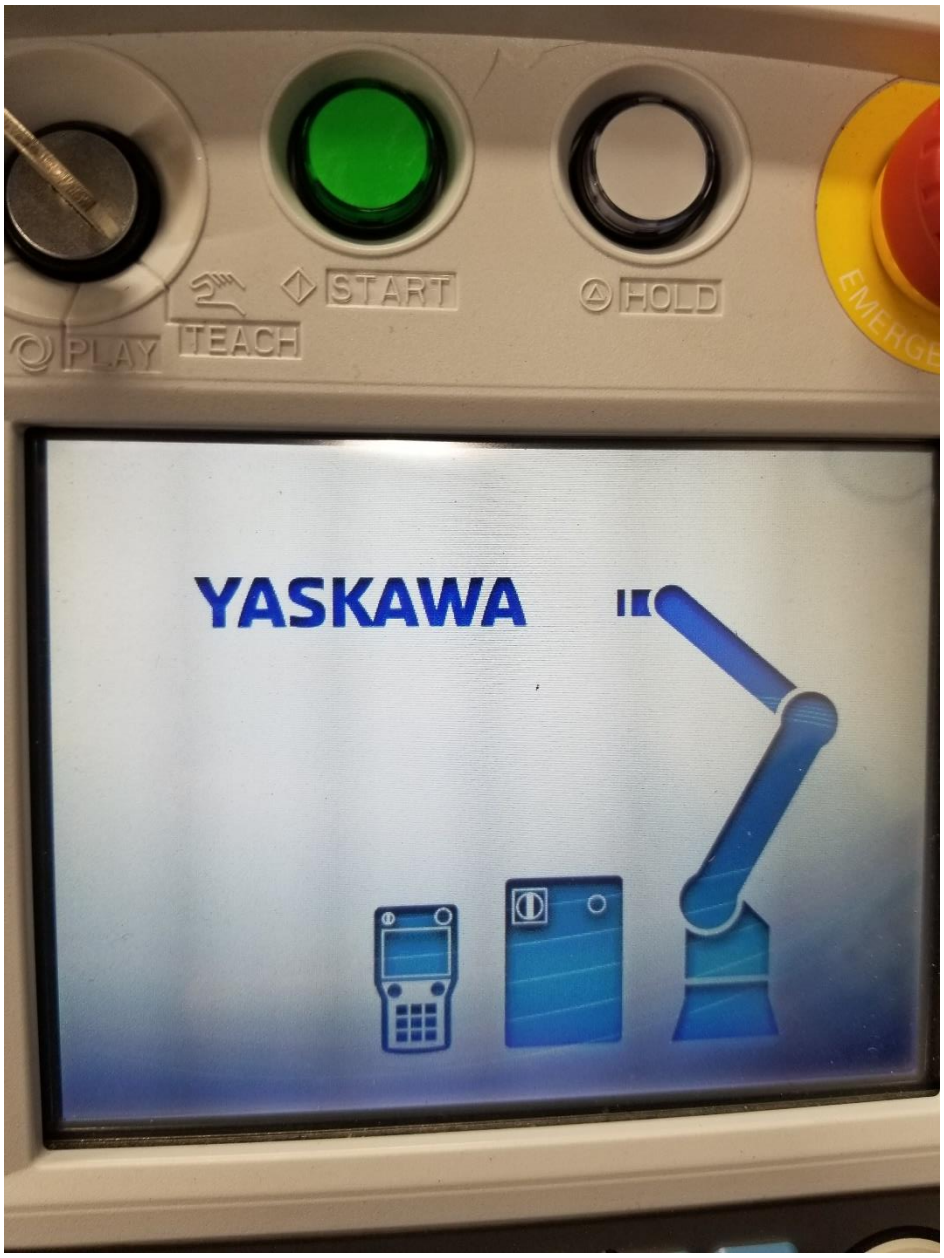

Figure G.11 - YASKAWA splash screen displayed after connection is successful.

Step 7: Select the robot job file “DFTHESIS”.

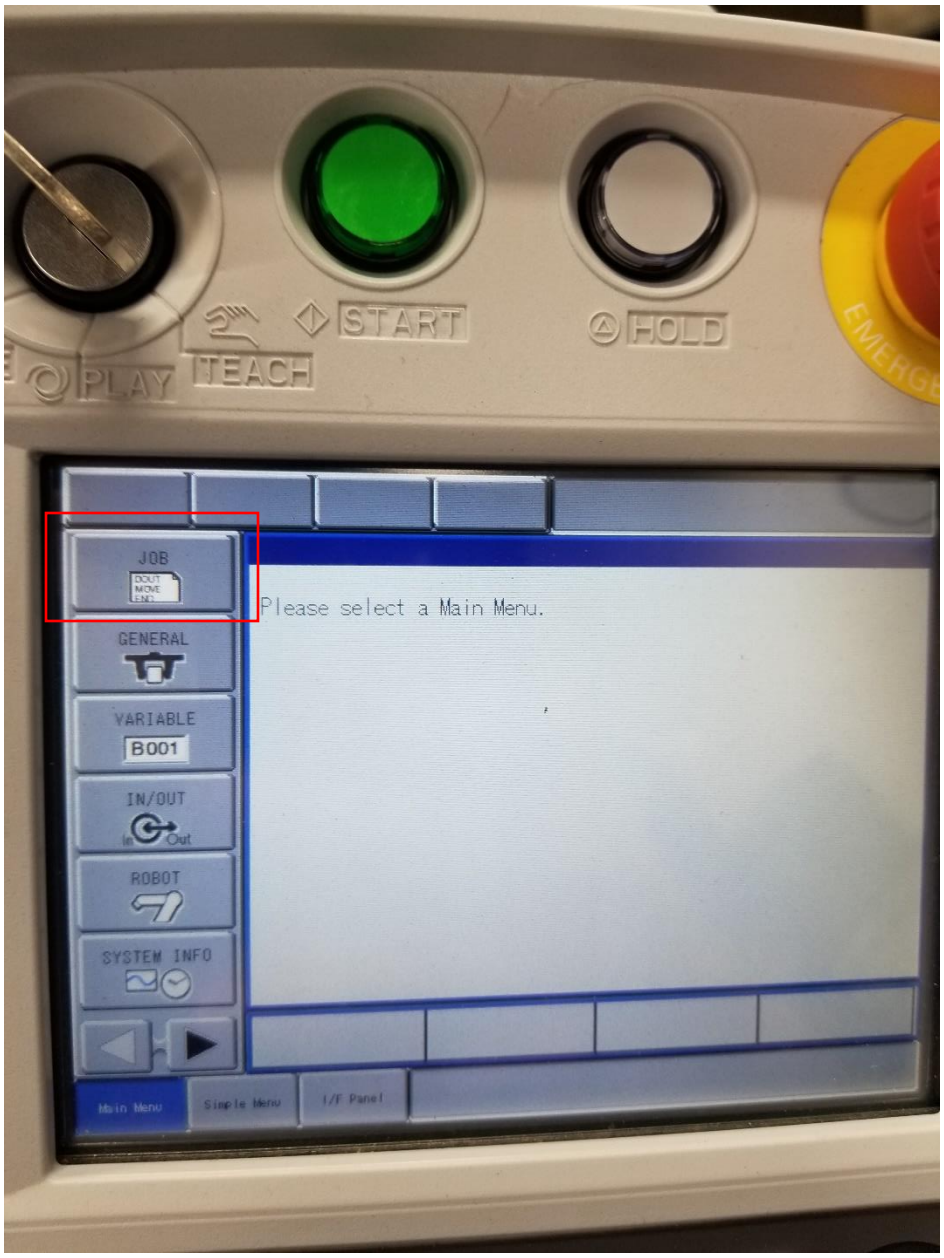

Figure G.12 - Main menu after connection completed.

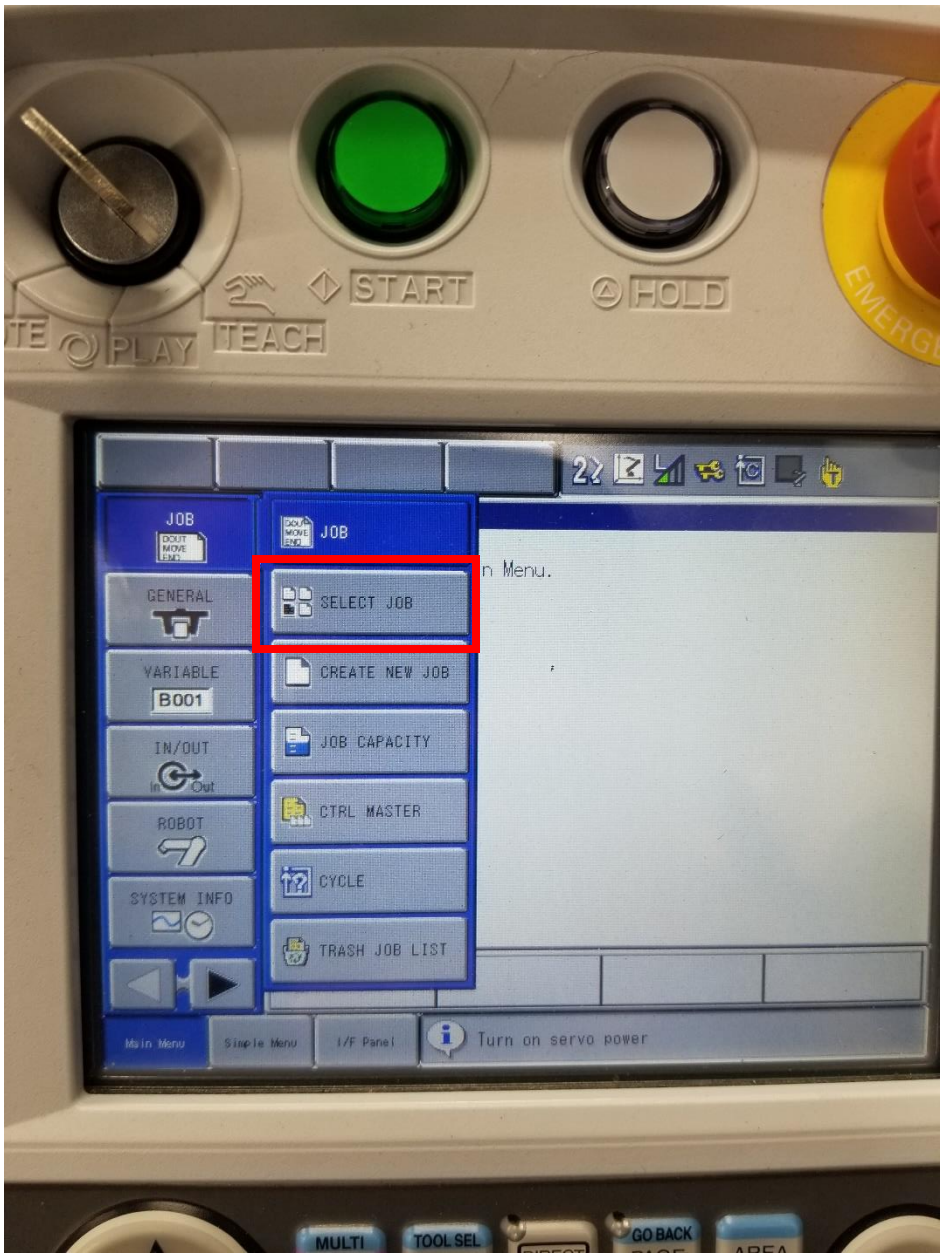

Figure G.13 - Screen after touching job on touchscreen controller.

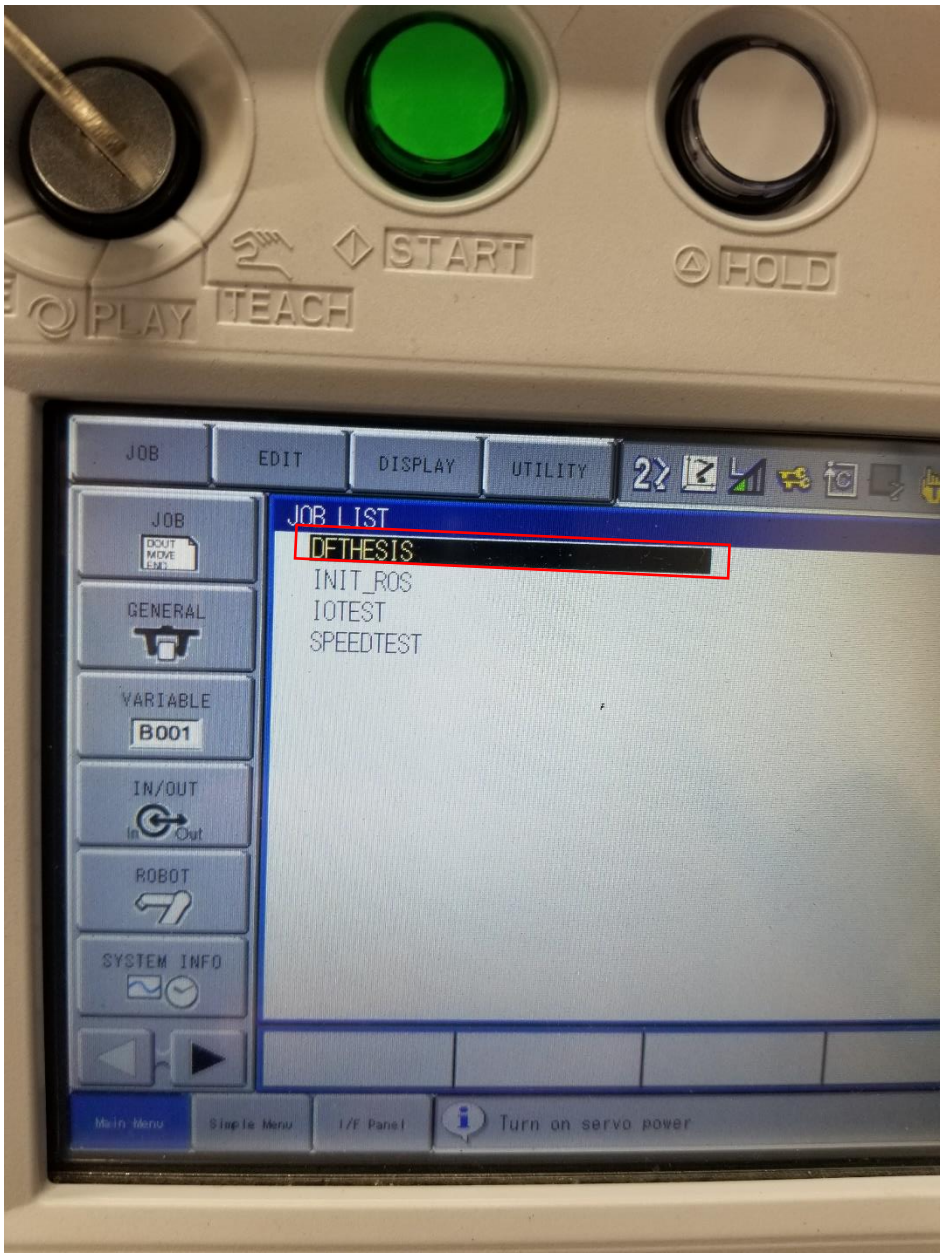

Figure G.14 - Job list after touching "Select Job". DFTHEIS job can selected using the "Select" button

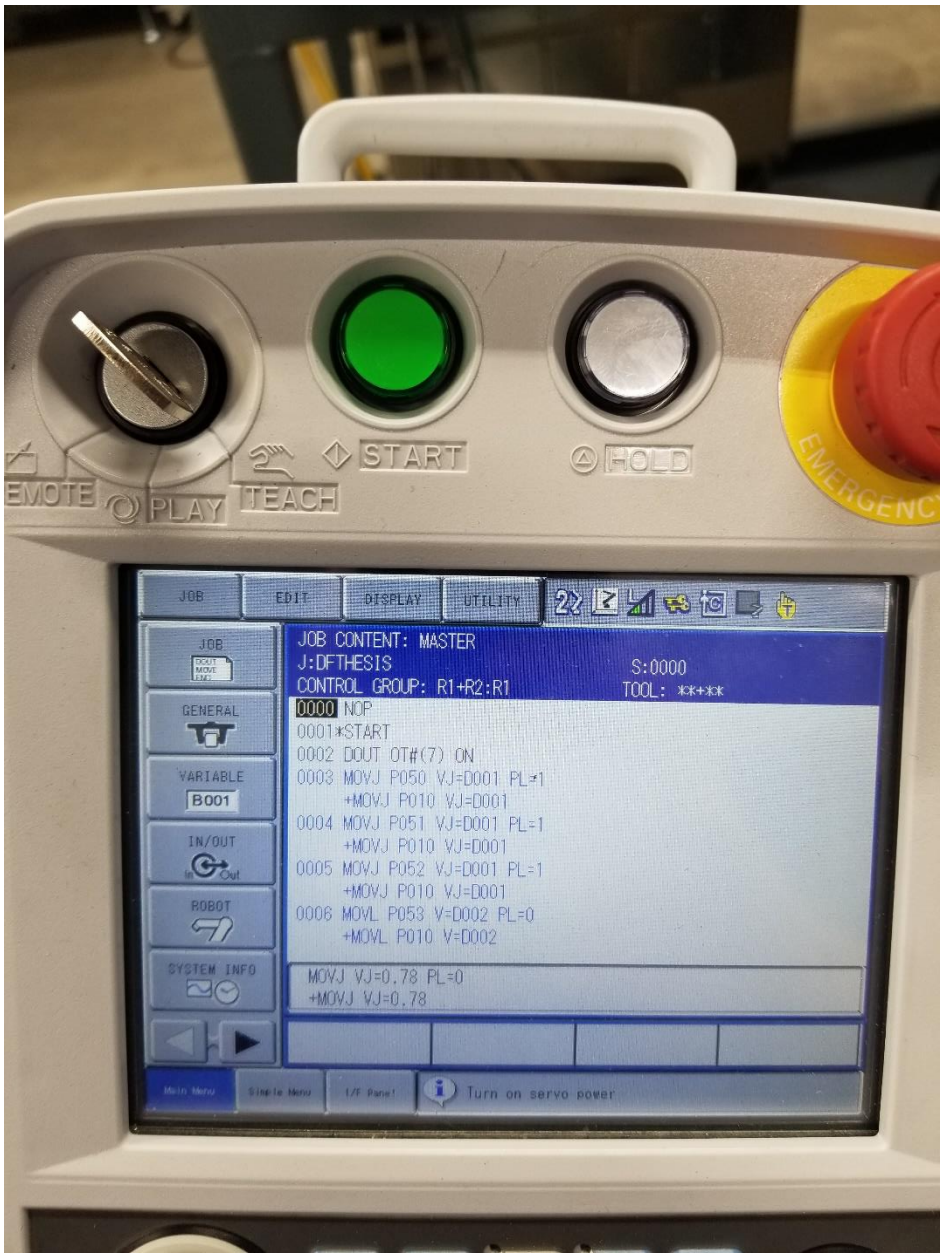

Figure G.15 - Job screen after selecing DFTHESIS job.

Step 8: Turn the key to “Play”.

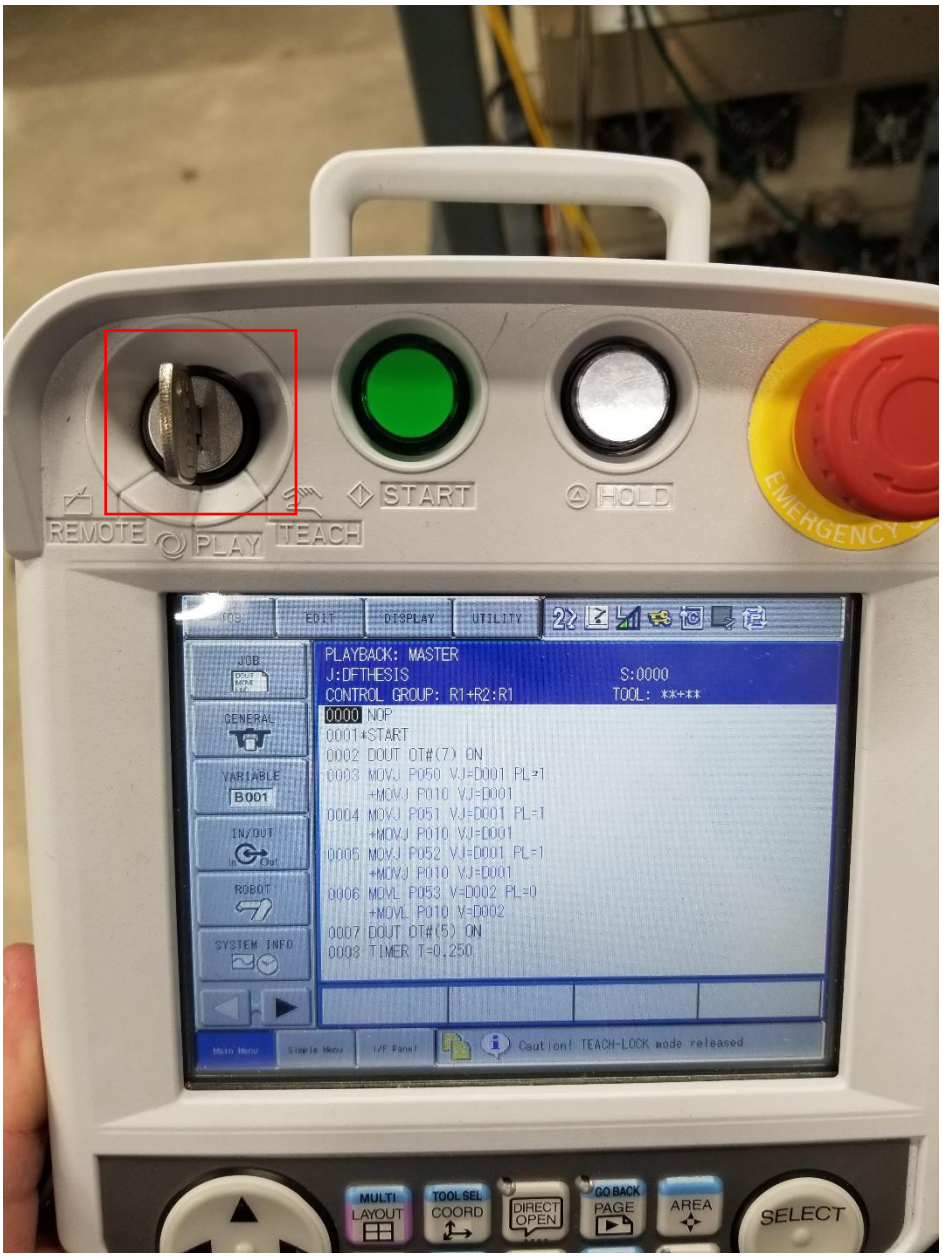

Figure G.16 - After switching the pendant key to play.

Step 9: Turn the servos on and press “Start”. Be aware that the robot will begin moving and accomplishing the job.

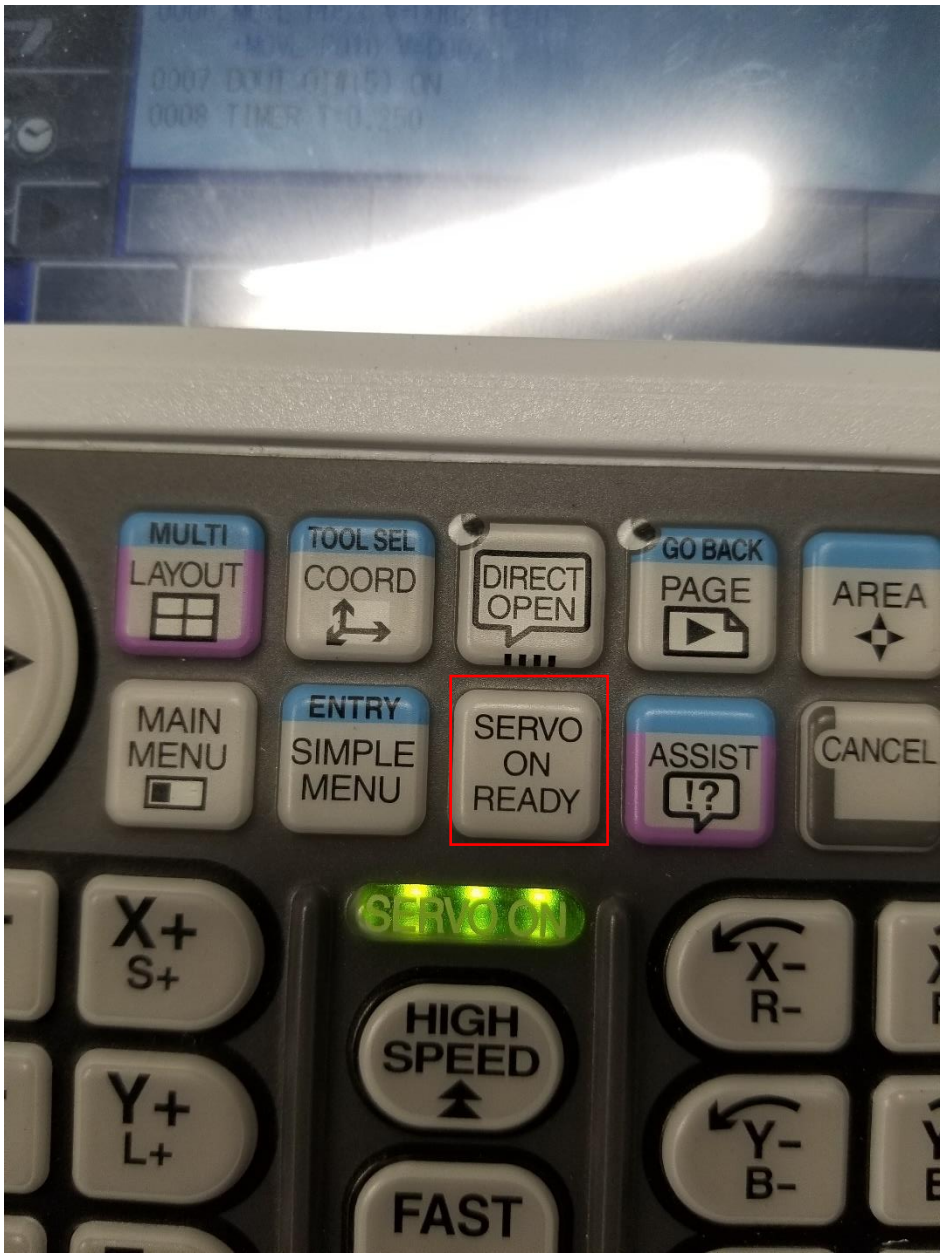

Figure G.17 - Press "SERVO ON READY" to enable robot servos. Wait a couple seconds for the servo brakes to disable and the servos to energize before pressing Start.

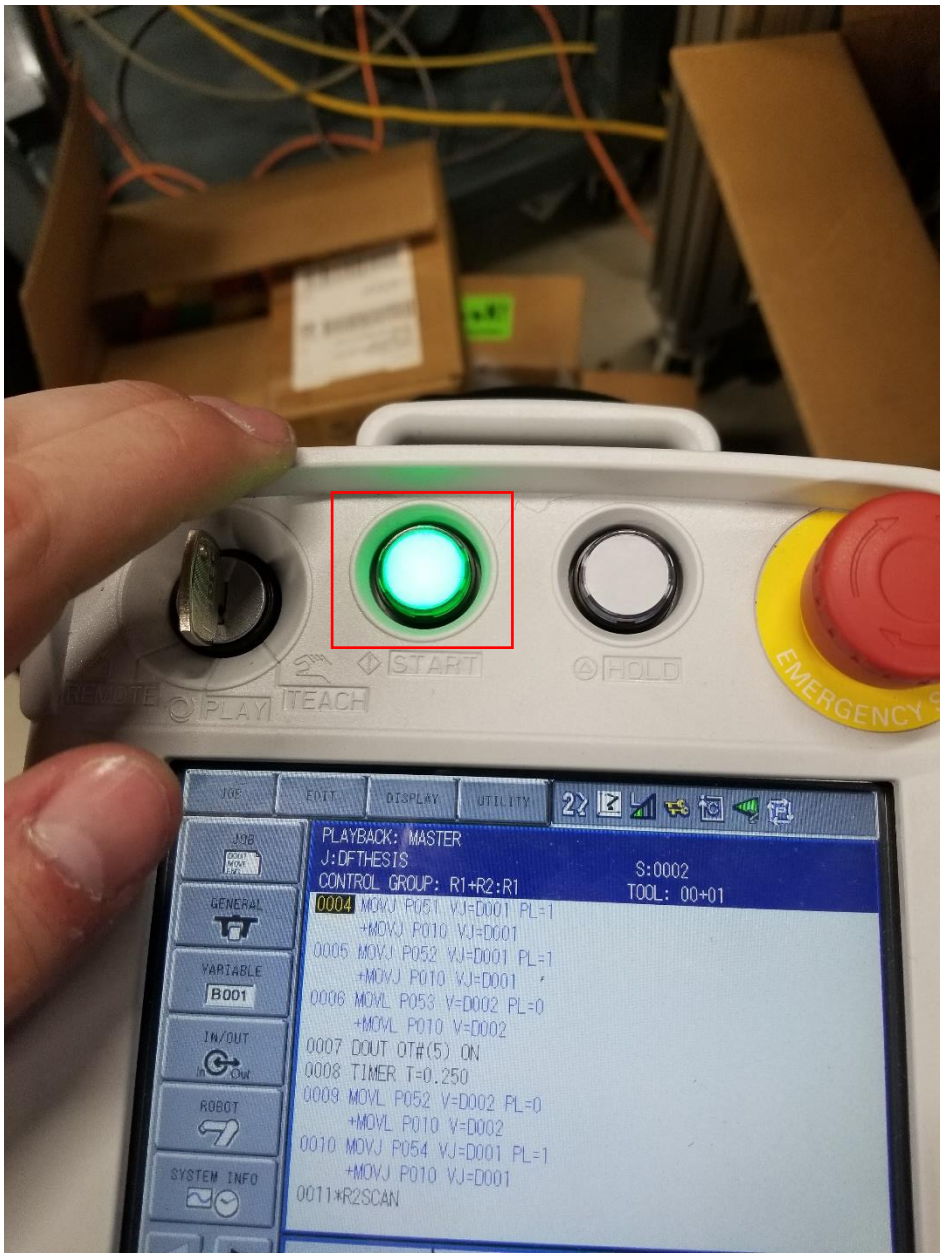

Figure G.18 - Press start on teach pendant to begin the program.